ΠΑΝΕΠΙΣΤΗΜΙΟ ΚΡΗΤΗΣ

ΤΜΗΜΑ ΙΑΤΡΙΚΗΣ

ΜΕΛΕΤΗ ΤΩΝ ΜΟΡΙΑΚΩΝ ΜΗΧΑΝΙΣΜΩΝ ΑΛΛΗΛΕΠΙΔΡΑΣΗΣ ΤΩΝ ΜΑΚΡΟΦΑΓΩΝ ΜΕ ΤΟ ΜΥΚΗΤΑ *MUCORALES*

ΔΙΔΑΚΤΟΡΙΚΗ ΔΙΑΤΡΙΒΗ

ΑΓΓΕΛΙΚΗ ΑΝΔΡΙΑΝΑΚΗ

ΙΑΤΡΟΣ

ΕΠΙΒΛΕΠΩΝ ΚΑΘΗΓΗΤΗΣ: ΓΕΩΡΓΙΟΣ ΧΑΜΗΛΟΣ

ΗΡΑΚΛΕΙΟ 2019

UNIVERSITY OF CRETE

FACULTY OF MEDICINE

STUDY OF THE MOLECULAR MECHANISMS OF THE INTERACTION OF MACROPHAGES WITH *MUCORALES*

PhD DISSERTATION

ANGELIKI ANDRIANAKI, MD

SUPERVISING PROFESSOR: GEORGIOS CHAMILOS

HERAKLION 2019

ΔΙΔΑΚΤΟΡΙΚΗ ΔΙΑΤΡΙΒΗ ΑΓΓΕΛΙΚΗΣ ΑΝΔΡΙΑΝΑΚΗ

Τίτλος: Μελέτη των μοριακών μηχανισμών αλληλεπίδρασης των μακροφάγων με το μύκητα Mucorales

Επιβλέπων Καθηγητής:

Γεώργιος Χαμηλός, Αναπληρωτής Καθηγητής Κλινικής Μικροβιολογίας - Μικροβιακής Παθογένεσης

Τριμελής Συμβουλευτική Επιτροπή:

1. Γεώργιος Χαμηλός, Αναπληρωτής Καθηγητής Κλινικής Μικροβιολογίας - Μικροβιακής Παθογένεσης Τμήματος Ιατρικής Πανεπιστημίου Κρήτης
2. Γεώργιος Σαμώνης, Ογκολόγος – Λοιμωξιολόγος, Καθηγητής Παθολογίας Τμήματος Ιατρικής Πανεπιστημίου Κρήτης
3. Διαμαντής Κοφτερίδης, Παθολόγος – Λοιμωξιολόγος, Αναπληρωτής Καθηγητής Παθολογίας Τμήματος Ιατρικής Πανεπιστημίου Κρήτης

Επταμελής Συμβουλευτική Επιτροπή:

1. Γεώργιος Χαμηλός, Αναπληρωτής Καθηγητής Κλινικής Μικροβιολογίας - Μικροβιακής Παθογένεσης
2. Γεώργιος Σαμώνης, Καθηγητής Παθολογίας
3. Διαμαντής Κοφτερίδης, Αναπληρωτής Καθηγητής Παθολογίας
4. Αχιλλέας Γκίκας, Καθηγητής Παθολογίας
5. Ελένη Παπαδάκη, Καθηγήτρια Αιματολογίας
6. Γεώργιος Τσατσάνης, Καθηγητής Κλινικής Χημείας
7. Ηλίας Δράκος, Επίκουρος Καθηγητής Παθολογικής Ανατομικής

ACKNOWLEDGEMENTS

As the poet would have said, my trip to «Ithaca» was long, full of adventures and knowledge. After my graduation, I started to work with enthusiasm on this new challenging field, expecting that this way was not going to be an easy one. Through the successes and the failures, I learned to work effectively, to interpret the negative and unexpected results, to be patient, and to think out of the box. All these valuable skills are the basis for my future career, with an ultimate goal to become a better scientist and doctor. With no doubt, this Thesis would not have been possible without the help of many people.

Firstly, I would like to thank my supervisor, Professor George Chamilos, the mind behind this project, who trusted me despite my initial lack of laboratory experience. He invested time to teach me techniques and most importantly a way of thinking on a totally new field for me. Without his expertise, his insight, feedback, and ideas this thesis would not have been possible. I will miss the brainstorming in every lab meeting and his enthusiasm after getting positive or unexpected results.

I will always be grateful to Professor George Samonis, whom I consider as my mentor and a great influence both in my professional life and on my personality. I started working with Dr Samonis as a research fellow right after my graduation. In fact, Dr Samonis was the person that encouraged me to engage with basic science. His thorough and deep knowledge of science, his enthusiasm with Medicine, his remarkable organization skills and love for perfectionism taught me many valuable lessons, which made me a better person and scientist. Moreover, I am thankful that he shared with me some of his wide knowledge on History and Arts, which helped me broaden my horizons and way of thinking.

I would like also to thank Professor Diamantis Kofteridis, who was the first to spot my interest on research, when I was young a medical student. Dr Kofteridis introduced me to clinical research and under his supervision we conducted many studies, which have been published in top Clinical Infectious Diseases journals. Moreover, as an attending physician, Dr Kofteridis helped me to build up my clinical skills and clinical knowledge during my residency in Internal Medicine at the University Hospital of Heraklionr.

I would like to acknowledge the contribution of the other members of my PhD committee, Professors A. Gikas, E. Papadaki, G. Tsatsanis and E. Drakos. Thank you for your support and advice every time I needed them.

I would like also to thank all our collaborators in University of Crete, Institute Pasteur, UCLA, Biomedical Research Foundation of the Academy of Athens, MD Anderson Cancer Centre and University of Sharjah for their valuable contribution to this project.

Many thanks go to the members of our lab, Dr. Tonia Akoumianaki, Dr. Irene Kyrmizi, Dr. Petros Ioannou and Afroditi Katsarou for their warm welcome, their patience, their insights and their knowledge that generously shared with me. I consider myself very lucky that except for valuable collaborators, these people also became close friends.

I owe a great gratitude to my family, my parents Michalis and Roula, and my sister, Maria, for their constant love and support. Thank you for believing in me more that I believed in myself and helped me to fulfil my dreams. Finally, I would like to thank my partner and husband-to-be, Christos, for his endless patience, his understanding with my crazy working hours and his confidence that I will succeed, even when the difficulties overwhelmed me. I love you so much.

CONTENTS

ΠΕΡΙΛΗΨΗ

Εισαγωγή

Η μουκορμύκωση αποτελεί μια σοβαρή λοίμωξη που συνοδεύεται από αρκετά υψηλή θνητότητα και προκαλείται από μύκητες της τάξης των Mucorales. Η μουκορμύκωση προσβάλλει κατά κύριο λόγο ανοσοκατεσταλμένους ασθενείς καθώς επίσης και ασθενείς με μεταβολικές διαταραχές που επηρεάζουν τη ρύθμιση του σιδήρου. Την τελευταία δεκαετία έχει καταγραφεί σημαντική αύξηση της επίπτωσής της μουκορμύκωσης, καθιστώντας την πλέον τη δεύτερη σημαντικότερη διηθητική λοίμωξη από υφομύκητες μετά την ασπεργίλλωση σε ανοσοκατασταλμένους ασθενείς.

Οι γνώσεις μας σχετικά με την παθοφυσιολογία της μουκορμύκωσης είναι λίγες. Μελέτες έχουν δείξει πως τόσο τα σπόρια όσο και οι υφές των Mucorales ανθίστανται στη θανάτωση από τα φαγοκύτταρα, γεγονός που αποδίδεται αφενός στην ιδιαίτερη σύνθεση του κυτταρικού τους τοιχώματος, που τους καθιστά εξαιρετικά ανθεκτικούς, και αφετέρου στην μη ικανοποιητική φαγοκυττάρωσή τους, συνεπεία του μεγάλου μεγέθους των σποριών τους, χωρίς όμως να έχουν μελετηθεί περαιτέρω οι υπεύθυνοι μηχανισμοί.

Στόχος της παρούσας διατριβής είναι η κατανόηση των μηχανισμών αλληλεπίδρασης των φαγοκυττάρων με το μύκητα *Rhizopus oryzae* της τάξης των *Mucorales* με έμφαση στη διαδικασία ωρίμανσης του φαγοσώματος κατά την φαγοκυττάρωσή του από τα μακροφάγα. Παράλληλα, αναζητήθηκαν οι αιτιολογικοί παράγοντες και οι μηχανισμοί που καθιστούν το μύκητα ανθεκτικό στη δράση των μακροφάγων, καθώς και ο ρόλος των τελευταίων στην παθοφυσιολογία της λοίμωξης.

Υλικά και Μέθοδοι

Σε όλα τα πειράματα χρησιμοποιήθηκαν ανοσοεπαρκή black 6 (B6), διαγονιδιακά GFP-LC3 και CD11c-DTR ποντίκια ηλικίας 8-12 εβδομάδων. Όλες οι διαδικασίες πραγματοποιήθηκαν σύμφωνα με τα υψηλότερα πρότυπα φροντίδας και διαχείρισης ζώων, έχοντας λάβει την σχετική έγκριση από την αρμόδια Κτηνιατρική Υπηρεσία. Τα ex vivo πειράματα πραγματοποιήθηκαν σε διαφοροποιημένα μακροφάγα προερχόμενα από τον μυελό των οστών των ποντικών (bone marrow derived macrophages – BMDMs). Για την μελέτη των διάφορων σταδίων της φαγοκυττάρωσης με ανοσοφθορισμό τα BMDMs μολύνθηκαν σε συγκεκριμένα χρονικά διαστήματα με ζωντανά σπόρια *Mucorales* και *Aspergillus fumigatus* (ως μάρτυρας-control) και εξετάσθηκαν σε συνεστιακό μικροσκόπιο (Confocal microscopy).

Για την μελέτη των μηχανισμών φαγοκυττάρωσης σε κυψελιδικά μακροφάγα (alveolar macrophages – AMs) χρησιμοποιήθηκαν GFP-LC3 ποντίκια τα οποία μολύνθηκαν ενδοτραχειακά με $5*10^6$ ζωντανά σπόρια *Mucorales* και *Aspergillus fumigatus* και αφού θυσιάστηκαν μετά από 2, 4 και 24 ώρες, ελήφθη βρογχοκυψελιδικό έκπλυμα (BAL). Τα απομονωθέντα κύτταρα μονιμοποιήθηκαν και στη συνέχεια ακολούθησε η σήμανση των διαφόρων μορίων-πρωτεινών με τα πρωτόκολλα ανοσοφθορισμού. Τα σημασμένα κύτταρα εξετάσθηκαν στο confocal.

Για τα in vivo πειράματα χρησιμοποιήθηκαν ανοσοεπαρκή black 6 (B6), διαγονιδιακά GFP-LC3 και CD11c-DTR ποντίκια, τα οποία θανατώθηκαν σε διαδοχικά χρονικά διαστήματα. Οι πνεύμονες αφαιρέθηκαν, μονιμοποιήθηκαν με παραφίνη και επεξεργαστηκαν με διάφορες χρώσεις, καθώς και ιστοχημικά. Σε διαφορετικά πειράματα απομονώθηκαν οι διαφορετικοί κυτταρικοί υποπληθυσμοί των φαγοκυττάρων του πνεύμονα σε διάφορα στάδια της λοίμωξης (1 και 5 ημέρες) με κυτταρομετρία ροής (sorting) και αναλύθηκαν με συνεστιακή μικροσκοπία Μελανίνη του κυτταρικού τοιχώματος ζωντανών σποριών *Rhizopus*, απομονώθηκε

με χημικές μεθόδους, αναλύθηκε δομικά με φασματομετρία μάζας και χρησιμοποιήθηκε σε ex vivo πειράματα φαγοκυττάρωσης.

BMDMs απο B6 ανοσοεπαρκή ποντίκια μολύνθηκαν με ζωντανά σπόρια Mucorales σε συγκεκριμένα χρονικά διαστήματα. Στη συνέχεια απομονώθηκε σύμφωνα με τις οδηγίες του κατασκευαστή RNA, τόσο απο τα μακροφάγα όσο και απο τα σπόρια του μύκητα. Με την τεχνική του υβριδισμού ακολούθησε ποσοτική ανάλυση του απομονωθέντος RNA και κατόπιν βιοπληροφορική ανάλυση της έκφρασης των γονιδίων.

Αποτελέσματα

Αρχικά, σε αντίθεση με την επικρατούσα άποψη, ότι το μεγάλο μέγεθος των σποριών Mucorales (με διάμετρο μέχρι και 10μm) συνεπάγεται την ανεπαρκή φαγοκυττάρωσή τους, διαπιστώσαμε οτι μολύνοντας τα BMDMs με ζωντανά σπόρια Mucorales, ο μύκητας όχι μόνο φαγοκυτταρώνεται επαρκώς αλλά ο ρυθμός της φαγοκυττάρωσης (phagocytic rate – PR) κυμαίνεται στα υψηλότερα επίπεδα σε σύγκριση με τον *A. fumigatus,* που χρησιμοποιήθηκε ως control.

Παράλληλα επιβεβαιώσαμε πως ενώ τα BMDMs θανατώνουν τα σπόρια του *A. fumigatus*, αδυνατουν να καταστρέψουν τα σπόρια Mucorales, που παραμένουν ζωντανά, ακόμα και 6 ώρες μετά τη φαγοκυττάρωσή τους από τα BMDMs, καταδεικνύοντας με τον τρόπο αυτό την ανθεκτικότητα του συγκεκριμένου μύκητα. Επίσης, διαπιστώσαμε την βιωσιμότητα των BMDMs μετά τη μόλυνση με τους δύο μύκητες, αποκλείοντας το ενδεχόμενο της επαγόμενης από τη μόλυνση απόπτωσης των BMDMs, αποδεικνύοντας με τον τρόπο αυτό ότι η παρατηρούμενη ανθεκτικότητα των σποριών Mucorales αποτελεί εγγενή ιδιότητα του μύκητα. Στην συνέχεια, εξετάσαμε την *in vitro* αποτελεσματικότητα των οξειδωτικών και μη οξειδωτικών μηχανισμών των μακροφάγων, επωάζοντας τα σπόρια Mucorales με H_20_2 και απομονωθέντα λυσσοσώματα αντίστοιχα. Από τα πειράματα προέκυψε

πως οι οξειδωτικοί και μη μηχανισμοί των μακροφάγων είναι ικανοί να θανατώσουν τα σπόρια του μύκητα. Μελετώντας περαιτέρω με *ex vivo* πειράματα το μονοπάτι της φαγοκυττάρωσης, διαπιστώσαμε πως τα σπόρια Mucorales προκαλούν ενεργητική αναστολή της διαδικασίας, ήδη από τα αρχικά της στάδια (Rab5, LC3), με απώτερο αποτέλεσμα την αναστολής της φαγολυσοσωμικής ένωσης. Αυτή η ανακάλυψη επιβεβαιώθηκε σε διάφορα ήδη μακροφάγων (BMDMs, AMs) τόσο ex vivo όσο και σε in vivo πειράματα με μετέπειτα απομόνωση AMs σε διαφορετικά διαστήματα μετά από την ενδοτραχειακή λοίμωξη.

Στην συνέχεια, έχοντας χαρακτηρίσει τη συμπεριφορά (τροπισμό) του μύκητα για τα μακροφάγα, μελετήσαμε τους υποκείμενους υπεύθυνους μηχανισμούς που συντελούν στην μακροχρόνια « ενδοκυττάρια λαθροβίωση» των σπορίων. Γνωρίζουμε ήδη πως τα σπόρια του *A. fumigatus*, αφού φαγοκυτταρωθούν, υφίστανται εξοίδηση (swelling). Επακολούθως, η απομάκρυνση της μελανίνης του κυτταρικού τους τοιχώματος οδηγεί σε αποκάλυψη της β-γλυκάνης, που μέσω σύνδεσής της με την dectin-1, οδηγεί σε ενεργοποίηση του μονοπατιού της NADPH oxidase και τελικά την παραγωγή ριζών οξυγόνου (ROS), που τελικά συντελούν στην θανάτωση των σποριών (Εικόνα 1).

Στη συνέχεια, αναλύθηκε η σημασία της μακροχρόνιας ενδοκυττάριας επιβίωσης των σποριών Mucorales στη φυσική εξέλιξη της λοίμωξης. Χρησιμοποιώντας φυσιολογικά μοντέλα πνευμονικής λοίμωξης σε πειραματόζωα αποδείξαμε πως τα ποντίκια παρέμειναν ζωντανά μετά την ενδοτραχειακή λοίμωξη με σπόρια Mucorales. Παράλληλα, αφού τα ζώα θυσιάστηκαν 5 ημέρες μετά την λοίμωξη, βρήκαμε πως τα σπόρια του μύκητα παραμένουν ζωντανά μέσα στα μακροφάγα. Το παραπάνω εύρημα επιβεβαιώθηκε και σε ιστοπαθολογική ανάλυση βιοψιών από ασθενή με μουκορμύκωση.

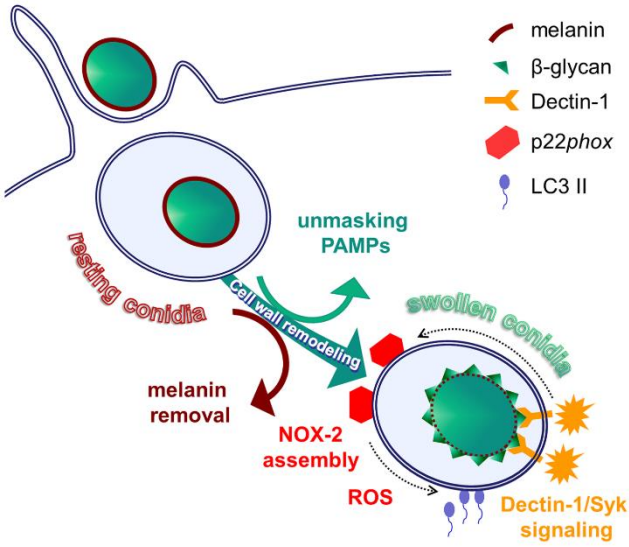

Εικόνα 1. Μοριακοί μηχανισμοί θανάτωσης του μύκητα *A.fumigatus* από τα φαγοκύτταρα (1).

Έπειτα, αφού επιβεβαιώσαμε την παρουσία μελανίνης στο κυτταρικό τοίχωμα των σποριών *Mucorales,* διατυπώσαμε την ερευνητική υπόθεση ότι η μελανίνη διαδραματίζει καταλυτικό ρόλο στην αναστολή της φαγολυσοσωμικής ένωσης. Παράλληλα μελετήσαμε ex vivo την μεταβολή του μεγέθους των σποριών *Mucorales* 1 ωρα και 24 ώρες μετά την φαγοκυττάρωση τους απο BMDMs σε σύγκριση με τα σπόρια *A.fumigatus* και παρατηρήσαμε πως τα σπόρια Mucorales δεν υπόκεινται σε ενδοκυττάρια εξοίδηση. Ως εκ τούτου συνάγεται το συμπέρασμα πως η αναστολή της ωριμάνσης του φαγοσώματος οφείλεται στο γεγονός οτι η μελανίνη παραμένει ανέπαφη στο κυτταρικό τοίχωμα των σποριών Mucorales μετά την φαγοκυττάρωση τους, σε αντίθεση με τα σπόρια *A. fumigatus*. Στην συνέχεια χρησιμοποιώντας σπόρια Mucorales από τα οποία είχε αφαιρεθεί χημικά η μελανίνη, μελετήσαμε την συγκέντρωση των πρωτεινών LC3 και Rab5 (δείκτες πρώιμων ενδοσωμάτων και λυσοσωμάτων αντίστοιχα) στα φαγοσώματα και παρατηρήσαμε πως αποκαθίσταται η ενεργοποίηση της ωρίμανσης του φαγοσώματος, γεγονός που αποδεικνύει τον καθοριστικό ρόλο της μελανίνης στο συγκεκριμένο μονοπάτι.

Μελετώντας περαιτέρω την φυσική εξέλιξη της πνευμονικής μουκορμύκωσης, αναζητήσαμε την κατηγορία φαγοκυττάρων που διαδραματίζει τον σημαντικότερο ρολο στην παθογενεση της λοίμωξη. Έπειτα από ενδοτραχειακή μόλυνση Β6 ποντικιών με σπόρια Mucorales, πάρθηκε βροχγοκυψελιδικό έκπλυμα (BAL). Χρησιμοποιώντας κυτταρομετρία ροής (FACS) και απομόνωση αμιγών κυτταρικών πληθυσμών διαφόρων φαγοκυττάρων του πνεύμονα (sorting) παρατηρήσαμε πως τα σπόρια Mucorales φαγοκυτταρώνονται κυρίως από τα κυψελιδικά μακροφάγα (AMs) (CD45+/CD11c+/MHC-II-low/F4/80+). Στην συνέχεια ακολούθησαν in vivo πειράματα, όπου μολύναμε ενδοτραχειακά ανοσοεπαρκή Β6 ποντίκια με σπόρια Mucorales και *A.fumigatus* και τα θυσιάσαμε 5 ημέρες αργότερα. Απομονώθηκαν οι πνεύμονες και τόσο με καλλιέργειες (CFUs) όσο και με ανοσοϊστοχημικές χρώσεις παρατηρήσαμε πως τα σπόρια Mucorales παρέμεναν ζωντανα μέσα στα AMs, σε αντίθεση με τα σπόρια *A.fumigatus*, που είχαν θανατωθεί. Στην συνέχεια, μολύνοντας ενδοτραχειακά με σπόρια Mucorales διαγονιδιακά CD11c-DTR ποντίκια, στα οποία μικρές συγκεντρώσεις τοξίνης της διφθερίτιδας προσδένονται εκλεκτικά στα κυψελιδικά μακροφάγα προκαλώντας την θανάτωσή τους, βρήκαμε πως στις 5 ημέρες μετά την μόλυνση με σπόρια Mucorales όλα τα CD11c-DTR ποντίκια απεβίωσαν, ενώ τα ανοσοεπαρκή Β6 ποντικια-μάρτυρες παρέμειναν ζωντανά και υγιή, καταδεικνύντας έτσι πως τα AMs αποτελούν τον ακρογωνιαίο λίθο της φυσικής ανοσίας απέναντι στα στελέχη Mucorales.

Τέλος, προσπαθήσαμε να συσχετίσουμε την ανοσολογική απάντηση με την χρήση του σιδήρου, που ως γνωστόν αποτελεί σημαντικό στοιχείο για την παθογένεση της λοίμωξης. Για τα πειράματά μας χρησιμοποιήσαμε BMDMs από GFP-LC3 ποντίκια, τα οποία μολύναμε για 30 λεπτά και 18 ωρες με ζωντανά σπόρια Mucorales. Το θρεπτικό υλικό εμπλουτίστηκε με τρισθενή σίδηρο ($FeCl_3$), δεφεροξαμίνη (σιδηροδεσμευτική πρωτεΐνη) ή τον συνδυασμό τους. Στις 18 ώρες

παρατηρήσαμε με το confocal μικροσκόπιο πως, ενώ στο control δείγμα (BMDMs - σπόρια Mucorales - standard θρεπτικό υλικό) τα σπόρια Mucorales παρέμειναν μέσα στα BMDMs χωρίς να έχει αλλάξει το μέγεθός τους, στα εμπλουτισμένα με τρισθενή σίδηρο και δεφεροξαμίνη δείγματα τα σπόρια Mucorales είχαν εξοιδηθεί (swollen) και σε πολλές περιπτώσεις είχαν προκαλέσει λύση των κυττάρων και εξωκυττάρια ανάπτυξη υφών. Ως εκ τούτου, καταφέραμε για πρώτη φορά να αποδείξουμε πως η ενδοκυττάρια στέρηση σιδήρου διαδραματίζει καταλυτικό ρόλο στην αναστολή ανάπτυξης του μύκητα από το μακροφάγο. Τα αποτελέσματα αυτά επιβεβαιώθηκαν περαιτέρω με RNAseq ανάλυση, όπου βρήκαμε πως μετά την φαγοκυττάρωση σποριων Mucorales από τα BMDMs, στον μεν ξενιστή ενεργοποιήθηκαν τα γονίδια που σχετίζονται με ομοιοστατικούς μηχανισμούς ενδοκυττάριας στέρησης σιδήρου, ενώ παράλληλα στον μύκητα αυξήθηκε η έκφραση των γονίδιων σχετιζόμενων με πρόσληψη σιδήρου.

Συζήτηση

Τα αποτελέσματα της μελέτης ρίχνουν φως στους μηχανισμούς μοριακής αλληλεπίδραση των μυκήτων Mucorales με τα μακροφάγα με σημαντικές προεκτάσεις στην παθογένεση της νόσου.

Δυο πολύ σημαντικά ευρήματα στην παθογένεση της νόσου προκύπτουν από τη μελέτη μας. Πρώτον, σε αντίθεση με όλους τους άλλους υφομύκητες οι Mucorales παρουσιάζουν μακροχρόνια ενδοκυττάρια λαθροβίωση στα μακροφάγα του πνεύμονα φυσιολογικών (μη ανοσοκατασταλμένων) ζώων. Η ικανότητα αυτή επιβεβαιώνεται και σε μεταγενέστερη μελέτη σε zebrafish (2). Αυτή η ανακάλυψη συνεπάγεται ότι, ενδεχομένως τα μακροφάγα να λειτουργούν σαν δούρειος ίππος της λοίμωξης και σε περίπτωση ανοσοκαταστολής η λοίμωξη να επέρχεται από την ενδοκυττάρια ανάπτυξη του μύκητα. Επιπλέον αυτό μπορεί να εξηγεί την αναζοπύρωση της λοίμωξης σε ανοσοκαταστολή, γεγονός που προκύπτει συχνά

στην κλινική πράξη, όπως στην περίπτωση του ασθενή της μελέτης μας. Αξίζει να αναφερθεί ότι πειραματικά μοντέλα αναζωπύρωσης μουκορμύκωσης μετά από ανοσοκαταστολή υπάρχουν ήδη από τη δεκαετία του 1960 χωρίς ωστόσο να είναι γνωστός ο μηχανισμός της λαθροβίωση. Τέλος, τα ευρήματα αυτά ίσως εξηγούν την αξιοσημείωτη αντοχή των Mucorales στην υπάρχουσα φαρμακευτική αγωγή, επειδή ενδεχομένως μέσα στο φαγόσωμα να μην είναι δυνατή η εκκρίζωση των σπορίων με τις υπάρχουσες θεραπείες.

Η μελέτη μας επίσης αναδεικνύει τον σημαντικό ρόλο της ανοσολογίας θρέψης στη φυσιολογική άμυνα των μακροφάγων και κατά συνέπεια των διαταραχών της στην παθογένεση της λοίμωξης. Στο σημείο αυτό ανοίγει ένα νέο κεφάλαιο στην ανοσοπαθογένεση αυτών των λοιμώξεων που αφορά την επίδραση του σιδήρου τόσο στην ανάπτυξη του παθογόνου όσο και στον μεταβολισμό και στη λειτουργία των μακροφάγων. Οι μοριακοί μηχανισμοί της ρύθμισης της άμυνας από το σίδηρο είναι ελάχιστα μελετημένοι και η κατανόηση τους θα οδηγήσει σε σημαντικές θεραπευτικές εφαρμογές.

Τα παραπάνω ευρήματα, που πρώτη φορά περιγράφονται στην βιβλιογραφία σχετικά με τον μύκητα Mucorales, ρίχουν φως στην παθογένεση της μουκορμύκωσης, που τα τελευταία χρόνια εχει αναδειχθεί σε σημαντική απείλή των ανοσοκατεσταλμένων ασθενών, και ανοίγουν τον δρόμο για την αναζήτηση νέων θεραπευτικών μέσων.

Μειονέκτημα της μελέτης μας είναι ότι δεν αποδείξαμε το ρόλο της διαταραχής της ανοσολογίας θρέψης στην αναζωπύρωση της λοίμωξης in vivo σε πειραματόζωα. Επιπλέον, το ότι η αναζωπύρωση της λοίμωξης ξεκινά από ενδοκυττάρια σπόρια παραμένει ακόμα υπόθεση. Τέλος η λειτουργία πολλών από τα μόρια που αναδείχθηκαν στην γονιδιωματική ανάλυση θα πρέπει να επιβεβαιωθούν με πειράματα εκλεκτικής γονιδιακής απαλοιφής σε μακροφάγα.

ABSTRACT

Introduction

Mucormycosis is an emerging fungal disease among immunocompromised patients with hematological malignancies, undergoing transplantations or chronic steroid treatment, associated with high mortality, which can reach up tp 90% in disseminated disease. Unlike other filamentous fungi Mucorales can infect patents with uncontrolled hyperglycemia, diabetic ketoacidosis and iron overload, as well as immunocompetent individuals suffering from severe burns or trauma. The epidemiology of mucormycosis is attributed to Mucorales unique virulent traits, regarding spores size, iron acquisition and angioinvasion. Several studies have shown that Mucorales is resistant to killing by phagocytes, without revealing the related mechanisms. The aim of this dissertation was to shed light in the mechanisms regarding the interaction of macrophages with Mucorales spores and address the role of iron in the pathogenesis of mucormycosis.

Materials and Methods

All animal studies were performed with GFP-LC3, C57BL/6 (B6) or CD11cDTR mice were maintained in grouped cages in a high-efficiency particulate air-filtered environmentally controlled virus-free facility.

Aspergillus fumigatus ATCC46645 and *Rhizopus* strains used (WT *R.oryzae* ATCC55796932; WT strain R. delemar 99-880) were grown on Yeast extract agar glucose agar plates. In addition, *Rhizopus* FTR1 and FOB1/2 mutants were delivered from the aforementioned *R.delemar* strain. Fungal melanin was extracted from *A. fumigatus* and *R. oryzae* conidia, which were treated with a combination of proteolytic and glycohydrolytic enzymes, denaturing guanidine thiocyanate, and hot

concentrated HCl. *Rhizopus* melanin was further characterized with liquid chromatography - mass spectrometry and electron paramagnetic resonance.

Bone marrow derived macrophages (BMDMs) were generated by culturing bone marrow cells obtained from 8- to 12-week-old female mice in culture medium supplemented with L929 cell-conditioned medium. For immunofluorescence experiments, BMDMs were stimulated with conidia of *Rhizopus* or *A. fumigatus* for the indicated time points. After infection, cells were fixed on the coverslips, which were then incubated with the indicated primary antibody (Ab), washed twice in PBS-BSA, then counterstained with the appropriate secondary Alexa Fluor secondary Ab. Images were acquired using a laser-scanning spectral confocal microscope (TCS SP2; Leica), LCS Lite software (Leica), and a ×40 Apochromat 1.25 NA oil objective using identical gain settings.

For the killing assays, 10^6 BMDMs were infected with either *R.oryzae* or *A. fumigatus* conidia, at an MOI of 1:1. At the indicated time point of infection (2 or 6 hours), BMDMs were lysed by sonication, centrifuged and the pellet containing intracellular conidia was resuspended in sterile PBS. *Aspergillus fumigatus* killing was assessed with confocal microscopy using propidium iodide staining, whereas killing of *R. oryzae* was assessed by photonic microscopy evaluating the germination of intracellular *Rhizopus* conidia.

For virulence studies, 8- to 12-week-old female mice were intratracheally infected with a standard dose of *A. fumigatus* or *Rhizopus* conidia and euthanized at the indicated time point. The lungs were homogenized, and CFU counts were assessed. For alveolar macrophages depletion studies, mice received by intratracheal administration 100 µl of clodronate liposomes or control liposomes. For CD11c cell depletion, CD11c-DTR mice received by intratracheal administration 20 ng/kg of diphtheria toxin (DT). The efficiency of cell depletion was assessed by

immunohistochemistry for CD11c and flow cytometry analysis of bronchoalveolar lavage.

For the histopathological studies, lungs were fixed in 10% formalin, paraffin embedded, cut in 4-μm sections, and stained with hematoxylin and eosin. For immunohistochemistry studies, the anti-CD11c Abs and anti-CD68 primary antibodies were used for detection of CD11c and CD68 in tissue.

RNA was isolated both from BMDMs and *R.oryzae* spores. Briefly, obtained from 12-week-old female C57BL/6 mice were infected with *R. delemar*. At the indicated time point of infection (1, 4, and 18 hours), BMDMs were lysed using the RNeasy Plant Mini Kit (Qiagen). Afterwards, isolation of RNAs was performed according to the manufacturer's instructions.

Results

In this study we showed that the alveolar macrophages play a predominant role during the host-*Rhizopus* interplay. *Rhizopus* conidia are phagocytosed by the alveolar macrophages of immunocompetent mice and establish prolonged intracellular dormancy, despite their in vitro vulnerability to the oxidative and non-oxidative killing mechanisms of the macrophages. Mechanistically, the resistance in killing is attributed to the melanin-induced phagosome maturation arrest. The alveolar macrophages selective depletion was associated with increased mortality and fungal burden in vivo experiments in immunocompetent mice, proving the essential role of macrophages on the natural course of mucormycosis. Furthermore, we discovered that inhibition of *Rhizopus* growth inside macrophages is a central host defense mechanism that depends on nutritional immunity via iron starvation. Finally, dual RNA sequencing (RNA-seq) and functional studies identify critical host and fungal modulators of iron homeostasis inside macrophages that promote invasive fungal growth.

Discussion

In this dissertation, we showed the essential role of macrophages for the outcome of mucormycosis. Furthermore, our experiments introduce the prolonged intracellular survival of the fungus inside these immune cells as a central pathogenetic event in development of the infection. In addition, we dissect the molecular mechanisms that allow *Rhizopus* to persist inside macrophages via melanin-induced phagosome maturation arrest. Finally, we identify nutritional immunity via iron restriction inside the phagosome as an important host defense mechanism during pulmonary mucormycosis. These findings lead to a novel pathogenetic model of mucormycosis that links abnormalities in iron metabolism with nutritional immunity inside macrophages, paving the way for important future therapeutic implications in the management of this devastating disease.

ABBREVIATIONS

AIDS	Acquired immunodeficiency syndrome
APCs	Antigen presenting cells
ATGs	Autophagy-related genes
BAL	Bronchoalveolar lavage
BCS	β-Citrylglutamate
BHB	β-hydroxy butyrate
BM	Bone marrow
BMDMs	Bone marrow derived macrophages
CFU	Colony-forming unit
CGD	Chronic granulomatous disease
CORVET	class C core vacuole/endosome tether complex
DCs	Dentritic cells
DFO	Deferoxamine
DHN	Dihydroxynaphthalene
DKA	Diabetic ketoacidosis
DMEM	Dulbecco's modified Eagle's medium
DT	Diphtheria toxin
EEA1	Early endosomal antigen 1
EEA1	Early endosome antigen 1
EPR	Electron paramagnetic resonance
FCS	Fetal calf serum
FcγRs	Fcgamma receptors
FITC	Fluorescein isothiocyanate-labeled
FTR1	High affinity iron permease gene

GM-CSF	Granulocyte-macrophage colony stimulating factor
GRP78	Endothelial cell glucose-regulated protein 78
HPLC	High Performance Liquid Chromatography
IACUC	Institutional Animal Care and Use Committee
IFN-γ	Interferon-γ
IL-12	Interkeukin-12
IL-2	Interkeukin-2
IMs	Interstitial macrophages
iNOS	Inducible nitric oxide synthase
IR	Infrared spectroscopy
LAMP-1	Lysosome-associated membrane protein 1
LAMP-1	Lysosome-associated membrane proteins 1
LAMP-2	Lysosome-associated membrane protein 2
LAP	LC3-assosiated phagocytosis
LAPosome	LC3+ phagosome
LC3	Microtubule-associated protein 1A/1B-light chain 3
LC-MS	Liquid chromatography with mass spectrometry
l-dopa	l-3,4-dihydroxyphenylalanine
MHC I	Major histocompatibility complex I
MOI	Multiple of infection
NADPH oxidase	Nicotinamide adenine dinucleotide phosphate oxidase
NETs	Neutrophil extracellular traps
NK cells	Natural killer cells
PAMPs	Pathogen-associated molecular patterns
PBS	Phosphate-buffered saline
PE	Phosphatidyl ethanolamine

PE	Phosphatidylethanolamine
PI(3)K	Phosphatidylinositol (PI) 3-kinases
PI	Propidium iodide
PI3P	Phosphatidylinositol-3-phosphate
P–L fusion	Phagolysosomal fusion
PMNs	Polymorphonuclear neutrophils
PRRs	Pattern recognition receptors
RBCs	Red blood cells
RNA	Ribonucleic acid
RNAi	RNA interference
ROS	Reactive oxygen species
ROS	Reactive oxygen species
SCB	Sodium cacodylate buffer
SD	Synthetic defined medium
SDS	Sodium dodecyl sulfate
Syk	Spleen tyrosine kinase
TCRs	T-cell receptors
TGF-β	Tumor growth factor- β
Th1	T-helper 1 cells
Th17	T-helper 17
Th2	T-helper 2
TLR	Toll-like receptor ligands
TNF	Tumor necrosis factor
Treg	T-regulatory cells
ULK	Unc-51-like kinase
ULK	Unc-51-like kinase

UV	Ultraviolet
v-ATPase	Vacuolar ATPase
Vps34	Vacuolar protein-sorting 34
WT	Wild type
XTT	(2,3)-bis (2-methoxy 4-nitro 5-sulfenyl)-2H-tetrazolium carboxanilide
YNB	Yeast nitrogen base

A. INTRODUCTION

A1. The Tree of Life

A fundamental breakthrough in Evolutionary Biology and Science in general occurred in 1977, with the work of Woese and Fox containing a single table with the first gene sequence-based quantitative assessment of phylogenetic relationships between representatives of the major known kinds of organisms (3). Based on analyses of genes coding for the production of ribosomal RNA, it was shown that all cellular life is categorized into three large groups: eukaryotes (cells with a nuclear envelope), eubacteria and archaebacteria (Figure 1).

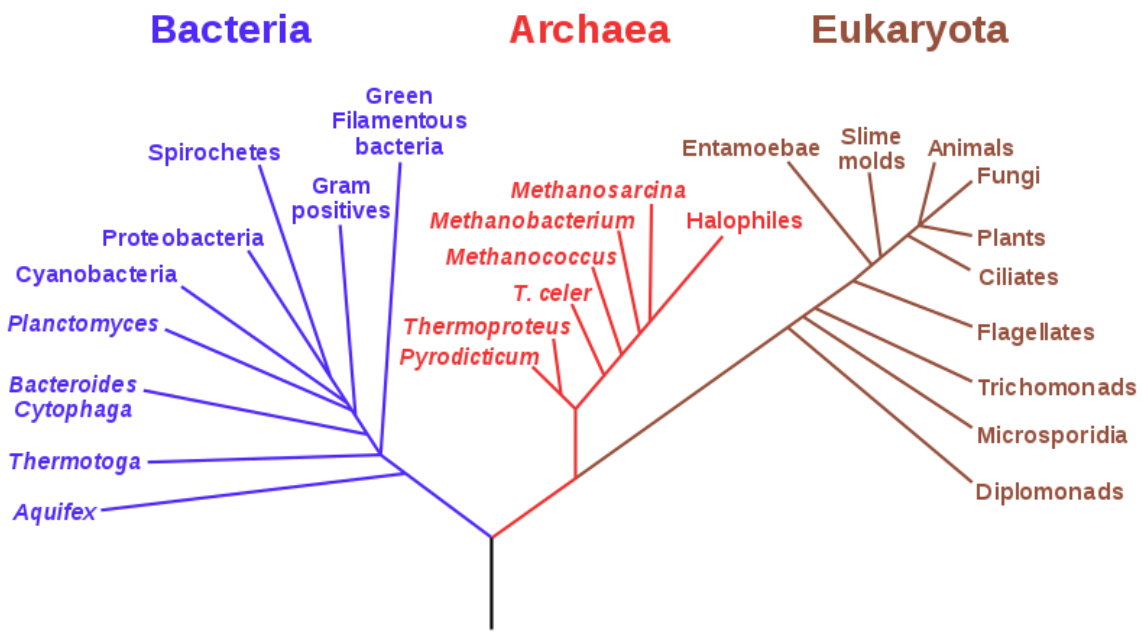

Figure 1: The phylogenetic Tree of Life (credit: modification of work by Eric Gaba)

The animals, plants and fungi, which are placed on the top of the Eucarya Domain, is believed to have diverged at approximately the same period, around half a billion

years ago. Based on fossils it is estimated that the first fungal species are dated in the Ordovician period, between 460 and 455 million years ago (4). Since then a major expansion and diversification has occurred, so that today about 90000 fungal species have been described and due to the increasing use of molecular techniques circa 1,800 new species are found per year, with the total number of fungal species estimated at 3.8 million (5) (6).

A2. The fungi

The fungi are eukaryotic organisms, which can be found in the ground, the air and the water, growing as a parasite of another living organism, as a pathogen causing disease to the host (termed mycosis), as a symbiont in association with another organism and finally as a saprophyte on nonliving materials. Their nutrition depends on pre-formed organic compounds; therefore they are included to the heterotrophic organisms.

Numerous fungi are adapted to grow as parasites of many different hosts, including plants, insects (entomopathogens), nematodes (nematophagous fungi) and other fungi (mycoparasites). The tissues of the host serve as the nutrient tank, from which the fungi obtain the necessary nutrients, without killing the host organism. It is reported that some fungi can infect only one type of host, and the association is occasionally so specific that they can grow only in the host tissues and not in laboratory cultures, making their study even more difficult. The most typical representatives of this kind of fungi are the rust fungi, the powdery mildew fungi and the plasmodiophorids (4).

The number of fungi that cause disease to plants, animals and humans is much smaller. Among humans the most common and relatively benign infection is caused by the dermatophytic fungi, impairing the skin, nails, and hair. The situation changes

dramatically among immunocompromised patients (with AIDS, transplant recipients, patients with hematological malignancies or sold tumors, patients with uncontrolled Diabetes mellitus or under prolonged corticosteroid treatment), who are endangered of life-threatening fungal infections, from fungal species, that to are no threat to healthy individuals (2).

As far as the symbiotic associations of fungi is concerned, the most common examples are two types of plants, lichens and mycorrhizas. Despite the differences between these two plant types, there is a common rule; the fungus supports and protects the photosynthetic plant cells, absorbing mineral nutrients from the environment, while the plant serves as a source of carbon nutrients for the fungus. Lichens and mycorrhizas are not the only examples of symbiosis. Additionally, the fungi are associated with the activations of plant genes responsible for the defense against insects and environmental toxins (2).

Fungi play also an important role as saprophytes, since they are capable to produce a wide range of degrading enzymes against complex polymers such as cellulose (the most abundant natural polymer on Earth and the main plant cell wall component) proteins, chitin, keratin and even large scale materials such wood. Each species has different decomposer capabilities and it is not unusual to find many fungal saprotrophs growing on a single plant or material.

Moreover, the fungal metabolites are the cornerstone in the production process of many foods, beverages and alcoholic drinks. Their pharmaceutical applications are of most importance, since their secondary metabolites are the basis of numerous of medications. The most characteristic example is the discovery of penicillin, produced by *Penicillium chrysogenum*, discovered in 1928 by the Scottish scientist Alexander Fleming, changing the route of human history (2).

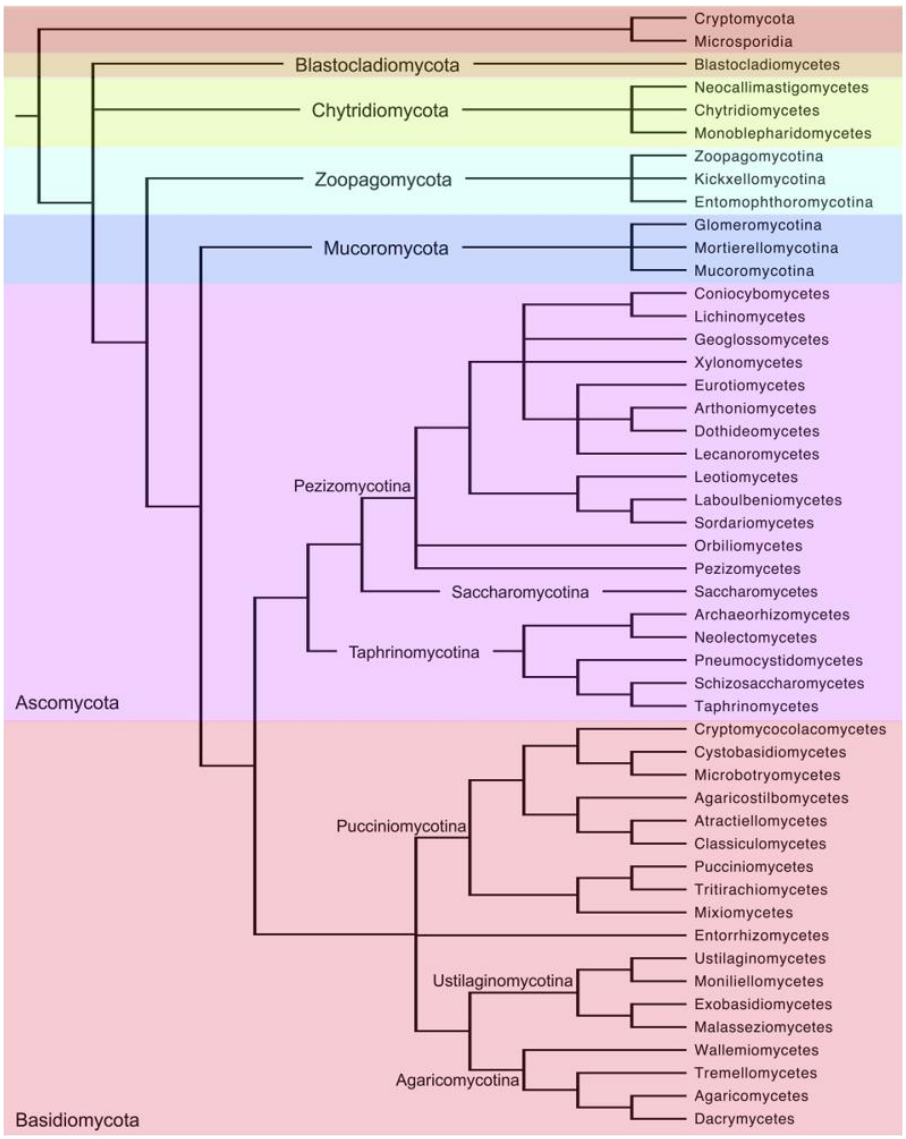

Figure 2. The fungal Tree of Life [Adopted from Ref. (7)]

According to a recent publication, the classification of the kingdom Fungi recognizes eight phyla (Figure 2), defined by morphological traits, reproduction forms and the results from the latest sequencing analysis using molecular and genome technologies (7).

Fungi reproduce sexually and asexually. There are several forms of asexual reproduction. The most common is the spore production through mitosis and cell division. Depending on the specific way of spore formation, numerous types have

been reported; arthrospores (produced from splitting of hyphae), chlamydospores (spores enclosed in a thick wall before separation), sporangiospores (spores are found in a sac at a hyphal tip), conidiospores (spores formed at the hyphal tips or sides) and blastospores (produced by budding from a mother cell) (Figure 3). The sexual reproduction involves the fusion of two compatible sex cells or gametes of opposite or same-sex mating types.

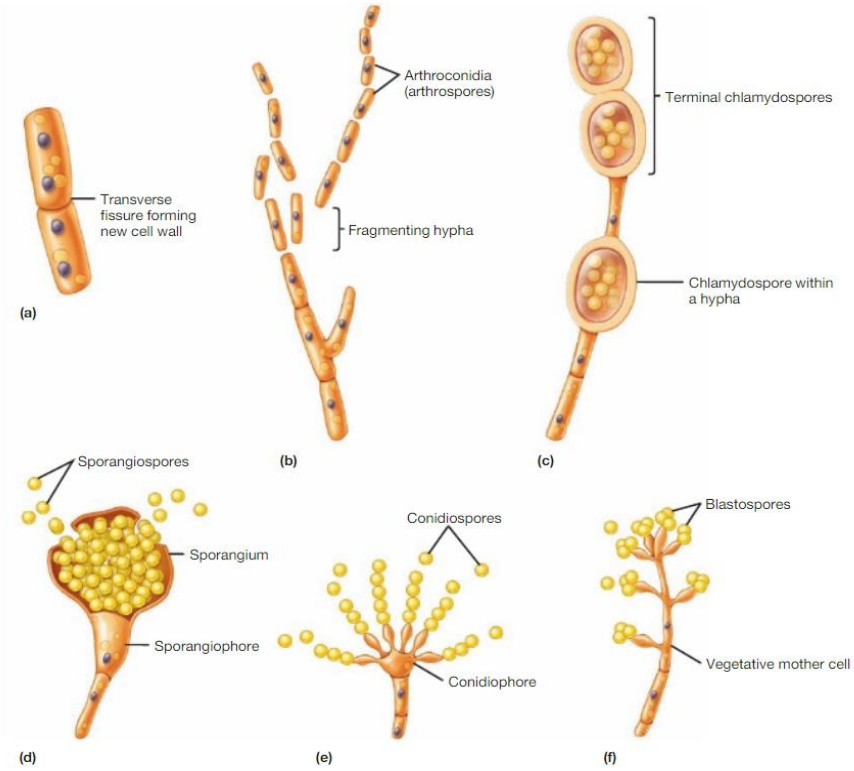

Figure 3: Types of asexual reproduction in the fungi (a) Transverse fission (b) Arthrospores (c) Chlamydospores (d) Sporangiospores in asporangium (e) Conidiospores at the end of a conidiophor (f) Blastospores [Adopted from Ref. (8)]

The fungus species may be homothallic or heterothallic, using gametes from the same or different (but sexually compatible) mycelium respectively. Three phases are reported; plasmogamy (in which a cell with two separated nuclei is formed, called

dikaryon), karyogamy (when the nuclei fusion occurs) and meiosis, with the final production of genetically different spores. Fungal spores are of outmost importance not only for the fungal survival against environmental stresses but also for the fungal dissemination, since they are able to spread through the air and adhere on various surfaces and bodies, surviving in a dormant state for long period of time (8).

Fungal cell wall is a unique form, consisting of a cross-linked network of components, which including chitin and glucans (polymers of glucose with predominantly β-1,3 and β-1,6 linkages), other polysaccharides, and glycoproteins. A great cell variability in the composition of the cell wall has been reported between different fungal species, mainly regulated by the environmental changes. This characteristic in combination with the great chemical adaptation serves as an important defense mechanism against the host immune system (9). Moreover, the fungal cell wall possesses various important roles in fungal viability and pathogenesis, including the maintenance of the morphology and integrity of developing fungal cells; a rapid generation and shape adaption in order to support the penetration of the environment and the protection against environmental stresses (10).

The body of a fungus is called a thallus, which has a great variety among the fungal species concerning its complexity and size, ranging from the mono- to multicellular fungi, macroscopic puffballs and mushrooms.

The majority of fungi are molds. Their thallus is a long apical filament, which is called hypha and contains a full spectrum of organelles, that are also found in many eukaryotic cells (e.g. mitochondria, endoplasmic reticulum, Golgi apparatus, endosomal vacuoles, vesicles). The hyphae usually gather together forming a mass, called mycelium. Moreover, the majority of hyphae is multinucleate, producing septa (cross walls), that facilitate cytoplasmic streaming. Different types of hyphae present distinct combinations of behavioral, structural and functional characteristics,

but in general this fungal type is characterized by an exceptional plasticity and flexibility, allowing them to form colonies, invade to the environment or host, defend against the host immune system by a rapid and massive production of enzymes and communicate through a long-distance signaling (8, 10).

Yeasts are typically a uninucleate single cells, principally larger than bacteria, with a wide range of size. They reproduce either asexually by budding or by binary fission or sexually resulting to spore formation. Despite the limited plasticity and adaptation capability compared to hyphae, they have the ability to reproduce rapid in nutrient-rich and aqueous environments, being a major threat for severe bloodstream infections in immunocompromised hosts. Many important fungal pathogens such as *Candida, Cryptococcus* and *Histoplasma* can produce yeast cells (8, 10).

It is to mention that numerous fungal species, especially the pathogenic ones, are dimorphic. Depending on the environmental conditions and nutritional adequacy these fungi are capable of changing from the yeast form in the animal to the mold or mycelial form in the external environment (8).

Many fungi have evolved a selective advantage to release their spores into the air for dispersal (Table 1) (11, 12). The last decades, the great progress on the treatment of hematological and solid tumors, as well as the increase of transplantations and the broad use of potent immunosuppressive therapy in many different patient groups led to a significantly higher number of immunosuppressed patients. The airborne fungi have become a great threat for those individuals, causing opportunistic infections with a high morbidity and mortality (13). Historically, *Aspergillus* spp. and *Candida* spp. collectively account for the majority of deeply invasive and life-threatening fungal infections (14). However, during the last decades an epidemiological shift towards infections by *Aspergillus* spp., nonalbicans *Candida* spp., as well as previously uncommon opportunistic fungi, such as *Trichosporon beigelii*, *Fusarium* spp. Mucorales and *Penicillium mamefei* is reported (15). The incidence of fungal

infections in patients with hematological malignancies is increasing. Moreover, due to the low sensitivity of microbiological culture techniques and the low specificity of radiological procedures, particularly in neutropenic patients, the diagnosis of the invasive opportunistic fungal infections remains challenging, a fact confirmed by a recent study with retrospective autopsy data, which showed that approximately 75% of such infections are not diagnosed prior to death (16, 17). The late diagnosis as wells as the limited therapeutic options contributed to the high mortality rates. However, the pathogenic mechanisms leading to these life-threatening infections remain relatively unexplored.

Absidia corymbifera	*Paecilomyces variotii*
Alternaria citri	*Penicillium brevicompactum*
Aspergillus candidus	*P. chrysogenum*
A. flavus	*P. citrinum*
A. fumigatus	*P. corylophilum*
A. niger	*P. expansum*
A. ochraceus	*P. frequentans*
A. restrictus	*P. griseofulvum*
A. sydowii	*P. spinulosum*
A. terreus	*Phoma herbarum*
A. versicolor	*Rhizopus microsporus*
A. wentii	*R. stolonifer*
Cladosporium cladosporioides	*R. oryzae*
Cladosporium sphaerospermum	*Scopulariopsis brevicaulis*
Eurotium[a] *amstelodami*	*Sistotrema brinkmannii*
Eurotium chevalieri	*Stachybotrys chartarum*
Emericella[a] *nidulans*	*Syncephalastrum racemosum*
Fusarium moniliforme	*Trichoderma harzianum*
Geomyces pannorum	*Wallemia sebi*
Mucor circinelloides	*Ulocladium chartarum*
M. plumbeus	*U. consortiale*

Table 1. List of the most common airborne fungi {adapted from (12) and modified}

A2.1. Zygomycetes

Zygomycetes is one of the two classes of the phylum formerly described as Zygomycota, further distributed over nine orders. Based on gene sequencing analysis and well preserved fossils the estimated divergence time of the zygomycetes on Earth is placed in the Precambrian era, ~ 1200–1400 million years ago, being an essential component of the ancient ecosystems. Since then, they managed to adapt prompt, adopting all types of nutrition, from saprophytic to parasitic end endophytic in plants, ultimately evolving to an important group of opportunistic and usually life-threatening human pathogens (18, 19). They possess four general characteristics; their cell walls are made of a mixture of chitin, chitosan and polyglucuronic acid; the hyphae are typically aseptate (without cross walls), also called coenocytic; they can reproduce either sexually forming a thick-walled resting spore, called zygospore, or asexually, that result to the production of spores by cytoplasmic cleavage within a sporangium; they have an haploid genome (4).

A2.2. Mucorales species

Mucorales have been recently reclassified into the subphylum Mucoromycotina of the Glomeromycota phylum of the Fungal Kingdom (20). Many Mucorales species account for some of the first appeared on Earth and most widespread terrestrial fungal lineages. They are can be found everywhere in nature and they grow rapid within 24-48 hours in an agar plate. They distinguish with their aseptate hyaline hyphae, the sexual formation of zygospores and the asexual reproduction with nonmotile sporangiospores, on which the dissemination is based, since the asexual reproduction of Mucorales occurs very fast (Figure 4) (4). The thalli of the

Mucorales consist of substrate mycelium, which develops rapidly to grow aerial hyphae, which is their main transmission way. Sporangia form at the pear – shaped sporangiophore apex a visible, well-shaped columella, which is the trademark of the Mucorales as a monophyletic order (18).

Mucorales embraces various species, which are potentially pathogenic to humans, causing an infection called mucormycosis, affecting primarily immunocompromised individuals. The last decades an increased incidence of mucormycosis is reported, being the third most common invasive fungal infection after candidiasis and aspergillosis (21). The predisposing factors for mucormycosis are hematological malignancies, chronic high-dose corticosteroid treatment, hemopoietic stem cells and solid organ transplantations, uncontrolled hyperglycemia, diabetic ketoacidosis and iron overload (due to multiple blood products transfusions in patients with thalassemias or leukemic states and patients under hemodialysis) (22). Nevertheless, because Mucorales can be found anywhere and also in decaying organic substrates, many causes of mucormycosis are reported, even in immunocompetent adults, after major natural disasters; from wound to pulmonary infections, caused also from unusual species (23, 24). The most common among them are the species *of Rhizopus, Lichtheimia, Mucor, Rhizomucor, Apophysomyces, Saksenaea, Syncephalastrum* and *Cunninghamella* (19).

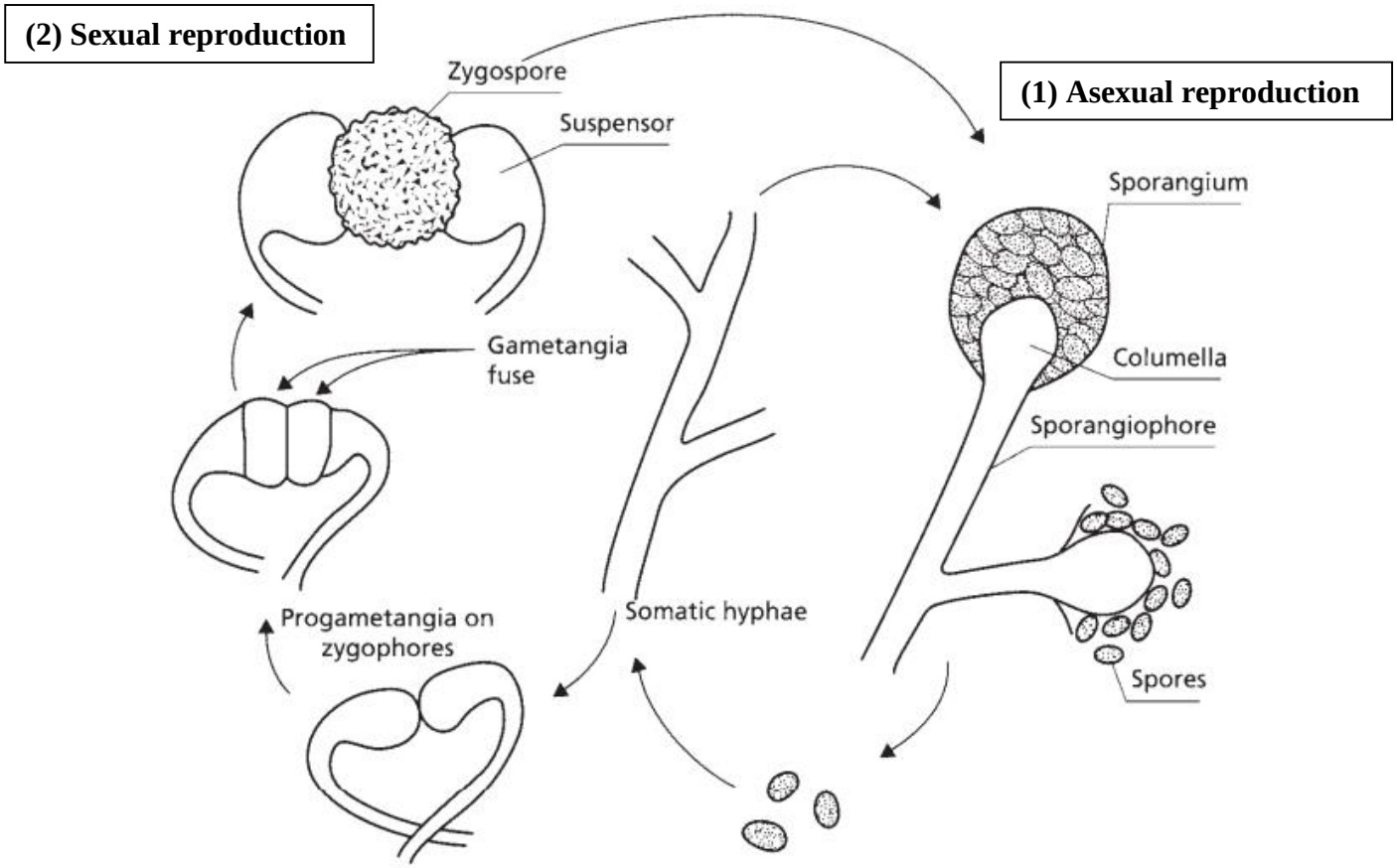

Figure 4. The life cycle Mucorales. (1) Asexual reproduction. The somatic growth of hyphae is followed by the production of aerial branches (sporangiophores). After that a thin-walled sporangium is formed at the pear-shaped tip and the sporangial contents split in order to produce many darkly pigmented uninucleate spores (sporangiospores). The released spores are wind-dispersed after the collapse of the thin sporangial wall. The species' trademark, columella, remains after the spores' dispersal. (2) Sexual reproduction. Under ideal culture conditions compatible mating aerial branches, termed zygophores, grow towards one another to form progametangia. Soon after a complete septum is developed by the latter, separating each gametangium from the subtending hypha. A thick-walled zygospore is then formed from the fusion of gametangia. After a small period of dormancy, the zygospores eventually germinate to produce a sporangium, releasing haploid spores. [Adopted from Ref. (4) and modified]

A2.3. Rhizopus spp. and their unique virulent factors

The predominant human pathogen of the Mucorales is *R. oryzae*, responsible for approximately 70% of all cases of mucormycosis (25). *Rhizopus delemar* and *Rhizopus stolonifer* are less common *Rhizopus* species, also causing opportunistic infections. *R. oryzae* is also found as *R. arrhizus* in the medical literature. It is characterized by a rapid growth, ideal at around 37°C, on standard media, producing dark brown or gray colonies. Microscopically, *R. oryzae* is identified by the presence of broad nonseptate root-like hyphae having four to eight branches, called rhizoids. Sporangiophores can be seen solitary or in clusters, with a length ranging from 750 to 2,000 μm (generally 1,500 μm) and they are usually unbranched. At the tip of the sporangiophores are found round, grayish black sporangia measuring 40 to 350 μm in diameter. The columella of *R. oryzae* is lightly pigmented gray and ellipsoidal to hemispherical in shape. Typically, a great amount of sporangiospores is produced, which are round to ovoid in shape, dark in color and their length is up to 8 μm. The zygospores, which are produced heterothallically range from 80 to 100 μm and are also dark in colour (26-28). Dormant spores are able to endure extreme climate conditions, as proved from the viable spores found both in arctic and desert climates. The transmission of *R. oryzae* is primarily airborne, causing opportunistic rhinocerebral and pulmonary mucormycosis in immunocompromised patients suffering from hematological malignancies, uncontrolled Diabetes mellitus, transplant recipients or patients long treated with corticosteroids. Due to the rapid fungal proliferation the mortality rate can reach up to 100% in disseminated disease. A highly suspicion is the key to a quick diagnosis. The cornerstone of treatment is the control of precipitating factors, surgical debridement and appropriate antifungal therapy (21, 25, 29). As far as the antifungal treatment is concerned, our armamentarium is limited, since only Amphotericin B and two triazoles,

posaconazole and isavuconzole, are approved for the management of mucormycosis (23). Less common transmission routes through the disruption of the mucocutaneous barrier are the percutaneous, gastrointestinal and oral, causing infections even in immunocompetent individuals (21, 26).

R. oryzae has some unique characteristics, that attribute as virulence factors in the process of host invasion and penetration, overcome of the host's immune system, leading ultimately to his survival and reproduction. In contrast to other molds like *Aspergillu*s spp., it was early observed that patients with iron overload (such as patients under dialysis or need of frequent blood transfusions), treated with an iron chelator called deferoxamine, were much more susceptible to mucormycosis (30, 31). In addition, the importance of iron metabolism in the pathogenesis of *R.oryzae* was highlighted in vitro experiments in the papers of Diamond et al (32, 33). Therefore, it is no surprise that *R.oryzae* possesses various receptors related to iron accumulation (34). A high-affinity iron permease (FTR1), encoded especially iron-depleted environments, plays an important role in iron uptake and transport. A reduced virulence and iron accumulation after the knock-down of FTR1 has been reported (35). It is of interest that passive immunization of infected mice with diabetic ketoacidosis (DKA) with anti-FTR1protein reduced the mortality rate, setting the basis for new therapeutic perspectives (36). Fob1 and Fob2 are two highly preserved receptors on the surface of the Mucorales, necessary for the binding of ferrioxamine. After the binding of the ferrioxamine/iron complex, iron is detached and transported into the fungal cell, without internalizing the siderophore (37). Besides iron accumulation, the ability of *R.oryzae* to invade vessels and endothelia is of outmost importance for the fungal pathogenicity. The angioinvasion is mediated through the binding of the spore coat (CotH) proteins to the endothelial cell glucose-regulated protein 78 (GRP78), which partially explains the susceptibility of patients

with DKA, who overexpress GRP78. In addition *R.oryzae* mutants with reduced CotH expression were less virulent in mouse models with DKA (38).

The discovery of rhixotoxin, a plant mycotoxin produced by bacterial endosymbiont (*Burkholderia*) from environmental isolates of *Rhizopus*, which let to plant destruction by inhibition of mitosis and cell cycle arrest, thought to be a new virulent factor from Rhizopus. However, following studies showed that the virulence of Rhizopus was independent from the bacterial endosymbionts (39-41).

A2.4. The pathogenesis of pulmonary mucormycosis

Mucormycosis is the second most common fungal infection, after candidiasis and aspergillosis, among immunocompromised patients. Initially mucormycosis has been described mostly in diabetic patients, but the last decades, due to the tremendous improvement in the diagnosis and treatment of hematological malignancies and autoimmune diseases, as well as the increase of transplantations (both from hemopoioetic stem cells and solid organs), the incidence of the infection is steadily rising, estimated approximately in 1.7 cases per 1000 000 inhabitants per year (21, 29). Pulmonary mucormycosis accounts for 20% of the total mucormycosis cases with the overall mortality reaching the 51% of the patients, according to a recently published meta-analysis (42). The infection is caused after the inhalation of airborne spores by patients with predisposing factors, as mentioned above. As the spores reach the lungs, they meet the first line of defense, the phagocytes. In healthy individuals, macrophages and polymorphonuclear neutrophils (PMNs) eliminate the Mucorales spores through oxidative and non-oxidative mechanisms, preventing the infection. In patients with severe neutropenia, hyperglycemia or undergoing corticosteroid treatment, the acquisition of phagocytes as well as their major killing

mechanisms are severely impaired, so that the proliferation of Mucorales cannot be restrained. The spores find themselves in an abundance of nutritional substances and the proliferate forming hyphae.

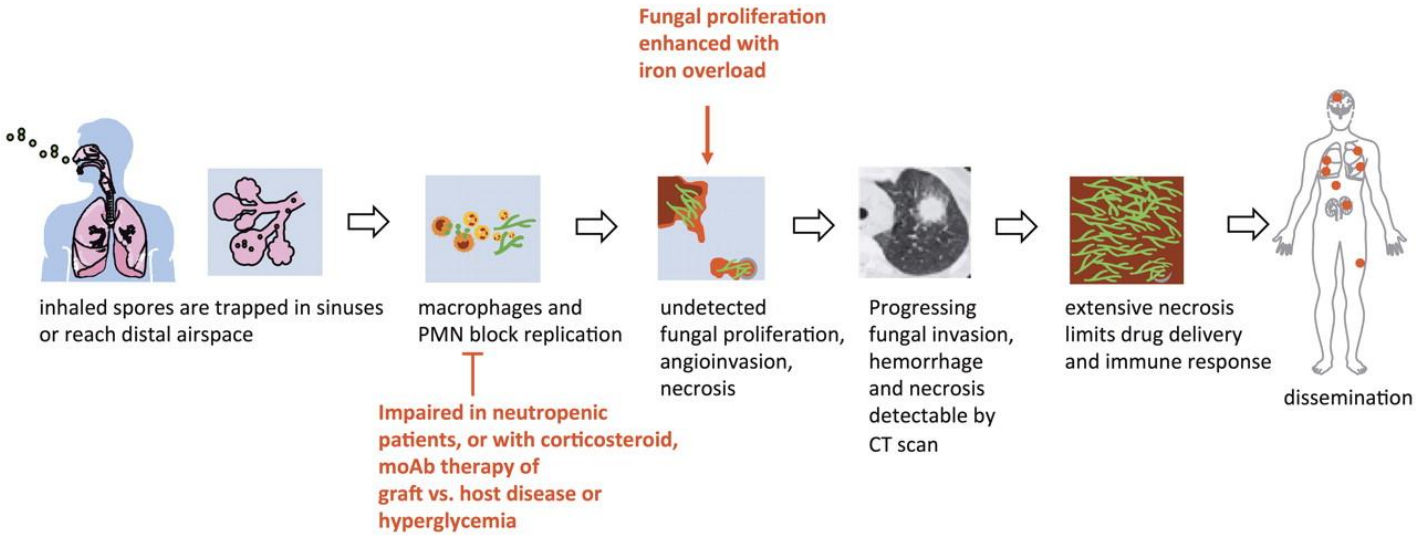

Figure 5. The pathogenesis of mucormycosis. Neutropenia, hyperglycemia and corticosteroids lead to impaired chemotaxis, phagocytosis and oxidative burst. The additional iron abundance in serum induces the Mucorales proliferation and subsequent endothelial damage and angioinvasion. The extensive vessel necrosis further restricts the immune responses and drug delivery, resulting to a disseminated infection with remarkably high mortality [Adopted from Ref. (22)]

The high concentration of iron in serum, as observed in DKA, since the acidic pH results to dissociation of free iron from bound proteins enhances the fungal pathogenicity. The hyphae adhere to the endothelial cells, causing a critical endothelial damage, which leads to angioinvasion, vessel thrombosis, consecutive tissue necrosis and ultimately to disseminated mucormycosis (22, 25, 29, 43, 44). A schematic figure of the pathogenesis of mucormycosis is shown on figure 5.

A3. An overview of the immune response to infections

The immune system is responsible for the prevention and management of infections. It is divided into two big categories, the innate and adaptive immunity. The innate immunity is the first line of defence, with circulating and scattered tissue cells, that recognize the invaders. Through a signalling cascade the adaptive immunity is activated. The adaptive immunity is the sophisticated branch of the immune system, pledged with the coordination and expansion of specific cells, that produce pathogen-specific proteins, called antibodies, that recognize unique proteins of each pathogen, leading to its death and ultimately to the restriction of the infection. Furthermore, the adaptive immune response is followed by the production of pathogen – specific memory cells, that guarantee the rapid reaction of the immune system in case of a future reinfection.

The immune responses are mediated by leukocytes, which differ from the majority of other cells, since they are motile, interact with pathogens and cellular debris and coordinate the inflammation. The leukocytes derive from a multipotent haemopoietic stem cells in the bone marrow. The innate leukocytes encompass the natural killer cells (NK cells), the mast cells, the eosinophils, the basophils and the phagocytic cells, which are the monocytes, the macrophages, the dendritic cells and the neutrophils (45). The NK cells are responsible for the recognition and destruction of compromised host cells, typically tumor cells and virus/infected cells, that lack the normal amount major histocompatibility complex I (MHC I) on their cell membrane. The mast cells are found in connective tissue and in the mucous membranes, mostly associated with allergy by releasing histamine. The basophils and eosinophils are granulocytes, which play a central role in the management of parasitic infection and allergic reactions (45).

The professional phagocytes orchestrate the pathogen recognition, phagocytosis, antigen-presentation and - through a signaling cascade – activation of the adaptive immunity. In addition, they maintain a key role to wound healing and tissue development, by removing the apoptotic cells or the pathogen-infected cells from the affected sites. The aforementioned functions are mediated through receptors, named pattern recognition receptors (PRRs), which recognize molecules typical for pathogens but absent on the host cells, referred to as pathogen-associated molecular patterns (PAMPs). As soon as a PRR recognizes a PAMP, inflammation mediators are released. As soon as phagocytosis occurs, the engulfed pathogen is enclosed in a phagosome and through a signaling cascade inside the cell, it is finally fused with lysosomes, organelles that excrete lytic enzymes, causing the pathogen degradation (46).

Monocytes circulate in the bloodstream for about 28 to 72 hours, equipped with chemokine receptors and PRRs. They produce inflammatory cytokines, such as tumor necrosis factor (TNF) and inducible nitric oxide synthase (iNOS), and upon inflammation, they migrate into the tissues, where they differentiate into macrophages and dendritic cells (45, 47). Dendritic cells lurk in peripheral tissues as immature phagocytes. Upon infection they ingest pathogens, present antigens on their surface and them they migrate to the draining lymph nodes, where they activate the adaptive immunity, stimulating the T-cells (48).

Neutrophils, which are also known as polymorphonuclear leukocytes due to their distinctive lobed nuclei, are of paramount importance for the inflammatory response. Every day approximately 10^{11} cells are produced in the bone marrow and then enter the circulation. Upon threat recognition they migrate to tissues to kill the invading pathogens. Their main functions are phagocytosis, degranulation, and the release of nuclear material in the form of neutrophil extracellular traps (NETs), which serve not only the microcode but also contribute to the pathogenesis of autoimmune

diseases, cancer and atherosclerosis. Upon phagocytosis neutrophils undergo respiratory burst producing reactive oxygen intermediates (ROIs), including hydrogen peroxide, free oxygen radicals and hypochlorite, which is the main mechanism for killing the phagocytosed pathogens. Additionally, neutrophils orchestrate the immune response by producing various cytokines such as TNF and interferon-γ, leading to attraction of monocytes and DCs inflammatory sites as well as differentiation of macrophages to a pro- or anti-inflammatory state. Additionally, neutrophils play an important role on proliferation and activation of B- an T-cells, as well as suppression of T-cells, which are of great importance for the pathogenesis of cancer (49, 50).

The adaptive immunity consists of two big cellular subsets, the T lymphocytes, which mediate the immune responses and the B lymphocytes, which produce pathogen- and cell-specific antibodies. Both T- and B- cells are produced in the bone marrow from a common progenitor stem cell and until their activation are morphologically indistinguishable. Lymphocytes are mobile and migrate from the primary lymphoid organs (thymus and bone marrow) to the secondary ones (lymph nodes and the spleen), where they are activated either from the antigen presenting cells (APCs) or the innate immune stimuli (51).

Mature T-cells are divided into two subgroups, CD8+ (cytotoxic) and CD4+ (T-helper) cells. They are activated upon interaction of their T-cell receptors (TCRs) with antigenic peptides bond with MHC class I and II respectively. CD4+ cells are divides into four categories; T-helper 1(Th1), T-helper 2 (Th2), T-helper 17 (Th17) and T-regulatory (Treg) cells, depending on cytokine production and function. Th1 cells facilitate the host defense against intracellular pathogens and fungi, by mainly producing IFNγ, lymphotoxin α, interkeukin-2 (IL-2) and interkeukin-12 (IL-12). The IFNγ secretion by Th1 cells lead to M1 macrophage activation, thus IL-12 has a key role for the immune responses against fungi. In addition, Th1 cells activation

and uncontrolled activity is related with the pathogenesis of various autoimmune diseases, including rheumatoid arthritis and multiple sclerosis. The immune response against extracellular parasites is mediated by Th2 cells, which produce various interleukins (IL-4, IL-5, IL-9, IL-10, IL-13, IL-25), and amphiregulin. Furthermore, Th2 cells through IL-4 secretion and the consequent IgE class switching in B cells are the cornerstone in the pathogenesis of asthma and allergic diseases. Among others, they favor the M2 macrophage polarization. Th17 cells mediate immune responses against extracellular bacteria and fungi, producing IL-17a, IL-17f, IL-21, and IL-22, that leads to stimulation of CD8 T cells, B cells, NK and dendritic cells, as well as PMNs activation. Treg cells guarantee the homeostasis, since they are responsible for the regulation and suppression of the immune responses, though the production of tumor growth factor- β (TGF-β), IL-10, and IL-35 (51-53).

The B-cells mediate the humoral immunity. Responding to cytokines from T-cells and APCs, B-cells are activated and either mature into plasma cells, producing antibodies or transform into memory cells, for a rapid immune response when the host has to encounter the same pathogen in the future. Many B-cells subsets are described, depending on their surface marker expression and their developmental stage. Furthermore, B-cells produce cytokines, like IL-2, TNF and IFN-γ, promoting the responses of memory Th2 and Th1 respectively. The production of IL-10 or IL-35 leads to negative regulation of immune responses in many bacterial infections and autoimmune diseases, mediated by Th1, Th2 and Th17 cells, such as experimental autoimmune encephalitis, systemic lupus erythematosus, ulcerative colitis and infection from *Listeria monocytogenes* (51, 54).

A3.1. Immune responses against fungal infections

The key phagocytes that mediate fungal killing are neutrophils and macrophages. The increased incidence of fungal infections among patients with neutropenia or impaired monocyte function (like those suffering from chronic granulomatous disease) indicates the outmost importance of these immune cells. Phagocytic clearance of fungal pathogens is mediated through the recognition of cell-wall fungal-specific PAMPs by PRRs of phagocytes, including Toll-like receptors (TLRs), C-type lectin receptors (CLRs) and NOD-like receptors (NLRs). This recognition leads to the engulfment of fungal cells and the subsequent degradation of the engulfed fungal cells within maturing phagosomal compartments. Moreover, the production of pro-inflammatory chemokines and cytokines by neutrophils and macrophages, leads to the stimulation of other phagocytic cells, antigen uptake and presentation, and ultimately, activation of adaptive immune responses. In addition to phagocytes, fungal pathogens also interact with phagocytic dendritic cells, which leads to the activation of TH_{17} and Treg cells (53, 55).

The fungal cell wall plays pivotal role, since it contains polysaccharide and lipid moieties that activate immune responses. Principally, the cell wall is arranged in layers: the innermost layer typically consists of chitin, an *N*-acetylglucosamine polymer and the adjacent external layer is formed by immunoreactive β-(1,3) and β-(1,6) glucans, over which other cell wall polysaccharides and glycoproteins are attached. β-1,3-glucan, which is the strongest fungal recognition signal, is recognized by dectin-1 (also known as CLEC7A), a C-type lectin receptor of the neutrophils and macrophages. This interaction leads to engulf of the fungal spores, phagosome maturation and ultimately fungal degradation via activation of downstream Syk kinase signaling and subsequent production of ROS. Since the exposure (unmasking) of β-1,3-glucan is required for initiation of phagosome

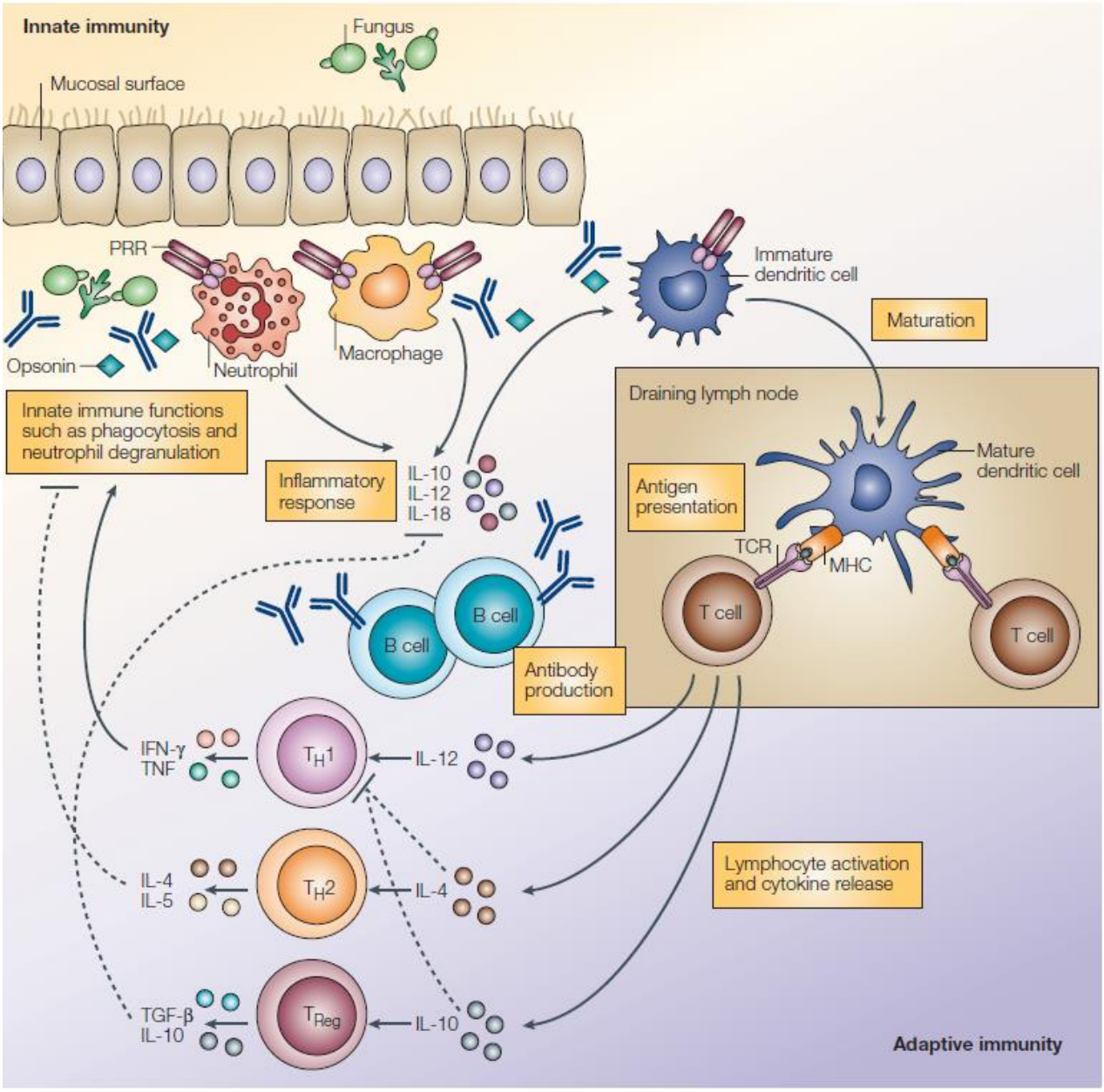

Figure 6. Overview of the immune responses and their regulation in fungal infections. As soon as the fungus overcomes the mucosal barrier, the endothelial cells through chemotactic signals orchestrate the gathering of the antigen presenting cells (APCs) - neutrophils, macrophages and dendritic cells - at the site of the infection within a few hours. The APCs through their PRRs recognize and subsequently engulf the fungal cells. They produce a panel of cytokines attracting more cells and keeping the infection under control. The mature dendritic cells migrate to the lymph nodes, where through the interactions of their MHC with TCRs leads to T-cell activation and differentiation. CD4+ T-cells differentiate Th1, Th2 and Th17cells, which produce various cytokines providing positive and negative feedback signals to effector phagocytes. All together activate the B-cells, which mature into plasma cells, producing pathogen-specific antibodies,

and to memory cells. Treg are responsible for the downregulation of the immune responses and contribute to the development of memory T-cells. Solid and broken lines refer to positive and negative signals, respectively. IFN-γ, interferon-γ; IL, interleukin; TCR, T-cell receptor; TGF-β, transforming growth factor-β; TNF, tumor-necrosis factor; PRRs, pattern recognition receptors. [Adopted from Ref. (53)]

maturation, the cell wall immunoinert polysaccharides and glycoproteins prevent the phagosome activation (9).

Beside the fungal spores killing via ROS production, the neutrophils have other killing mechanisms. Fungal hyphae of *A. fumigatus* and pseudohyphae and *C. albicans* induce NADPH oxidase–dependent NETs formation, which contain extracellular nucleic acids, histones, and granular proteins, including calprotectin and PTX3. In vitro experiments have shown that fungal hyphae, which are too large to be phagocytosed, are trapped in NETs and destroyed (55, 56). An overview of the immune responses in fungal infections is shown in figure 6.

A3.2. Macrophages

The macrophages are large phagocytic cells, that take part in almost all of procedures of the human body, from homeostasis, tissue repair and of course immune responses. They migrate through the capillary walls to place themselves in the tissues, where they differentiate to different phenotypes (for example alveolar macrophages in the lungs, Kuppfer cells in the liver etc.). Since the macrophages possess a great spectrum of functions, they are highly adaptive in order to recognise the environmental changes and rapidly react to them. Their upregulation or uncontrolled activity is associated with the development of cancer and various inflammatory diseases, such as atherosclerosis, asthma, inflammatory bowel disease, rheumatoid arthritis, and fibrosis (57). Focusing on their role for the immune defence, as soon as the macrophages recognize a pathogen, they engulf and destroy it through

oxidative and non-oxidative mechanisms, facilitated by ROS and the lysosomal enzymes respectively. Additionally, the macrophages produce cytokines, initiating the cascade of immune response. Depending on the inflammatory state, macrophages are classified into two groups, M1, stimulated by Toll-like receptor (TLR) ligands and Interferon-γ (IFN-γ), and M2, stimulated by IL-4/IL-13. The M1/M2 polarization corresponds to the Th1–Th2 polarization of T cells (Figure 7).

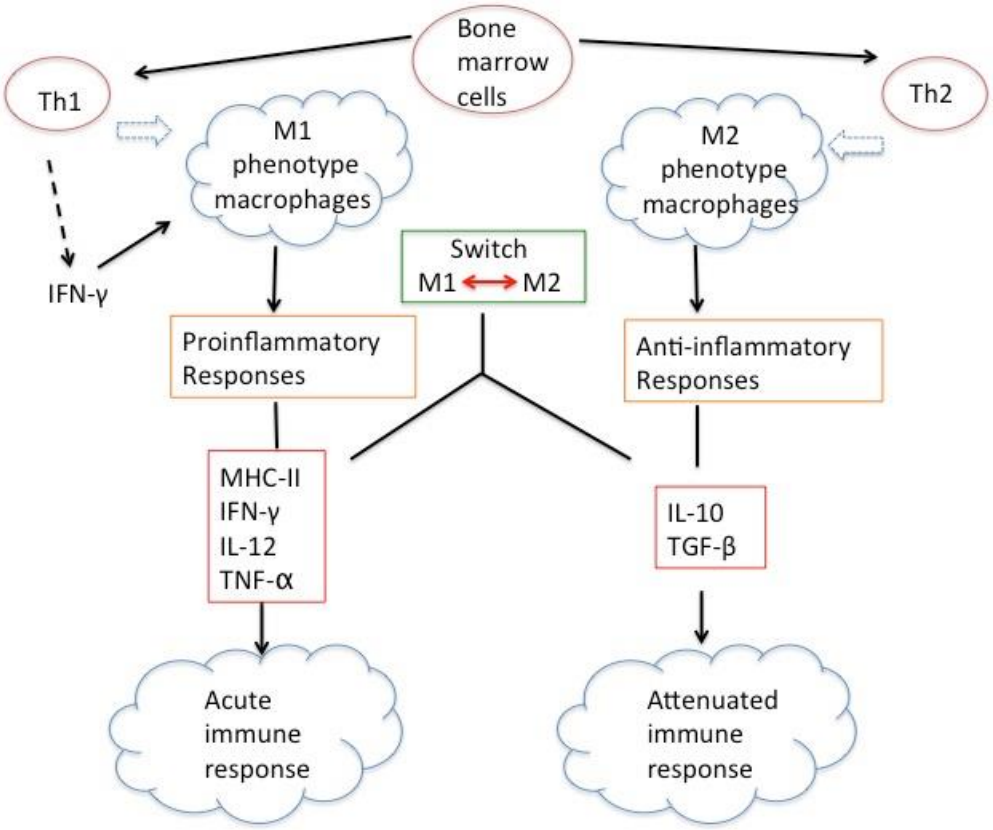

Figure 7. The macrophages polarization and the related functions [Adopted from (58)]

The expression of proinflammatory cytokines, such as IL-12, IL-23 and TNF, as well as the production of reactive nitrogen and oxygen species are the distinguish characteristics of M1 phenotype, which is associated with microcidal function and

tumor inhibition. On the other hand, M2 macrophages are considered to have immunoregulatory and anti-inflammatory functions, down-regulating the expression of TLR2 and IL-12, and their main characteristics are the enhanced phagocytic activity, the expression of mannose and galactose receptors and the production of ornithine and polyamines. The have a key role on the control of the parasitic infections, tissue remodeling and tumor progression. The M1/M2 switch is a control mechanism for the regulation of immune responses, deterring the unrestrained inflammation and consequent tissue damage. Nevertheless, some pathogens, like *Coxiela burneti*, *Yersinia enterocolitica* and *Mycobacterium tuberculosis*, exploit the M1/M2 switch for their favor, overcoming the M1- microcidal activity (59-62).
The alveolar macrophages (AMs) are considered to be at the first line of immune defense against airborne fungi (63). Although neutrophils are the main immune cells responsible for phagocytosis and killing of the *A.fumigatus*, AMs play also an important role. *A. fumigatus* conidia are endocytosed with pseudopods in an actin-dependent manner. The endosomes fuse with phagosomes, while the cell wall of the conidia swells exposing β-1,3, glucan on the fungal cell surface, resulting in phagolysosomal fusion and killing of *A.fumigatus* via a NADPH-oxidase ROS production (64, 65). Furthermore, the interaction of dectin-1 on AMs with β-1,3, glucan stimulates the production of proinflammatory cytokines TNFα, IL-6, and IL-18 (66). On the other hand, the role of AMs in infection with *C. neoformans* is crucial. Experiments in CD11c-DTR mice, were AMs and DCs are selectively depleted, showed enhanced mortality with severe lung inflammation and neutrophil infiltration (67). Moreover, other studies suggest that *C. neoformans* stays dormant inside the AMs. When an immunosuppressive state is induced, such as during advanced HIV infection, *C. neoformans* escapes from the AMs, which leads to a rekindling of the infection (68). The importance of AMs in mucormycosis remains to be explored.

A3.3. The phagosome maturation

The recognition of the pathogen is followed by its engulfment in an intracellular vacuole with a single membrane bilayer, termed phagosome. Intracellularly the binding of signaling proteins on the phagosome membrane leads to phagosome maturation by the interaction with various vacuoles, the endosomes. This interplay has been characterized as a 'kiss and run' mechanism, since the different organelles exchange molecules and they rarely fuse completely (69). The ultimate goal is the fusion of the phagosome with lysosomes, to form the phagolysosome, in order the pathogen to be degraded (58, 70).

The first step of the phagosome maturation is mediated by Rab5 protein, a GTPase, which induces the fusion of phagosome with early endosomes and recruits the class III phosphoinositide 3-kinase complex (PI3K) with its subunit vacuolar protein-sorting 34 (Vps34). Then phosphatidylinositol-3-phosphate (PI3P) is accumulated, mediating the acquisition of early endosomal antigen 1 (EEA1) and the class C core vacuole/endosome tether (CORVET) complex to the phagosomal membrane. The shift from early to late phagosome occurs with the replacement of Rab5 with Rab7 and the subsequent acquisition of lysosome-associated membrane proteins 1 and 2 (LAMP-1 and LAMP-2), which are essential for phagolysosomal fusion. Upon the formation of phagolysosome, its degradative and killing activity is enhanced through the accumulation of hydrolytic enzymes, such as cathepsins (71).

A crucial step of the phagosome maturation is the gradual acidification, which begins shortly after the pathogen engulfment. In M2 macrophages, the pH values tend to be very low, reaching 4.5-5.0. On the other hand, in neutrophils and M1 macrophages the phagolysosomal environment is more neutral or even slightly alkaline, due to the vast ROS production (71). Necessary component of the acidification is the v-ATPase, which pumps protons from the cytoplasm to the

phagosomal lumen and is accumulated shortly after the formation of early endosomes (72). The respiratory burst with the production of ROS is of outmost importance for the microbicidal activity of the phagocytes and it is mediated by the nicotinamide adenine dinucleotide phosphate (NADPH) oxidase, and particularly, by its catalytic, membrane-bound NOX2, which transfers electrons from the cytosol to luminal O_2, generating superoxide, a major killing effector (73).

In 2007 another form of phagocytosis was described, which is termed LC3-associated phagocytosis (LAP). LAP is a noncanonical autophagy pathway linking classical phagocytosis with pattern recognition receptor (PRR) signaling. (74). Many proteins from the autophagy machinery participate in the formation LC3 II-positive phagosomes (LAPosomes), composed of a single membrane instead of the double lipid membrane of the autophagosomes (75). The recognition of pathogens via TLRs or Fcgamma receptors (FcγRs) triggers the recruitment of Beclin-1- PI3K complex, which is a major difference in contrast to canonical autophagy, since there is no need of a pre-initiation complex, known as Unc-51-like kinase (ULK) complex (76). Up next, the production of PI3P by Vps34, leads to the accumulation of two ubiquitin-like conjugation systems, Ub-I and Ub-II, formed by the autophagy proteins ATG5-ATG12-ATG16L1, and ATG8 (LC3 II). Rubicon, a LAP-specific protein, is crucial for this step and also for the recruitment and stabilization of NADPH oxidase NOX2, for the subsequent production of ROS (77, 78). In addition, Rubicon, which is regulated from the interaction of intracellular calcium and calmodulin (79), inhibits the canonical autophagy and promotes the accumulation of LC3-I on the phagosome membrane and its lipidation to LC3-II by phosphatidyl ethanolamine (PE). The last step is vital for the recruitment of LAMP-1 and the subsequent phagolysosomal fusion (77, 80).

A number of studies from our group and others highlighted the role of LAP against fungal infections. In particular, we have previously demonstrated that Dectin-1, a C-

type lectin receptor on the surface of macrophages, recognizes β-1,3-glucan in *Aspergillus* cell wall and triggers LAP. In macrophages a spleen tyrosine kinase (Syk) is required for Dectin-1 activation and LC3 is recruited to the phagosome in a NADPH oxidase- and Atg5-dependant manner (81, 82). Polymorphisms leading to a functionally impaired dectin-1 are associated with increased susceptibility in invasive aspergillosis in immunocompromised patients, addressing the pivotal role of dectin-1 in host defense (83).

Furthermore, corticosteroids have proved to also block the LC3 II recruitment in *A. fumigatus* phagosomes, by inhibiting the phosphorylation Syk kinase–dependent ROS production (84). Additionally, the proteins of the autophagy machinery are of outmost importance, since the conditional inactivation of Atg5 leads to attenuated phagolysosomal fusion and killing of *A. fumigatus* spores (84). A following study showed that cell wall melanin of *A. fumigatus* conidia, which covers the immunostimulatory β-glucan, inhibits the NADPH oxidase-dependent activation of LAP by selectively blockade of p22phox subunit from the phagosome membrane. In vivo, the pigmentless *A.fumigatus* mutant was significant less virulent compared to the wild-type in cyclophosphamide-immunosuppressed control mice, whereas its virulence was restored upon infection of cyclophosphamide-immunosuppressed Atg5 conditional knock-out mice, addressing the importance of the autophagy machinery (1). The LAP pathway against *Aspergillus fumigatus* is summarised in Figure 8.

LAP is also associated with *Candida* infections. In vitro, upon infection of macrophages with *C.albicans*, LC3 is recruited in phagosomes, after a Dectin-1/Syk signaling cascade. In addition, LAP modulates the production of proinflammatory cytokines (TNF-α, IL-6, and IL-1β) by macrophages, promoting their fungicidal activity (85). Conditional knock-out of Atg5 in vitro leads to decreased phagocytosis in J774.16 macrophage cell line, whereas in vivo a significant decrease in survival

rate among conditional knock-out of Atg5 mice was observed upon intravenous infection with *C.albicans* (86). More studies are needed to enlighten the role of LAP and autophagic machinery in *C. albicans* infections, since the current data imply that the mechanisms may be strain-specific (76).

Furthermore, the microbicidal activity mediated by LAP is also of great interest. *Listeria monocytogenes* relies its virulence on escaping from macrophages using them as a proliferative niche. Nevertheless, in 20–25% of *L. monocytogenes*-containing phagosomes LC3 is recruited. LAP is initiated by the surface receptor Mac-1, which mediates ROS production by Nox2 and subsequent LC3 recruitment. The rapid phagolysosomal fusion results to killing and degradation of *L. monocytogenes*. In contrast to *A.fumigatus*, NOX2 and ROS do not have a listericidal role but they are crucial for the lysosomal recruitment and the subsequent killing of *L.monocytogenes* by the lysosomal hydrolases (87). *Mycobacterium. tuberculosis* has also evolved to overcome the killing properties of macrophages, by producing the virulence factor CpsA to prevent NOX2 recruitment to the phagosome and, as a result, induction of LAP and phagosome maturation. Unlike the wildtype *M. tuberculosis*, CpsA-deficient *M. tuberculosis* are able to reverse the blockade of NOX2 recruitment and induce LC3 recruitment to the phagosomes. Phagolysosomal fusion occurs successfully resulting in killing of the pathogen (88).

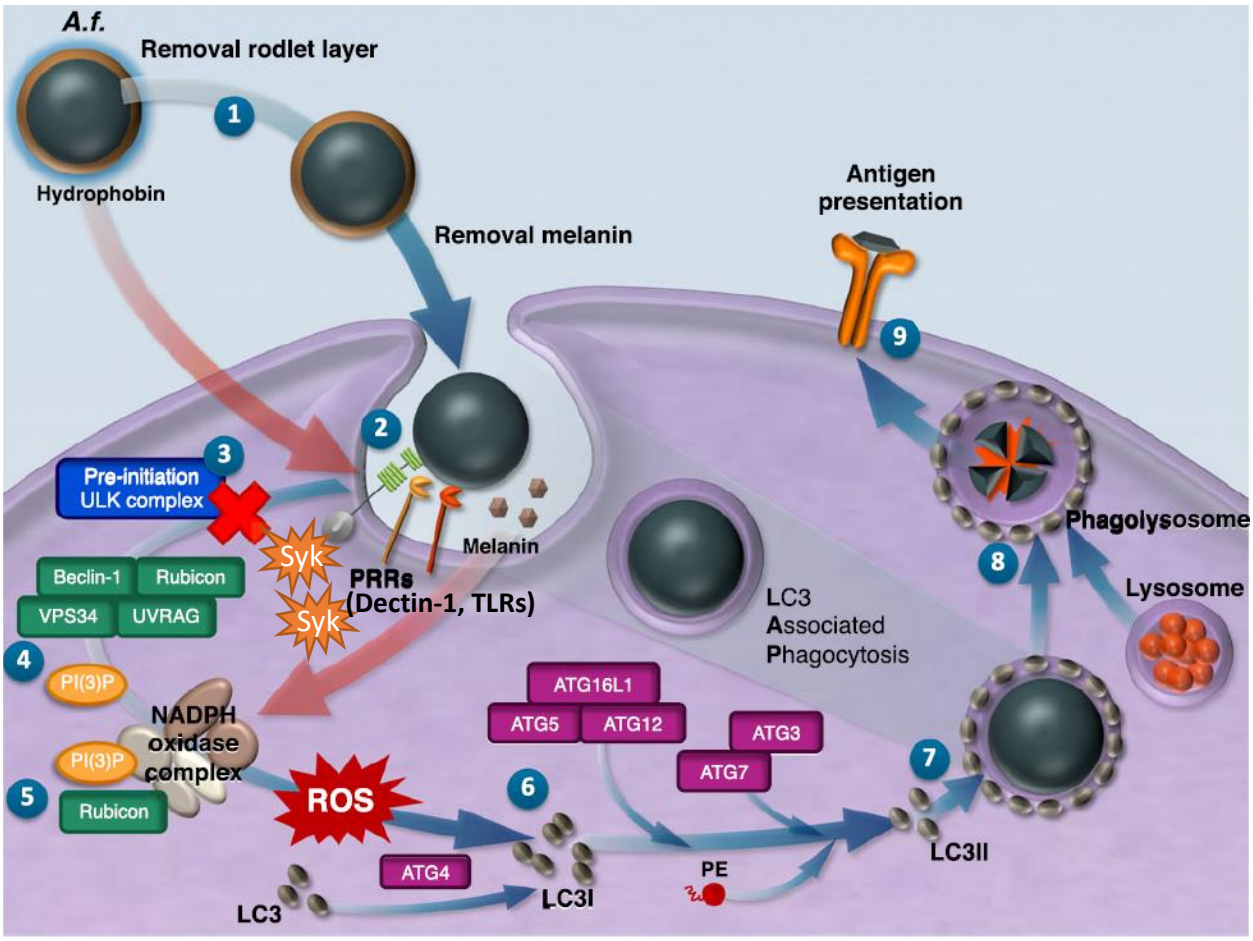

Figure 8. The LAP pathway upon *Aspergillus fumigatus* infection. 1) Swelling of the *Aspergillus fumigatus* spores leads to removal of hydrophobic rodlet proteins and melanin from the cell wall, revealing the immunostimmulatory β-glucan. 2) Engulfment of *A. fumigatus* spores after recognition from PRRs (Dectin-1 and TLRs) on phagocytes. Upon phagocytosis Dectin-1/Syk kinase complex is triggered. 3) LAP does not require the pre-initiation ULK complex, in contrast to canonical autophagy. 4) The class III PI3K complex (green) is recruited, generating PI(3)P that associates with the to the single-membrane phagosome. 5) PI(3)P and Rubicon stabilize the NADPH oxidase complex. Complete assembly of the NOX2 NADPH oxidase complex is essential for the optimal ROS production. Melanin inhibits NADPH oxidase-dependent ROS production, by blocking the phosphorylation of p22 subunit. 6) Formation of PI(3)P and ROS leads to the recruitment autophagy proteins (purple),which conjugate LC3I to PE to form LC3II. 7) Deposition of LC3II on the single-membrane phagosome enhances the phagosomal maturation. 8) Fusion with LAMP-1 lysosome and formation of the phagolysosome with subsequent degradation of *A. fumigatus*. 9) LAP is also a link between innate and adaptive immunity, since it facilitates the adaptive immune response by enhancing major histocompatibility complex II antigen presentation. Red and blue arrows represent the negative and positive regulation respectively. LAP: LC3-assosiated phagocytosis, PRRs: Pattern

recognition receptors, TLRs: Toll-like receptors, ULK: Unc-51-like kinase, PE: phosphatidylethanolamine, PI(3)P: Phosphatidylinositol 3-phosphate, PI(3)K: Phosphatidylinositol (PI) 3-kinases, NADPH oxidase: Nicotinamide adenine dinucleotide phosphate oxidase, ROS: Reactive oxygen species, LAMP-1: Lysosome-associated membrane proteins 1, LC3: Microtubule-associated protein 1A/1B-light chain 3, ATGs: Autophagy-related genes [Adopted from (89) and modified]

A4. Host defense mechanisms against Mucorales

The studies of Diamond et al. shed light to the pathogenic mechanisms of mucormycosis. The investigators showed that neutrophils are recruited and they capable of attaching on *A.fumigatus* und *R.oryzae* hyphae, resulting to pronounced hyphae damage and eventually hyphal killing (32). They proved that *R.oryzae* hyphae are susceptible to the oxidative and non-oxidative killing mechanisms of the neutrophils, and, interestingly, significantly more than *A.fumigatus* hyphae (90). Exploring the interaction of the innate immune system with Mucorales, the researchers showed that, like neutrophils, monocytes attached to and damaged *R.oryzae* hyphae by a serum-independent manner. The monocyte-mediated damage depended mostly on oxidative mechanisms (91). By this time, the profound susceptibility of diabetic patients to mucormycosis was well described (92). Since only rarely PMNs were observed in the histopathological pulmonary lesions of diabetic patients suffering from mucormycosis, the writers tried to elucidate the role of alveolar macrophages (AM) against *R.oryzae* spores and hyphae in a diabetic mouse model. Intranasal infection of diabetic mice with *R.oryzae* spores was associated with increased mortality. In addition, the pulmonary lesions contained irregularly branching hyphal filaments, massive hemorrhage and tissue necrosis. Infection of the diabetic mice with *A.fumigatus* spores did not affect their survival. Moreover, in ex vivo experiments with AMs from bronchoalveolar lavage (BAL) of

diabetic mice a significant germination of *R.oryzae* spores was observed, although the viability and number of AMs were the same as in the normal mice. The macrophage-mediated hyphal damage was comparable with the one caused from PMNs and monocytes as described above. Of interest, in vitro, no differences were found regarding the germination of *Rhizopus* spores lavaged from diabetic and normal mice. In addition, both spores were not easily killed, despite the intact oxidative killing mechanisms of the AMs, so that 10 days after the intranasal infection viable *Rhizopus* spores were recovered from the lungs of normal mice (33). The same group published another study showing that AMs from normal, diabetic and cortisone-treated mice were unable to kill *R.oryzae* spores in vivo, in contrast to *A.fumigatus* spores, which showed a profound resistance in killing only in the cortisone-treated group. Moreover, the resistance of *R.orzyae* spores in killing was confirmed again, since viable spores were obtained from normal murine lungs 10 days after the intranasal infection, unlike the *A.fumigatus* spores, which seemed to be killed shortly after the infection (93). These results implied that the inhibition of *Rhizopus* germination is the key point for the prevention of pulmonary mucormycosis, whereas for *Aspergillus* an early killing seemed to be more important for the prevention of aspergillosis. On the other hand, the aforementioned results showed that although the germination is restricted, the phagocytes still fail to kill the *Rhizopus* spores. Another aspect elucidated by the Diamond group is that although the resting spores of both *A.fumigatus* and *R.oryzae* are resistant in killing upon incubation with neutrophilic cationic peptides, the spores pretreated in culture medium, which become swollen and metabolically active are highly susceptible to non-oxidative killing mechanisms in vitro. It was intriguing, that the greater the swelling of spores, the greater the killing efficacy of macrophage activity. In addition, swollen *A.fumigatus* spores were found significantly susceptible upon

incubation with rabbit AMs, suggesting that the morphological cell wall change upon swelling favors the host defense mechanisms against the fungus (94).

All the previously stated observations do not explain why the phagocytic cells fail to eliminate Mucorales. It is known that hyperglycemia and acidosis impair chemotaxis and the killing activity of neutrophils against *R.oryzae* by impairing oxidative and non-oxidative mechanisms (95). Similarly, corticosteroids hinder migration, phagocytosis and phagolysosome fusion in human macrophages. Despite that, the mechanisms related to attenuated phagocytosis and phagolysosomal fusion are poorly studied. It is of interest that unlike *Aspergillus* patients with CGD are rarely susceptible to Mucorales and the role of NADPH-oxidase and ROS production in the pathogenesis of the infection is unclear (91, 96). Taking into consideration that ca 60% of CGD patients never develop invasive aspergillosis, despite the daily exposure to airborne conidia, a study discovered a novel Aspergillus killing mechanism, non-oxidative burst-dependent, mediated via iron sequestration by lactoferrin, found within neutrophil secondary granules. Based on these findings, non-oxidative mechanisms could be also involved in host defense against Mucorales (97).

Drosophila melanogaster, or fruit fly, is simple genetically amenable minihost with well characterized innate immune responses, mediated by induction of the evolutionarily conserved *Toll* pathway. Schneider 2 (S2) embryonic phagocytic cells of *D.melanogaster* have many common characteristics with mammalian phagocytic cells, placing *D.melanogaster* as a very useful model for the study of bacterial and fungal infections (98). A study showed that *R.oryzae* infects and kills *D. melanogaster* wild type (WT) flies despite the prompt activation of the *Toll* pathway, with both spores and hyphae being resistant to killing from phagocytes. Upon infection of S2 phagocytes, the phagocytosis rate of *R.oryzae* spores was significantly lower that the *A.fumigatus* ones. The authors posited that

the considerable bigger size of Mucorales spores could be the reason. In addition, WT flies infected with *R. oryzae* and *A.fumigatus* spores showed higher mortality rates, impaired phagocytosis and decreased hyphal damage compared to control flies (99).

The exposure of human neutrophils to *R.oryzae* hyphae in vitro was associated with robust expression of proinflammatory cytokines, upregulation in TLR2 mRNA, induction of NF-kappaB pathway-related genes and induced intracellular and extracellular production of superoxide anion (O2−), despite the impaired hyphal damage from the neutrophils (100).

Little is known regarding the interactions of Mucorales with the DCs and the adaptive immunity. An in vitro study showed that *Rhizopus* spores do activate human DCs, unlike *Rhizopus* hyphae. Upon germination, the β-glucan exposure triggers the dectin-1-signaling in human DCs, which leads to IL-23 production and subsequent induction of T_h-17 responses. Moreover, DCs upon interaction with *Rhizopus* hyphae release TNF-α, triggering T_h-1 responses (101).

Another study showed that the coincubating anti–*R. oryzae* T cells with autologous *R. oryzae*–loaded APCs led to a significant production of IFN-γ and TNF-α upon restimulation, indicating that the T cells differentiated to a Th1 population, although the reaction was less profound compared to stimulation with *A.fumigatus* and *C.albicans*. Additionally, a small but significant fraction of T cells producing IL-17 was also found. Interestingly, granulocytes cultured in the supernatant of anti–*R. oryzae* T cells coincubated with *R. oryzae*– loaded APCs had a significantly higher oxidative burst activity compared to controls. The observed decreased alloreactivity of anti–*R. oryzae* T cells can lead to new immunotherapeutic strategies in hematopoietic stem cell transplant recipients due to much milder graft- versus-host reactions (102).

Angioinvasion is a hallmark for the dissemination of mucormycosis. Histopathological studies on lung biopsies from patients with pulmonary mucormycosis showed significantly more extensive angioinvasion among neutropenic patients compared to those with normal neutrophil counts (103), suggesting that a attenuated inflammatory response favors the angioinvasion, the subsequent vessel thrombosis and ultimately tissue necrosis. *R.oryzae* spores and hyphae found to be able to adhere and damage human umbilical vein endothelial cells (HUVECs) in vitro. Presupposition for the endothelial cell damage was the direct contact of the spores with the cells and their subsequent phagocytosis (104). Of interest, the viability of *R.oryzae* was irrelevant for the endothelial damage, suggesting that a toxin substance of *R.oryzae* could mediate the adherence to endothelial cells (104). Recently, the importance of the interactions of endothelia cells with Mucorales was elucidated through the discovery of GRP78 (105). The latter is a required receptor of the endothelia cells, member of the Hsp70 chaperone family, which can specifically recognize Mucorales and but not other fungal pathogens like *A. fumigatus* and *C.albicans.* Elevated glucose and iron levels, stimulating the conditions of DKA, upregulate GRP78 expression, mediating the invasion and damage of endothelia cells by *R.oryzae*. Interestingly, GRP78-specific immune serum protected mice with DKA from mucormycosis (105),

CotH proteins, which are also a unique characteristic of Mucorales, bind to GRP78 during invasion of endothelial cells. *R. oryzae* mutants with attenuated expression of CotH proteins fail to invade endothelial cells and are significantly less virulent in a DKA mouse model of mucormycosis (96). Similarly to GRP78, another study showed that the expression of *R. oryzae* CotH was increased upon incubation with DKA-associated concentrations of β-hydroxy butyrate (BHB), glucose, and iron, enhancing the ability of *R. oryzae* to damage endothelial cells in vitro (106). Furthermore, the BHB related acidosis positively affected the expression of both

GRP78 and CotH (106). These unique virulent traits can partially explain why patients with DKA are so specifically susceptible to mucormycosis and not to other fungal infections.

A5. Fungal cell wall: Immune responses and virulence

The cell wall of the fungi is an important element not only for their survival and growth but also for their pathogenicity. It protects the fungal cell from environmental stress and toxic molecules, whereas it helps the fungi invade the host tissues and escape from phagocytosis. It is organized similarly among the different species. Principally, the cell wall is arranged in layers: the innermost layer typically consists of chitin, an *N*-acetylglucosamine polymer and the adjacent external layer is formed by immunoreactive β-(1,3) and β-(1,6) glucans, over which other cell wall polysaccharides and glycoproteins are attached (107, 108). The fungal cell wall is also a target of choice for antifungal drugs, such as echinocandins which act by inhibiting beta-(1,3)-D-glucan synthase, destabilizing the cell wall (109).

As far as the filamentous fungi are concerned, the cell wall of *Aspergillus fumigatus* is the most studied. It consists of an outer layer of polysaccharides, which are bound in a complex composed of a branched β-(1,3)-glucan found in the inner layer of chitin, galactomannan, and β-(1,4)-glucans. Other polysaccharides, such as α-(1,3)-glucan and galactosaminogalactan, are filling the pores between fibrillar polysaccharides. *A.fumigatus* conidia have a supplementary outer layer composed of melanin, which is covered by a RodA hydrophobin rodlet protein layer that confers hydrophobic properties (107, 110). Moreover, the rodlet layer covers β-(1,3)-glucan and other immunostimulatory cell wall polysaccharides, making the dormant conidia of *A. fumigatus* immunologically inert (111). After phagocytosis, an

intraphagolysosomal swelling of the conidium occurs and the rodlets as wells as the melanin layer are degraded, exposing the immunostimulatory β-(1,3)-glucan. Melanins are negatively charged hydrophobic pigments of high molecular weight that are composed of polymerized phenolic or/and indolic compounds. Based on their biochemical precursors, pathways and components melanins are categorized in several types. The two main types of melanin of the fungal cell wall are the DHN-melanin of *Aspergillus* species and black fungal pathogens such as *W. dermatitidis* or *Sporothrix schenckii* and the 3,4-dihydroxyphenylalamine (DOPA)-melanin found in *C. neoformans*, called eumelanin (108). Catechol-melanin, pyomelanin and paminophenol (PAP)-melanin as well as the heterogeneous melanins are also described (112). Melanin is an essential virulent component for *A.fumigatus*, since it inhibits conidial killing with two mechanisms: 1) blocking of phagosome biogenesis and acidification of phagolysosomes and 2) inhibition of phagocyte apoptosis by activation of the PI3K/Akt survival signaling pathway (110). Mechanistically, melanin blocks LAP by masking β-(1,3)-glucan, preventing the binding with dectin-1 on the neutrophils, an essential step for NADPH-oxidase dependent ROS production and subsequent killing of *A. fumigatus* conidia (1, 113). Regarding the cell wall of Mucorales little is known (114). Diamond et al. observed that in contrast to resting *Rhizopus* conidia, that are resistant to killing by phagocytes, the swollen ones are ultimately killed upon incubation with cationic peptides, assuming that the cell wall would need to become permeable to macrophage microbicidal products and/or the conidia become metabolically active inside the phagosome (94). A study from 1968 showed that the spore cell wall of *M. ramannianus* is composed of two layers: an outer electron-dense layer and an inner thicker layer composed of microfibrils containing glucans (115). The presence of β-glucan was confirmed in another study, where b-glucan exposure in the cell wall of *R.oryzae* proved to be essential for the induction of IL-23/T(H)-17 axis (101).

Moreover, glucan was found to be the major component of the spore cell wall in *M. circinelloides* in association with melanin, glucosamine, mannans, and proteins (116). Based on the studies of *A.fumigatus* rodlet layer and its significance on immune response, investigators using high-resolution scanning electron microscopy found no morphologic correlate of a rodlet layer in resting spores of *R. oryzae, C. bertholletiae,* and *R. pusillus*. Moreover, treatment of *R. oryzae* spores with hydrofluoric acid did not lead to a significantly altered morphology in the outermost cell wall layer, whereas the *A. fumigatus* spores lost their typical rodlet surface pattern. These data showed that cell wall of Mucorales lacks the immunoprotective rodlet hydrophobic outer layer (117). In contrast to *Aspergillus* spp. a morphological and chemical characterization of melanin as well as its significance on the virulence of Mucorales remains to be explored.

A6. Role of iron in immune response and in mucormycosis

Iron metabolism and the immune response are intimately linked, since the iron availability is crucial not only for the efficacy of antimicrobial immune pathways but also for the pathogen proliferation. The macrophages play an important role in iron sequestration, since they act as cellular guardians. Through their scavenger receptors, they engulf the aged or damaged red blood cells, which are the main source of iron (118). After the intracellular hemoglobin catabolism, iron is released and stored by binding to ferritin, in order to avoid an oxidative damage (119). Upon infection, pro-inflammatory cytokines (IL-1 and IL-6) and nuclear factor-κB (NF-κB) stimulate ferritin production (120). This mechanism limits the availability of this essential nutrient for circulating pathogens, a host defense strategy known as ‘nutritional immunity’. Macrophages have also the ability to adjust the iron

availability according to the different types of microorganisms. Infections with extracellular bacteria such as *Staphylococcus aureus, Streptococcus, Klebsiella* or *Yersinia* stimulate the expression of the iron-regulatory hormone hepcidin which targets the cellular iron-exporter ferroportin-1 causing its internalization. Consequently, iron remains intracellularly, keeping the infection under control. The hypoferraemia of the acute phase response subsequently results in the development of anemia of inflammation (118, 121-124). Regarding intracellular pathogens, such as *Chlamydia, Mycobacterium tuberculosis, Listeria monocytogenes or Salmonella Typhimurium,* ferroportin-1-mediated iron export is turned on for the removal of iron from infected cells, leading to reduced iron availability for intra-macrophage pathogens (125-128). This mechanism inhibits the pathogens' growth and in the same time strengthens antimicrobial effector pathways of macrophages including the formation of inducible nitric oxide synthase and tumour necrosis factor (118).

The fungi acquire iron mainly by two mechanisms. By producing iron reductases, they manage to covert ferric iron to ferrous iron, a non-toxic iron form which can be stored. Under conditions of iron starvation, fungi produce low-molecular-weight ferric iron chelators known as siderophores. Most of the latter are hydroxamates, whereas the zygomycetes form polycarboxylates (129). Already in the early 80s, Artis al. showed that the attenuated iron binding capacity of transferrin in the serum of patients suffering from DKA due to its excessive glycosylation led to excessed *R.oryzae* growth (130). Their findings elucidated the outmost importance of iron acquisition in the pathogenesis of mucormycosis, paving the way for the further study of the related mechanisms.

It is well established that patients with increased risk of iron overload (for example patients under renal replacement therapy or patients undergoing multiple blood transfusions) are susceptible to mucormycosis and therefore were treated with deferoxamine (DFO), an iron chelator (22, 23, 43, 96, 131). Ferrioxamine is a

xenosiderophore and iron-rich form of DFO, which binds with the specific Mucorales cell surface receptors FOB1 and FOB2. Through an energy dependent reductive step ferrous iron is released and transported across the fungal cell membrane without deferoxamine internalization (37, 132) . Interestingly, DFO-mediated growth was not observed among *Aspergillus* and *Candida* spp., which proves that iron acquisition through DFO is a unique virulent trait of Mucorales (133). DFO treatment and subsequent infection with *R.oryzae* in a Drosophila melanogaster model led to rapidly disseminated infections with higher fungal burdens and a significantly higher mortality rate (99). In contrast to DFO, deferiprone and deferasirox, modern iron chelators that *Rhizopus* is unable to use as xenosiderophores, act protectively against mucormycosis. Deferiprone was as effective as liposomal Amphotericin B at improving survival and decreasing brain fungal burden in DKA mice after an intravenous infection with *R.oryzae* (134). Although, a recent clinical trial failed to find a therapeutic benefit (135), indicating that more light has to be shed to the iron related pathogenesis of mucormycosis.

The key role of iron utilization in pathogenesis of mucormycosis is further illustrated by the fact that Mucorales express a high affinity iron permease gene (FTR1), which is essential for the iron transport upon iron starvation. Conditional inactivation of FTR1 resulted to impaired in vivo virulence of *R.oryzae* through attenuated iron uptake (36).

A7. Aim of the study

The recent therapeutic advances of hematological malignancies and hematopoietic stem cell transplantations led to increased survival of immunocompromised patients. As a result, the respiratory fungal infections caused by opportunistic filamentous

fungi, like Aspergillus and Mucorales, present the last decades an increased incidence among those patients. Mucormycosis is related with high mortality rate, which can reach up to 90% in disseminated disease. Unlike the other filamentous fungi, such Aspergillus, Mucorales frequently cause lethal infections not only in immunocompromised patients but also in patients suffering from metabolic disorders, such as diabetic ketoacidosis, and also immunocompetent individuals after extensive trauma and burns. These unique epidemiological characteristics made the researchers wonder what makes Mucorales so different. The initial studies revealed that Mucorales grow rapidly in culture medium and serum from patients with DKA. Besides, Mucorales spores are found to be highly resistant to killing from neutrophils and macrophages. The last decade studies highlighted the importance of iron acquisition for the pathogenicity of mucormycosis.

Despite the progress, at the molecular level little is known about the mechanisms of intracellular killing of Mucorales conidia inside phagocytes. The aim of the present study was to shed light on the virulence mechanisms that protect Mucorales conidia from killing by phagocytes, not only from the pathogen- but also from the host perspective. Based on previous studies from the literature and our laboratory, we focused on the intracellular events of phagolysosomal fusion, searching for a possible blockade that could explain the remarkable resistance of killing Mucorales by phagocytes. Furthermore, we intended to elucidate the physiological immune response of pulmonary mucormycosis and the role of macrophages. In addition, we aimed to explore the role of iron homeostasis upon infection of macrophages with Mucorales. We intended to identify a mechanistic link between iron starvation and intracellular growth of Mucorales, as well as to address possible host and fungal modulators of iron homeostasis that promote invasive fungal growth.

C. Materials and Methods

C1. Microorganisms and culture conditions

For the experiments all the fungal strains used were obtained from University of Texas Health Science Center at San Antonio. *Aspergillus fumigatus* ATCC22, WT *Rhizopus oryzae* ATCC55796932 and a brain isolate WT strain *R. delemar* 99- 880, which had its genome sequenced (36, 37). The aforementioned strains were grown on Yeast extract agar glucose agar plates for 3 days at 37 °C. For a final volume of 500ml, were used 2.5gr Yeast Extract, 7,5gr Agar, 5gr Dextrose 0,5ml Trace elements ($Na_2B_4O_7$:$10H_2O$, $CuSO_4$:$5H_2O$, Ferric Citrate, $MnSO_4$: H_2O, $NaMoO_4$:2 H_2O, $ZnSO_4$:7 H_2O) 1ml Vitamin Mix (p-Aminobenzoic acid, Niacin, Pyridoxine HCl, Riboflavin, Thiamine HCl, Choline HCl and d-Biotin) and 5ml MgSO4 (1M). The plates were filled with 25-30ml autoclaved medium and kept at room temperature in the dark before experimental use.

Rhizopus delemar M16 is a pyrf-null mutant that is derived from *Rhizopus delemar* 99-880 and is unable to synthesize its own uracil (136), and was grown on YPD medium (MP Biomedicals) supplemented with 100 μg/ml uracil. *Rhizopus delemar* with reduced FTR1 copy number, and *Rhizopus delemar* transformed with RNA interference (RNAi) targeting FTR1 expression were all derived from strain M169. In experiments including RNAi mutants, a chemically defined synthetic medium containing yeast nitrogen base (YNB) supplemented with complete supplemental mixture without uracil (CSM-URA) (MP Biomedicals) (i.e., YNB + CSM-URA). The culture medium per liter consisted of 17 g YNB without amino acids, 20 g dextrose, and 7.7 g complete supplemental mixture minus uracil. These strains were grown for 3 days in 37 °C.

Fungal conidia (spores) were harvested by gentle shaking in the presence of sterile 0.1% Tween-20 in phosphate-buffered saline (PBS), washed twice with PBS, filtered through a 40 μm pore size cell strainer (Falcon) to separate conidia from contaminating mycelium, counted by a hemocytometer, and suspended at a concentration of 10^7 and 10^8 spores/ml for *Rhizopus* and *Aspergillus* strains, respectively.

Inactivation of *Rhizopus* conidia was done by exposure to Ultraviolet (UV) irradiation, suspended in PBS in a 6-well plate for 1 hour in room temperature. To achieve synchronized swelling of *Rhizopus* conidia, 10^6/ml dormant conidia were incubated at 28 °C in a 6-well plate with RPMI-MOPS [3-(N-morpholino)propanesulfonic acid] (ThermoFischer Scientific and Gibco BRL Products, Life Technology, Gaithersburg, Md. respectively) supplemented with 2% glucose for 4 hours. The synchronized swelling was evaluated under optical microscopy.

For fluorescence labeling of *Rhizopus*, 10^6 conidia were stained in 100 μl PBS containing 100 μg/ml Fluorescent Brightener 28 (Sigma-Aldrich, #475300) and 0.1M NaHCO3 for 30 min protected from light in a bench-top rotator. Afterwards, conidia were washed three times with PBS and the concentration was adjusted to 10^7 or 10^8 conidia/ml.

C2. Melanin extraction and characterization

C2.1. Fungal melanin extraction

A. fumigatus and *R. oryzae* were collected by centrifugation at 3000 rpm for 30 min, washed with PBS, and suspended in 1.0 M sorbitol–0.1 M sodium citrate in pH 5.5. Glycohydrolytic enzymes (Glucanex; Novo), which contain protease, cellulase and

chitinase, were added at 1 mg/ml and the suspension was incubated overnight at 30ºC to generate melanin particles. They were then collected by centrifugation, washed with PBS and incubated in 4.0 M guanidine thiocyanate for 12 hours at room temperature with frequent vortexing. The suspension consisting of melanin and cellular debris was collected by centrifugation and washed with PBS. The particulate was then treated with 1.0 mg/ml Proteinase K in a reaction buffer with 10.0 mM Tris, 1.0 mM CaCl and 0.5% Sodium dodecyl sulfate (SDS) at pH 7.5 for 4 h at 37ºC overnight. After washing with PBS, the suspension was boiled in 6.0 M HCl for 1.5 hour to hydrolyze cellular debris, which may still be associated with the melanin. Melanin particles were collected by centrifugation, washed thoroughly with PBS, re-suspended in PBS and kept in 4ºC. This treatment resulted in an electron-dense layer similar in size and shape to the original conidial melanin layer without underlying cell components, for which reason these electron-dense materials were called melanin ghosts.

C2.2. Chemical characterization of *Rhizopus oryzae* melanin

Rhizopus conidia of 1.6 g was ground with mortar and pestle under liquid nitrogen into very fine powder. The black fine powder was extracted by boiling with 5% KOH under reflux for 1 h followed by filtration. The black colored filtrate was left to cool at room temperature and then precipitated with 1 N HCl. The black precipitate was collected by filtration using filter paper. The black precipitate was left to dry on the filter paper followed by washing several times with 1 N HCl, then 3 N HCl, water, and methanol. The remaining black/brown precipitate was dried at room temperature and used for further analysis. The solubility of the black pigment was tested in distilled deionized water, 0.1 N HCl, 1 N HCl, 3 N HCl, 1 N KOH, methanol, ethanol, acetone, chloroform, benzene, and dimethyl sulfoxide (DMSO). Reactions

with oxidizing agents such as 6% sodium hypochlorite and 30% H_2O_2 were determined by measuring solubility of the pigments in these reagents. The precipitation of the pigments with FeCl3 which reacts to polyphenols was also tested.

C2.3. UV absorbance and infrared (IR) spectroscopy analysis of *Rhizopus* melanin

The melanin extract in 1 N KOH was measured at 200–700 nm with the use of a SPECTRO UV–VIS spectrophotometer. One normal KOH was used as blank. For IR measurement, melanin powder was mixed with KBr and used to measure IR absorbance using a Bruker machine with KBr disc used as a blank.

C2.4. Melanin alkaline H_2O_2 oxidation

To identify the production of various pyrrole acids (PTCA, PDCA, isoPTCA, and PTeCA) from melanin samples by liquid chromatography-mass spectrometry (LC-MS), alkaline H_2O_2 degradation was performed. The extracted *Rhizopus* melanin was taken in a 5-ml screw-capped conical test tube, to which 500 µl of 1 mol/L K_2CO_3 and 50 µl of 30% H_2O_2 in a final concentration of 1.5% were added. The mixture was vigorously mixed and then kept on a shaker at 25 °C for 20 h. The residual H_2O_2 was decomposed by adding 100 µl 10% Na_2SO_3 and the mixture was then acidified with the addition of 200 µl of 6M HCl. The reaction mixture was centrifuged at 4000 × g for 5 min and then subjected to thin linear chromatography (TLC) along with total KOH extract. The TLC developing system comprised of water:1M HCl:chloroform:methanol (0.5:0.5:1:6).

C2.5. LC-MS of melanin hydrolyses product

The combination of liquid chromatography (LS) with mass spectrometry (MS) was a great challenge due to the totally opposite properties of the two methods. Therefore, their combination, which was established on early 70s, was a breakthrough in clinical biochemistry for the characterization and detection of various molecules. LS separates mixtures with multiple components, while MS provides structural identity of the individual components with high molecular specificity and detection sensitivity (137). LS-MS analyses were carried out in negative ion mode by electrospray ionization on (Waters) ACQUITY UPLC triple Quadrupole (Xevo TQD) instrument equipped with the MassLynx software, at a flow rate of 0.3 ml/min, run time of 5 min, and the use of a solvent system containing 85% methanol, 15% water, and 0.1% formic acid. All solvents and reagents were High Performance Liquid Chromatography (HPLC) grade and used without further purification.

C2.6. Electron paramagnetic resonance (EPR) studies

EPR spectra were recorded at room temperature on an ELEXSYS Bruker spectrometer equipped with a Super High Q Sensitivity resonator operating at X-band (9.9 GHz). Microwave power was 1 mW for synthetic melanin and 0.1 mW for A. fumigatus or R. oryzae. Magnetic field modulation amplitude and frequency were, respectively, set to 0.2 mT and 100 kHz.

C3. Virulence studies in mice

GFP-LC3 (obtained from RIKEN BioResource Center) and C57BL/6 (B6) mice were maintained in grouped cages in a high-efficiency particulate air-filtered

environmentally controlled virus-free facility (24 °C, 12/12-h light/dark cycle), and fed by standard chow diet and water ad libitum. All experiments were approved by the local ethics committee of the University of Crete Medical School, Greece in line with the corresponding National and European Union legislation. Animal studies on virulence of albino *Rhizopus* were approved by the Institutional Animal Care and Use Committee (IACUC) of the Los Angeles Biomedical Research Institute at Harbor-UCLA Medical Center, according to the National Institute of Health guidelines for animal housing and care.

For virulence studies, 8- to 12-week-old female C57BL/6 (B6) mice were challenged by intratracheal installation with *A. fumigatus* or *Rhizopus* conidia, 10^7 and 5×10^6 conidia/mouse respectively. Mice were euthanized 48 hours later, lungs were homogenized, plated on potato dextrose agar + 0.1% Triton plates and incubated at 37 °C. Colony-forming unit (CFU) counts were assessed after 24 hours.

For AM depletion studies, mice received by intratracheal administration 100 μl of clodronate liposomes (containing 500 μg of clodronate; http://www.clodronateliposomes.org) or control (empty) liposomes. Each group consisted of 10 and 5 mice respectively. After 48 hours they were challenged with 10^7 *Rhizopus* conidia and the survival rate was observed.

For CD11c cell depletion, CD11c-DTR mice received by intratracheal administration 20 ng/kg of diphtheria toxin (DT). The efficiency of cell depletion was assessed by immunohistochemistry for CD11c and flow cytometry analysis of BAL. 48 hours later, three groups of 5 CD11c-DTR mice each, were challenged either with 5×10^6 conidia of *R. delemar*, or PBS or plain DT. The last two groups were the control ones.

Immunocompetent CD-1 male mice were infected with 10^6 spores of *R. delemar* strain 99-880 grown in two different condition: on synthetic defined (SD) medium complete plates and on SD complete plates + 1mM of the copper chelator, β-

Citrylglutamate (BCS). Sporulation on plates with BCS was subjected to copper deprivation and thus conidia appeared pigmentless (referred to in experiments as albino). Infection was carried out intratracheally, with 9 mice per group. Lungs were collected at three different time points: 4 h post infection, at day +1, and at day +3. At each time point, three mice per group were sacrificed. Right after infection, two mice have been sacrificed for inoculum verification. After collection, the samples were plated on potato dextrose agar + 0.1% Triton plates and incubated at 37 °C. For lung samples, after homogenization in 2ml of PBS, 200 µl were plated directly from the concentrated samples and also from serial dilutions to facilitate counting.

C4. Generation, isolation and stimulation of murine BMDMs

L929 cell line has the ability to produce Granulocyte-macrophage colony stimulating factor (GM-CSF), which is required to induce hematopoietic cell differentiation into macrophages. L929 are cultured in complete Dulbecco's modified Eagle's medium (DMEM), i.e. DMEM supplemented with 10% fetal calf serum (FCS), 2 mM glutamine, 100 U/ml penicillin and 100 µg/ml streptomycin, at 37 °C, 5% CO_2 within 175cm^2 flasks for 10 days. The supernatants are then collected, pooled and centrifuge at 1300 rpm for 5 min. The cell pellets were discarded and the supernatants were stored in 15 ml tubes at -20 °C.

For the generation of BMDMs 8-12 weeks old mouse was sacrificed by cervical dislocation. After the skin disinfection with 70% alcohol, using sterile surgical blades the skin und muscles from every hind leg were removed. The bones were placed in a sterile Petri dish containing sterile, ice-cold PBS. The bone marrow (BM) from tibias and femurs was then flushed using a 20g syringe needle with ca 10ml complete DMEM under sterile conditions. The obtained BM cells were thoroughly flushed through a 18G syringe needle to lyse the red blood cells. Finally, the

remaining BM cells were cultured in DMEM complete with L929 cell-conditioned medium (30%) for 7 days to generate BMDMs. The cell growth was checked periodically with light microscopy. To harvest the BMDMs, supernatants were removed and the cells were washed with complete DMEM, that has been warmed to 37 °C. Then 5 ml of warm complete DMEM were added to the flasks and BMDMs were detached by gently scraping with a rubber policeman. The collected BMDMs were centrifuged at 1500 rpm for 5 min. The cells pellets were gently dissociated in complete DMEM. BMDMs were counted a Bürker counting chamber in the presence of trypan blue, to check their viability, which was always > 90%. They were finally resuspended in complete DMEM and their number was adjusted to 10^6/ml. The resulting cultures consisted of macrophages (>95% purity), as determined by staining for F4/80 and flow cytometry.

For immunofluorescence experiments, a total of 1×10^5 BMDMs per condition in a final volume of 100 µl were allowed to adhere to polylysine-treated glass coverslips (Ø 12 mm) for 1 h followed by stimulation with conidia of *Rhizopus* or *A. fumigatus* at a multiplicity of infection (MOI) of 2:1 and 5:1, respectively, at 37 °C in a 5% CO_2 incubator for the indicated time point. After infection, cells were washed twice with PBS to remove medium and non-phagocytosed spores and cells were fixed on the coverslips for 15 min in 4% paraformaldehyde, followed by 10 min fixation with 100% ice-cold methanol and then stored in PBS at 4°C until immunofluorescence staining.

C5. Immunofluorescence staining

For immunofluorescence imaging, cells were seeded on coverslips pretreated with polylysine, fixed with 4% paraformaldehyde for 15 min at room temperature, and followed by 10 min of fixation with ice-cold methanol at −20 °C. Next, the

coverslips were washed twice with PBS, permeabilized by using 0.1% saponin (Sigma-Aldrich) prior to blocking for 30 min in PBS-BSA (PBS + 2% Bovine serum albumin - BSA). The coverslips were then incubated for 1 hour with the indicated primary antibody (Ab), washed twice in PBS-BSA, then counterstained with the appropriate secondary Alexa Fluor secondary Ab (Molecular Probes), and followed by DNA staining with 10 μM TOPRO-3 iodide (642/661; Invitrogen). After extensive washing, slides were mounted in Prolong Gold antifade media (Molecular Probes). The following antibodies and reagents were used for ex vivo studies in BMDMs: anti-GFP polyclonal Ab (Minotech, #721-1, dilution 1:500), Cathepsin D (Santa Cruz, #sc-377299, dilution 1:100), Rab5B (clone A20, Santa Cruz, # sc-598, dilution 1:100), Alexa 555 (Life Technologies, #A21425, dilution 1:1000) and Alexa 488 (CF488A, Biotium, #20012-1, dilution 1:1000).

Images were acquired using a laser-scanning spectral confocal microscope (TCS SP2; Leica), LCS Lite software (Leica), and a ×40 Apochromat 1.25 NA oil objective using identical gain settings. A low fluorescence immersion oil (11513859; Leica) was used, and imaging was performed at room temperature. Serial confocal sections at 0.5 μm steps within a z-stack spanning a total thickness of 10 to 12 μm of the cell were taken and 3D images were generated using the LCS Lite software to assess for internalized conidia contained within phagosomes. Unless otherwise stated, mean projections of image stacks were obtained using the LCS Lite software and processed with Adobe Photoshop CS2. Phagosomes surrounded by a rim of fluorescence of the indicated protein marker were scored as positive.

C6. FITC-dextran experiments

FITC-dextran (Sigma, #46945) was diluted in sterile Water for Injection (WFI) for a stock of 2mg/ml. BMDMs were collected as left to adhere on polylysine treated

coverslips in 24-well plates as described above. FITC-dextran was added to the cells in a final concentration of 0.5mg/ml and left to be accumulated from the BMDMs for 16 hours. Then the cells were gently washed with warm 1x PBS, left to rest for 2 hours and followed by stimulation with conidia of *Rhizopus* or *A. fumigatus* at MOI of 2:1 and 5:1, respectively, at 37 °C in a 5% CO_2 incubator for 4 hours. After infection, cells were washed very gently twice with PBS to remove the remaining FITC-dextran, medium and non-phagocytosed spores. The cells were then fixed on the coverslips for 15 min in 4% paraformaldehyde. The slides were mounted in Prolong Gold antifade media and the image analysis with confocal microscopy, as described above, was performed the same day.

C7. Lysosomal extracts

C7.1. Lysosomal extract preparation

Crude BMDM lysosomal extracts were obtained using the lysosome isolation kit instructions (Thermo Scientific, Boston, MA, USA). At least 3×10^8 freshly collected BMDMs were counted, centrifuged at 400 × g for 5 min at 4 °C and then washed twice with cold 1xPBS. The supernatant was removed, the pellet was resuspended with reagent A and 1% (v/v) protease inhibitor, and then incubated in ice for exactly 2 min. Next, the cells were mildly sonicated on ice for 10 s and checked under a microscope with Tryptan blue solution staining to verify lysis of BMDMs. Subsequently, reagent B with 1% (v/v) protease inhibitor was added and the tube was inverted several times to mix the solution, which was then centrifuged at 500 × g for 10 min at 4 °C. The supernatant was collected and gradient dilution buffer was added. The solution was centrifuged at 18000 × g for 30 min at 4 °C and

the pellet was dissolved in 250 μl gradient dilution buffer. Two rounds of sonication for 10 s each were performed, resulting in the generation of crude lysosome extract.

C7.2. In vitro studies with crude lysosomal extracts

Crude lysosomal extracts were added to a 96-well plate in increasing concentration of 10%, 25%, and 50% with culture medium (DMEM-Glutamax supplemented with 10% FBS and 1% streptomycin) at pH 5.5. *R.oryzae* and *A. fumigatus* conidia were counted and added at a number of 5×10^4/well, reaching a total volume of 100 μl in each well. Culture medium at pH 5.5 was added to control wells. Plates were incubated for 24 h at 37°C in a 5% CO2 incubator. The fungal metabolic activity was assessed with XTT ((2,3)-bis (2-methoxy 4-nitro 5-sulfenyl)-2H-tetrazolium carboxanilide; Sigma-Aldrich) reduction assay. One hundred microliters of tetrazolium salt XTT and menadione was added to each well at a final concentration of 0.25 mg/ml and 25 μM, respectively, and the plate was incubated for an additional 1 h. The absorbance of formazan, the XTT reduction product, was read at 450 and 655 nm on a Bio-Rad 680 microplate spectrophotometer. The percentage of the metabolic activity was determined as follows: % metabolic activity = 100% × (OD450 − OD655) experiment/(OD450 − OD655) control. Fungal killing was evaluated by plating on a Sabouraud agar plate a 100-fold dilution of each well in sterile PBS.

C8. Electron microscopy studies

BMDMs were collected, counted, and inoculated in DMEM-Glutamax, 10% FBS, 1% streptomycin in 6-well plates. BMDMs were infected with conidia of either R. oryzae or A. fumigatus and cells were removed at the indicated time point of

infection. Accordingly, infected BMDMs were fixed for 30 min at 4 °C with 2% glutaraldehyde in cold sodium cacodylate buffer (SCB) (0.1M sodium cacodylate, 0.25M sucrose, pH 7.4), and washed again with SCB. This was followed by two 30-min incubations in acid phosphatase reaction buffer (0.1M sodium acetate, 1 mM glycerophosphate, and 2 mM CeCl3), pH 5.2, at 37 °C. The cells were then rinsed three times with acid phosphatase reaction buffer, and re-fixed in 3% glutaraldehyde in SCB for 1 h at 4 ° C. After two more washes in SCB, the obtained monolayers were post-fixed in cacodylate-buffered 1% OsO4 for 2 h, dehydrated, and embedded in Epon 812 (Merck, Darmstadt, Germany). An ultratome (Leica, Reichert Ultracuts, Wien, Austria) was used to cut ultrathin sections, which were contrasted with 4% uranyl acetate for 45 min and lead citrate for 4 min at room temperature. Finally, the sections were examined using a Jeol 1200 EX2 electron microscope (JEOL, Tokyo, Japan).

C9. Phagocytosis and killing assays in BMDMs and PMNs

For the killing assays, $5x10^5$ and 10^6 BMDMs were left to adhere in 6-well plates for 1 h in 2 ml of DMEM complete media at 37 °C in a 5% CO2 incubator, and subsequently infected with *R. oryzae* and FITC stained *A. fumigatus* conidia, at an MOI of 1:1 respectively. BMDMs were washed three times with warm 1xPBS 30 minutes after the infection to remove non-phagocytosed conidia. At the indicated time point of infection (2 or 6 h), BMDMs were harvested by scraping, placed in Eppendorf tubes, lysed by sonication (three times for 10 s and once for 5 s for *A. fumigatus*-infected and *R. oryzae*-infected BMDMs, respectively), centrifuged at 1000 rpm for 10 min at 4 °C, and the pellet containing intracellular conidia was resuspended in 200 μl sterile PBS.

A. fumigatus killing was assessed using propidium iodide (PI) (Sigma, #P4170) staining, which binds and labels DNA. In each Eppendorf containing the intracellular *A.fumigatus* conidia 2.5µl PI were added for 10 minutes in a dark room. The conidia were centrifuged twice at 1000rpm for 10 minutes at 4 °C. The pellet was mounted on slides mixed with Prolong Gold antifade media and the killing, indicated by PI-positiv conidia, was assessed by confocal microscopy. FITC labeled live *A. fumigatus* conidia served as controls for PI staining

For the evaluation of killing of *Rhizopus* conidia by BMDMs a differend approach was followed, since live *Rhizopus* conidia tend to absorb PI. Intracellular conidia recovered after BMDM lysis were incubated at 37 °C in a 5% CO2 incubator with DMEM complete medium for ~4 h, until germination was microscopically observed. Killing of *R. oryzae* was assessed using a Bürker counting chamber based on the percentage of germinating conidia. Germination of intracellular *Rhizopus* conidia by BMDMs was always normalized to the germination of control *R. oryzae* conidia following sonication (5 s) and cultured in DMEM complete medium for ~4 h in the absence of BMDMs, which was typically always >95%. In representative experiments, killing of *A. fumigatus* was also assessed based on the germination assay.

For phagocytosis assay, BMDMs and PMNs from GFP-LC3 mice were stimulated with *R. oryzae* and *A. fumigatus* conidia at a multiple of infection (MOI) of 2:1 at 37 °C in a 5% CO_2 incubator for different time points. Cells were then fixed and stained for confocal microscopy as previously mentioned. Phagocytic index was expressed with the following formula: (total number of engulfed cells/total number of counted macrophages) × (number of macrophages containing engulfed cells/total number of counted macrophages) × 100.

C10. Murine PMN isolation

Murine PMNs were isolated using a Percoll (Sigma) double gradient density centrifugation technique. Bone marrow from two immunocompetent GFP-LC3 mice was collected and flushed in room temperature in a sterile solution of PBS/EDTA. The cells were centrifuged at room temperature for 10 min at 350 × g and resuspended in 2ml PBS/EDTA. The cells were carefully placed on top of 2ml of three different Percoll concentrations (75%, 67%, and 52%) in a 15ml Falcon tube. The solution was centrifuged at room temperature for 30 min at 1100 × g, resulting in three zones, peripheral blood mononuclear cells, PMNs, and red blood cells (RBCs), from the top to the bottom, respectively. PMNs were collected and centrifuged in 4 °C for 10 min at 350 × g. The pellet was collected and resuspended in 0.5 ml water for 25 s to lyse the remaining RBCs. Subsequently, 0.5 ml of 1.8% NaCl was added and the cells were centrifuged in 4 °C for 10 min at 350 × g, washed with 2ml HEPES buffer, and centrifuged again in 4 °C for 10 min at 350 × g. Finally, the pellet was re-diluted in 1ml DMEM complete. The viability of PMNs, checked with trypan blue dye, was over 98% and purity of PMNs (identified as CD11b+/Ly6G+ cells) was >90% by flow cytometry.

C11. FACS sorting and flow cytometry studies

To obtain single lung cell suspensions, lungs were perfused with 20 ml PBS through the right ventricle, cut into small pieces, and digested for 1 h at 37 °C in 1 mg/ml collagenase A (Roche) and 0.05 mg/ ml DNase I (Roche) in Hank's balanced salt solution. For flow cytometric analysis, single lung cells were stained with the following antibodies: anti-CD45-APC (Clone 30-F11, BioLegend, #103111, 1:200 dilution), anti-MHCII-FITC (Clone M5/ 114.15.2, BioLegend, #107605, 1:100

dilution), anti-F4/80-PE (Clone BM8, Bio- Legend, #123109, 1:100 dilution), anti-CD11c-PerCP-Cy5.5 (Clone N418, BioLegend, #117328, 1:100 dilution), anti-CD11b-PE-Cy7 (Clone M1/70, BioLegend, #101215, 1:200 dilution), anti-Ly6G-PE (Clone 1A8, BioLegend, #127607, 1:200 dilution), and anti-Ly6C-FITC (Clone HK1.4, BioLegend, #128005, 1:200 dilution). Flow cytometric data were collected on a MoFloT High-Performance Cell Sorter and were analyzed with FlowJo, version 8.7.1 (Treestar). AMs and interstitial macrophages (IMs) were sorted by flow cytometry based on their differential F4/80/CD11c/MHCII expression [IMs (F4/80+CD11c–/ MHC-II-high), AMs (F4/80+CD11c+/ MHC-II-low), both CD68 positive] (138). PMNs were sorted as MHCII−/CD11b+/Ly6G+ cells. Isolated cells were cultured in RPMI-1640 medium supplemented with 10% fetal calf serum, 2mM L-glutamine, 1mM sodium pyruvate, 0.1mM nonessential amino acids, 50 μM β-mercaptoethanol, 50 μg/ml streptomycin, and 50 IU/ml penicillin (all from Invitrogen), fixed and stained for confocal imaging. Flow cytometric data were collected on a MoFloT High-Performance Cell Sorter and were analyzed with FlowJo, version 8.7.1 (Treestar).

For FACS analysis in CD11c-DTR mice, the following antibodies were used: anti-CD45-APC-Cy7 (Clone 30-F11, BioLegend, #103116, 1:200), anti-CD11c-PerCP-Cy5.5 (Clone N418, BioLegend, #117328, 1:200), anti-I-A/I-E-PE-Cy7 (M5/114.15.2, BioLegend, #107630, 1:200), and anti-Singlec-F Alexa Fluor® 647 (E50-2440, BD Pharmingen, #562680, 1:200). Cells were acquired in a FACS Aria IIu (BD Biosciences) and data were analyzed with the FACSDIVA software (BD Biosciences).

C12. Histopathological and immunohistochemistry studies

Lungs were fixed in 10% formalin, paraffin embedded, cut in 4-μm sections, and stained with hematoxylin and eosin. For immunohistochemistry studies, the anti-CD11c Abs (HL3; BD Biosciences, 1:200 dilution) and anti-CD68 (FA-11, 137001, BioLegend, 1:200 dilution) primary antibodies were used for detection of CD11c and CD68 in tissue. The slide-mounted sections were baked for 10 min at 60 °C, deparaffinized with two xylene washes, rehydrated through a series of graded alcohol washes, rinsed in water, and washed with 0.1M PBS (pH 7.4) containing 0.01% Tween-20. Heatinduced antigen retrieval was performed in a steamer using target retrieval solution (Dako S1700). Endogenous peroxidase was blocked with 3% H_2O_2 for 10 min. The slides were then incubated in blocking solution, i.e. serum-free protein block, Dako X0909, for 20 min to block nonspecific binding. The primary antibodies were added to the slides and incubated overnight in a humidified chamber at 40 °C. Detection was accomplished using an Envision_Horseradish Peroxidase Kit (Dako K0679). Immunostaining was revealed using 3,3′-diaminobenzidine. The slides were lightly counterstained with hematoxylin, progressively dehydrated through graded alcohols and xylene, and finally covered with a coverslip after mounting in distyrene, plasticiser (tricresyl phosphate), and xylene (DPX) mounting medium. Slides were examined under an Olympus light microscope that was equipped with a ×40 objective. In certain experiments fungal conidia were counterstained with periodic acid-Schiff (PAS).

C13. RNA isolation from *Rhizopus*-infected BMDMs

BMDMs, 2×10^6 per condition, obtained following 6 days of differentiation of BM cells of 12-week-old female C57BL/6 mice, were seeded in 12-well plates and left

overnight at 37 °C in DMEM media. Next, BMDMs were washed twice with DMEM complete, infected at an MOI of 1:2 (macrophage:fungal conidia) with *R. delemar* (strain 99-880), and 1 hour later washed five times to remove extracellular conidia. At the indicated time point of infection (1, 4, and 18 h), BMDMs were removed by scraping, centrifuged at 400 × g, and lysed with 450 µl of RLT buffer plus β-mercaptoethanol using the RNeasy Plant Mini Kit (Qiagen). As a negative control, 1×10^7 *R. delemar* conidia were added to the tissue culture plates containing medium alone without host cells and processed in parallel. Another control included RNA extracted from uninfected BMDMs. Then, each sample was sonicated using a sonication probe on ice 20 × 1 s (set 40). Afterwards, isolation of RNAs was performed according to the manufacturer's instructions. More specifically, the lysates were transferred to a QIAshredder spin column, placed in a 2 ml collection tube, and centrifuge for 2 minures at full speed. The supernatant was gently transferred to a new microcentrifuge tube, while the cell-debris pellet in the collection tube remained intact. In the supernatant 0.5 volume of ethanol (96–100%) was added. The sample, including any precipitate that may have formed, was then transferred to an RNeasy spin column, placed in a 2 ml collection tube and centrifuged for 15 seconds at 8000 x g. The flow-through was discarded, 700 µl Buffer RW1 were added to the RNeasy spin column and re-centrifuge at the same conditions. The pellet was suspended with 500 µl Buffer RPE and centrifuged as stated above. Lastly, 500 µl Buffer RPE were added to the RNeasy spin column and the sample was centrifuged for 2 minutes at 8000 x g. The RNeasy spin column was placed in a new 1.5 ml collection tube, 30–50 µl RNase-free water was added directly to the spin column membrane. Centrifuge for 1 minute at 8000 x g followed to elute the RNA.

C14. RNA-seq analysis

All RNA-seq libraries (strand-specific, paired-end) were prepared with the TruSeq RNA Sample Prep Kit (Illumina). The total RNA samples were subjected to poly (A) enrichment as part of the TruSeq protocol. One hundred and fifty nucleotide sequences were determined from both ends of each complementary DNA fragment using the HiSeq platform (Illumina) as per the manufacturer's protocol. Sequencing reads were annotated and aligned to the University of California Santa Cruz (UCSC) mouse reference genome (mm10, GRCm38.75) as well as the *R. delemar* (strain 99-880) genome using TopHat2, a splice junction mapper for RNA-Seq reads. TopHat 2 aligns RNA-Seq reads to mammalian-sized genomes using the latest sequencing technologies, and then analyzes the mapping results to identify splice junctions between exons (139). The alignment files from TopHat2 were used to generate read counts for each gene and a statistical analysis of differential gene expression was performed using the DE-seq package from the open source biostatistical software Bioconductor (140). A gene was considered differentially expressed if the P value for differential expression was <0.05 and the absolute log (base 2) fold change, relative to single organism control, was ≥ 1.

C15. Human studies

Approval for the collection of clinical information and tissue samples from the patient with mucormycosis was obtained and the Ethics Committee of the University Hospital of Heraklion, Crete, Greece (5159/2014). The patient provided written informed consent in accordance with the Declaration of Helsinki.

C16. Statistical analysis

The data were expressed as mean ± SEM. Statistical significance of differences was determined by two-sided nonparametric Mann–Whitney test and one-way analysis of variance with the indicated post hoc test for multiple comparisons ($P < 0.05$ was considered statistically significant). Survival analysis was performed by log-rank (Mantel–Cox) test. Analysis was performed using the GraphPad Prism software (version V). All in vitro experiments were performed at least in triplicate and replicated at least twice.

D. Results

D1. *Rhizopus* conidia persist inside alveolar macrophages of immunocompetent mice

To begin with, we tried to understand general aspects of the physiological immune response against Mucorales. Therefore, we performed an intratracheal infection of immunocompetent B6 mice with $5x10^6$ conidia of either *Aspergillus fumigatus* or two clinical isolates of *Rhizopus* (*Rhizopus oryzae* and *Rhizopus delemar*). Fungal clearance was compared by CFU counts. In addition, at different time points of

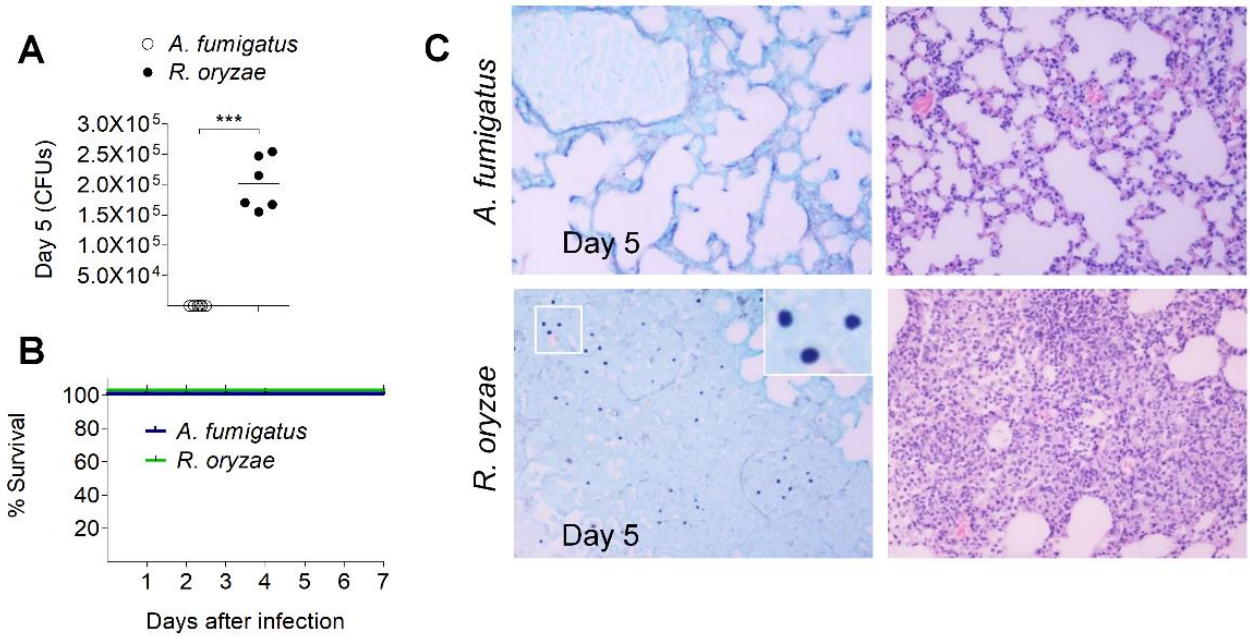

Figure 9. Rhizopus conidia are resistant to killing and remain dormant inside lung phagocytes.

A. Fungal loads in lungs of immunocompetent C57BL/6 (B6) mice (n = 3 per group) infected via intratracheal administration of a standardized inoculum (5 × 106 conidia per mice) of *A. fumigatus*, *R. oryzae*, or *R. delemar*. ***P < 0.0001, Mann–Whitney test. B. Survival of immunocompetent C57BL/6 (B6) mice (n =8 per group) infected as in A, with either *A. fumigatus*, *R. oryzae*, or *R.delemar*. C. Representative photomicrographs of the lungs from mice infected as in B with either *A. fumigatus* or *R.*

oryzae and sacrificed on day 5. Histopathological sections were stained with Grocott methenamine silver (GMS; left panels) or hematoxylin and eosin (H&E; right panels). Excessive tissue oedema and neutrophil infiltration are found in the lungs of mice infected with *R.oryzae.* The presence of *R. oryzae* conidia (black color) in the lungs is shown by GME stain, which remained dormant inside the lung phagocytes. Original magnification ×400.

infection (0, 2, 5, and 10 days) the infected mice were sacrificed and histopathological studies of total lung homogenates were conducted. We found that opposite to *A. fumigatus* conidia, a significant proportion of each *Rhizopus* isolate conidia remained viable in the lungs of immunocompetent mice as late as 10 days post infection (Fig. 9A), whereas none of the infected animals died (Fig. 9B). Histopathology of lung tissue sections collected on day 5 post infecting immunocompetent mice with *R. oryzae* confirmed the presence of abundant conidia in the lungs, which resulted in considerable tissue edema and neutrophil infiltration (Fig. 9C). Interestingly, there was no apparent evidence of *R. oryzae* germination in infected lungs (Fig. 9C).

Up next, we tried to figure out which type of cells are predominantly responsible for the host defence against Mucorales upon pulmonary infection. Immunohistochemistry studies revealed that *R. oryzae* conidia predominantly resided inside CD11c+/CD68+cells, which are consistent with AMs. There was also evidence of extracellular conidia associated with areas of intensive neutrophil infiltration (Fig. 10). For a specific characterization of these cells, we obtained BAL 1 and 5 days after infection of immunocompetent B6 mice with fluorescence-labeled conidia of *R. oryzae* and assessed kinetics of recruitment as well as degree of association of myeloid cells using FACS.

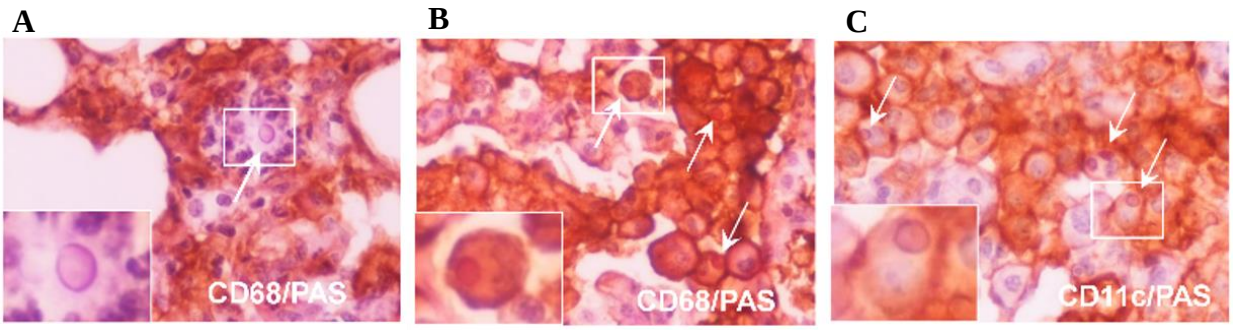

Figure 10. Rhizopus conidia reside inside AMs. Representative photomicrographs of the lungs from C57BL/6 (B6) mice (n = 3 per group) infected via intratracheal administration of a standardized inoculum (5×10^6 conidia per mice) of *A. fumigatus, R. oryzae,* or *R. delemar,* sacrificed on day 5. Lungs were stained by IHC for CD68 or CD11 and counterstained with hematoxylin and PAS. There is evidence of extracellular *R. oryzae* conidia surrounded by neutrophils (A), and intracellular *R. oryzae* conidia inside AMs (B and C).

Although we found a significant influx of neutrophils (identified as CD45+/CD11b+/Ly6G+/Ly6C− cells; Fig. 11A) and Ly6Chigh inflammatory monocytes (identified as CD45+/CD11b+/Ly6G−/CD11c−/Ly6C+ cells; Fig. 11B) in the lungs on days 1 and 5 of infection (Fig. 11C), most *R. oryzae* conidia were associated with AMs (identified as CD45+/F4/80+/CD11c+/MHCII low cells), interstitial macrophages (IMs; identified as CD45+/F4/80+/CD11c−/MHCII+), and DCs (identified as CD45+/F4/80−/CD11c +/MHCII+) in the lungs of immunocompetent mice (Fig. 11D). To distinguish which cell type was associated with *R.oryzae* phagocytosis, neutrophils, AMs, and IMs on day 5 post infection were sorted, stained with Cathepsin D (a cytoplasmic staining) and finally assessed with confocal microscopy. Our results confirmed that *R. oryzae* conidia were predominantly phagocytosed by AMs (Fig. 11 E,F) and not neutrophils. Collectively, these studies demonstrate that AMs are the cornerstone of host defense upon pulmonary Mucormycosis. Moreover, we proved that a significant proportion of *Rhizopus* conidia remain viable inside AMs for several days following infection of immunocompetent mice.

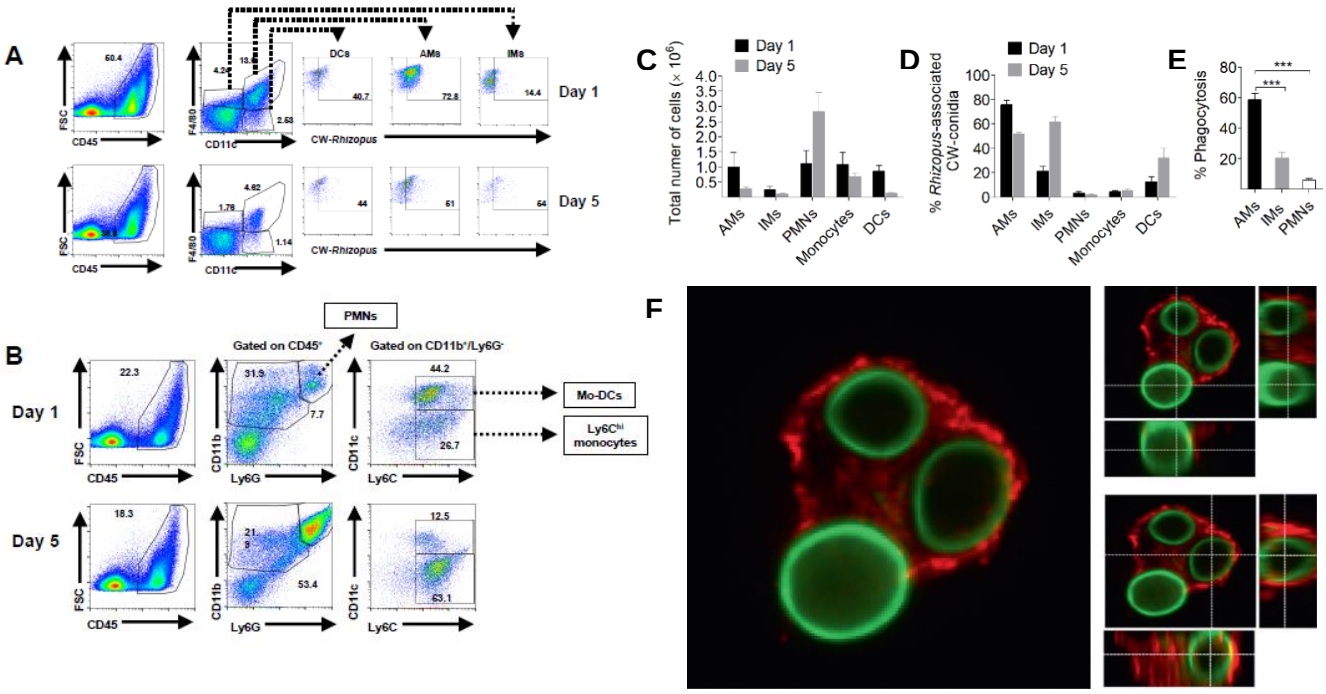

Figure 11. Selective tropism and prolonged intracellular persistence of *Rhizopus* conidia inside AMs. **A-B.** FACS analysis of lung professional phagocytes following infection of C57BL/6 (B6) mice with R. oryzae. Gating strategy for identification of professional phagocytic cells in the lung following R. oryzae infection by FACS analysis. (A). Identification of AMs, IMs, and DCs based on CD11c and F4/80 expression of CD45+ cells. Association of fluorescent Brightener 28; CW-labeled R. oryzae conidia with each cell population is shown. (B). Identification of Neutrophils, monocyte-derived DCs (mo-DCs) and Ly6Chimonocytes based on expression of CD11b, Ly6G, Ly6C, and CD11c of CD45+ cells. **C**. FACS analysis of total number of professional phagocytes in the lungs of C57BL/6 (B6) mice immunocompetent mice (n = 3 per group) infected via intratracheal administration of a standardized inoculum (5×10^6 conidia per mice) with *R. oryzae* assessed on days 1 and 5. **D**. FACS analysis of association of labeled (Fluorescent Brightener 28; CW) conidia of *R. oryzae* with professional phagocytes of mice infected as in **C**, assessed on days 1 and 5. **E.** In vivo phagocytosis rates of R. oryzae conidia on day 5 of infection of mice infected as in **C**. ***P < 0.0001 Mann–Whitney test. **F.** Representative confocal image of sorted AM from mice infected as in a with fluorescent-labeled, live conidia of R. oryzae (day 1), fixed and stained with Cathepsin Cross-section analysis was performed to discriminate intracellular conidia from conidia associated/bound to the cell surface of AM.

D2. *Rhizopus* conidia are resistant to killing by macrophages

In order to shed light on the mechanisms of intracellular persistence of *Rhizopus*, we studied interactions of BMDMs and neutrophils with conidia of *A. fumigatus* or *R. oryzae*. Hypothesizing that the relative big size of *R. oryzae* conidia is associated with impaired phagocytosis, we performed ex vivo experiments using BMDMs and neutrophils from GFP-LC3 mice. Both were infected with 10^5 *A. fumigatus* or *R. oryzae* dormant conidia at MOI 1:2 (effector cells: fungi), the cells were fixed with 4% PFA. Phagocytosis was assessed in different time points over 2 hours with confocal microscopy. As expected, *A. fumigatus* conidia were comparably phagocytosed by BMDMs and neutrophils. On the contrary, *R. oryzae* were almost exclusively phagocytosed by BMDMs and, despite their larger size, at a significantly higher index rate than *A. fumigatus* conidia (Fig. 12A–C).

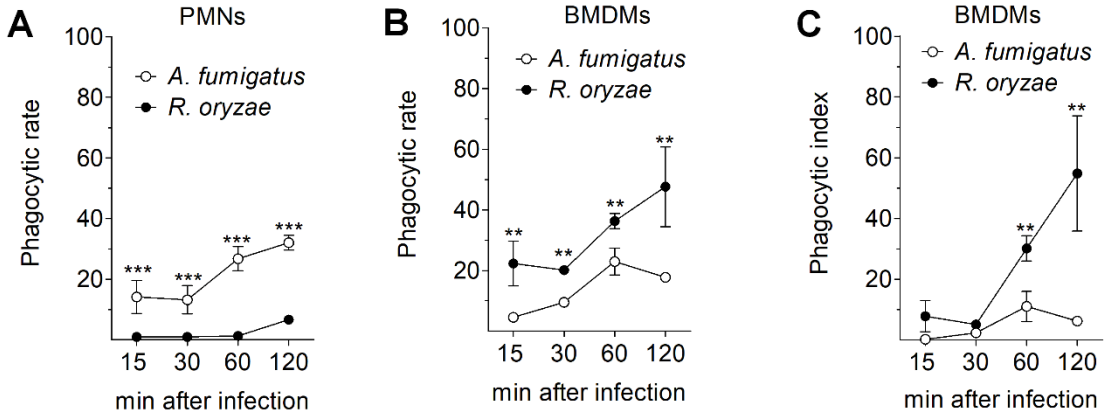

Figure 12. *Rhizopus* conidia are phagocytosed by BMDMs. Comparative studies on phagocytosis of *A. fumigatus* and *R. oryzae* conidia by (A) neutrophils (PMNs) and (B,C) BMDMs, assessed by confocal imaging. Data on quantification of phagocytosis are presented as mean ± SEM of five independent experiments ***P < 0.0001, **P < 0.001, Mann–Whitney test.

Next, we compared killing rates of *A. fumigatus* vs. different strains of *Rhizopus* conidia by BMDMs ex vivo. BMDMs were infected with the indicated *Rhizopus* and *A. fumigatus* strains ($5x10^5$ and 10^6 conidia respectively) at a MOI of 1:1 and unbound conidia were removed by extensive washing. Cells were lysed 2 or 6 hours post-infection and the assessment of percentage of killing of conidia was counted based on viability intracellular conidia. We found that unlike *A. fumigatus*, different clinical isolates of *Rhizopus* were resistant to killing by BMDMs (Fig.13).

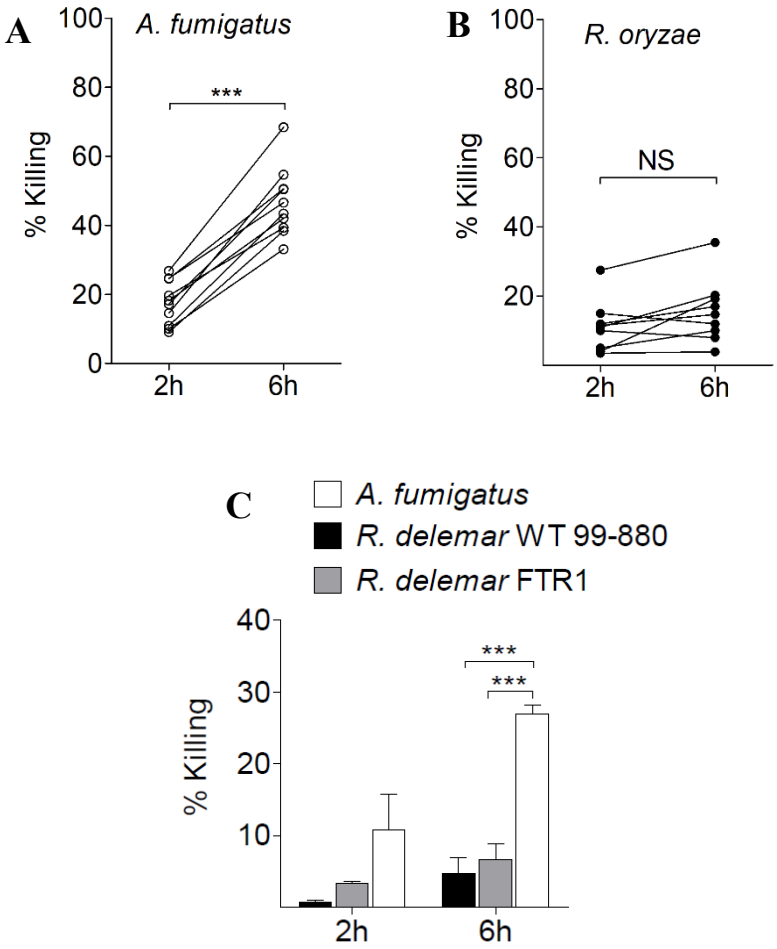

Figure 13. Mucorales is resistant to killing by BMDMs. **A-B.** Intracellular killing of (A) *A. fumigatus* and (B) R. oryzae conidia by BMDMs. Symbols connected with a line represent time points of the same independent experiment (n = 9 per group). ***P < 0.0001, Mann–Whitney test. **C.** Intracellular killing of different *Rhizopus* clinical isolates compared to *A.fumigatus.* Data on quantification of killing are presented as mean ± SEM of three independent experiments. *** *P*< 0.0001, unpaired Student's *t* test

D2.1. Comparable in vitro susceptibility of *Rhizopus* and *A. fumigatus* conidia to oxidative and non-oxidative immune effector mechanisms of macrophages.

Since the phagocytosis of *Rhizopus* conidia proved to be intact, the mechanisms of *Rhizopus* persistence inside macrophages remained unclear. Therefore, we tested whether fungal conidia are resistant to damage by phagocyte effector mechanisms. We compared susceptibility of *A. fumigatus vs. R. oryzae* conidia to (i) oxidative damage induced by hydrogen peroxide (H_2O_2) and (ii) non-oxidative damage mediated by lysosomal hydrolases. $5x10^4$ conidia from each fungus were incubated for 24 hours either with increasing concentrations of H_2O_2 or crude lysosomal extracts in RPMI-MOPS-2% Glucose medium with pH 5.5. The fungal metabolic activity was assessed with XTT colorometric assay. In addition, fungal viability was further estimated with plating in triton X plates and CFUs. Conidia of both fungi displayed comparable degree of susceptibility to killing by increasing concentrations of either H_2O_2 (Fig. 14C) or crude lysosomal extracts (Fig. 14 A,B,D). Therefore, the inability of BMDMs to kill *Rhizopus* could not be explained by resistance to oxidative or non-oxidative damage. Next, we investigated if *A. fumigatus* and *R. oryzae* vary in their ability to induce host cell apoptosis or necrosis, as a survival strategy that allows the fungus to escape host defense. BMDMs were infected with *A. fumigatus* and *R. oryzae* dormant conidia at MOI 3:1 (effector: fungal cells). 30 minutes after the infection the wells were washed to remove the non-phagocytosed spores. After 6 hours the BMDMs were collected, stained with Annexin-PI and their viability was assessed with FACS. We found no difference between the two fungi in induction of either form of host cell death during interaction with murine BMDMs (Fig. 15)

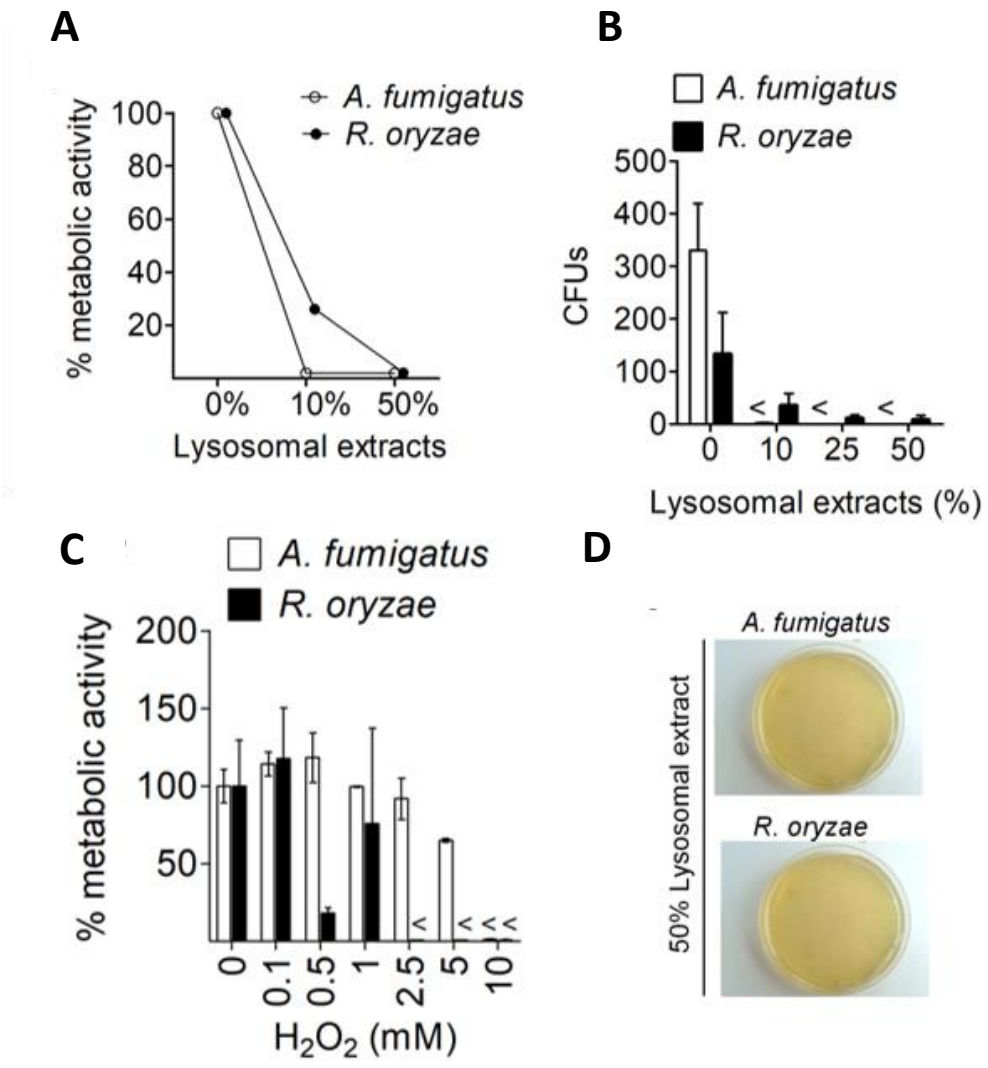

Figure 14. Rhizopus conidia are susceptible to phagocyte effector mechanisms. Assessment of in vitro susceptibility of *A. fumigatus* and *R. oryzae* conidia to **(A)** damage induced by enzymatic activity of increasing concentrations of lysosomal extracts of BMDMs or to **(C)** oxidative damage induced by increasing concentrations of H_2O_2 assessed by measurement of fungal metabolic activity using the XTT assay at 24 hours. **B.** In vitro fungicidal activity of increasing concentrations of lysosomal extracts against conidia of *A. fumigatus* or *R. oryzae* assessed by CFU plating. **D**. Lack of CFUs formation after plating *A.fumigatus* and *R.oryzae* incubated for 24 hours with 50% crude lysosomal extracts.

.

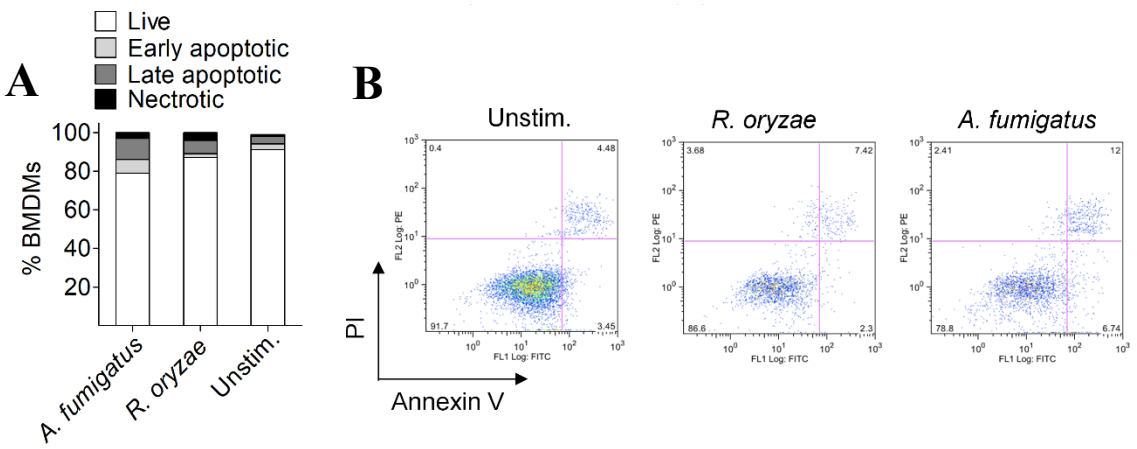

Figure 15. BMDMs remain viable upon infection with Rhizopus conidia. **A.** Induction of apoptosis in unstimulated BMDMs or BMDMs infected with *A. fumigatus* or *R. oryzae* for 6 h. **B.** Apoptotic BMDMs were assessed by FACS analysis following Annexin V/PI staining. Data are representative of one out of three independent experiments. NS not significant

Collectively, these data demonstrate that Mucorales is satisfactory phagocytosed by macrophages, can be killed by their effector mechanisms but yet it survives inside macrophages by avoiding phagocyte-mediated killing.

D3. *Rhizopus* conidia induce phagosome maturation arrest via targeting LAP

To understand the mechanism of establishment of *Rhizopus* intracellular persistence, we performed comparative phagosome biogenesis studies following phagocytosis of *A. fumigatus* or *R. oryzae* by BMDMs. As previously described, LC3-associated phagocytosis (LAP) is a major antifungal pathway regulating early events in biogenesis of *A. fumigatus* phagosome. Nevertheless, there is lacking knowledge concerning LAP and *Rhizopus* phagosome. We initially analyzed LC3+ phagosome (LAPosome) formation at different time points of infection by confocal imaging. BMDMs from GFP-LC3 mice were infected with live *A.fumigatus* and *R.oryzae* conidia at MOI 1:5 and 1:2 respectively (effector: fungal cells). In sharp contrast to

the robust activation of LAP pathway upon infection with *A. fumigatus*, we found no evidence of LAPosome formation during infection of BMDMs with *R. oryzae* (Fig. 16 A,B).

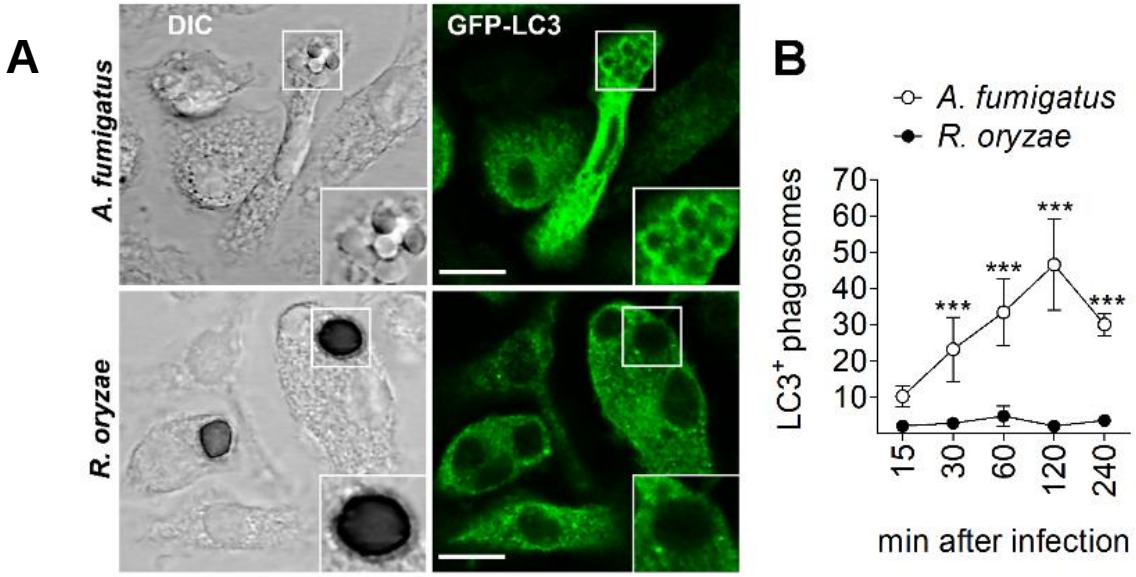

Figure 16. *Rhizopus* actively blocks LAP. BMDMs from GFP-LC3 mice were infected at different time points with live conidia of A. fumigatus or R. oryzae. At the indicated time point, cells were fixed and analyzed by confocal microscopy.**A.** Representative fluorescence images. Bar, 5 μm. **B.** Data on quantification of LC3+ phagosomes are presented as mean ± SEM of five independent experiments. ***P < 0.0001, Mann–Whitney test. Bar 5μm

As described above, the accumulation of Rab5, an early phagosomal marker, was evaluated. Similarly, Rab5 recruitment to the phagosome selectively and transiently occurred at early time points of BMDM infection with *A. fumigatus*, while there was no evidence of Rab5 localization in *R. oryzae*-containing phagosomes (Fig. 17).

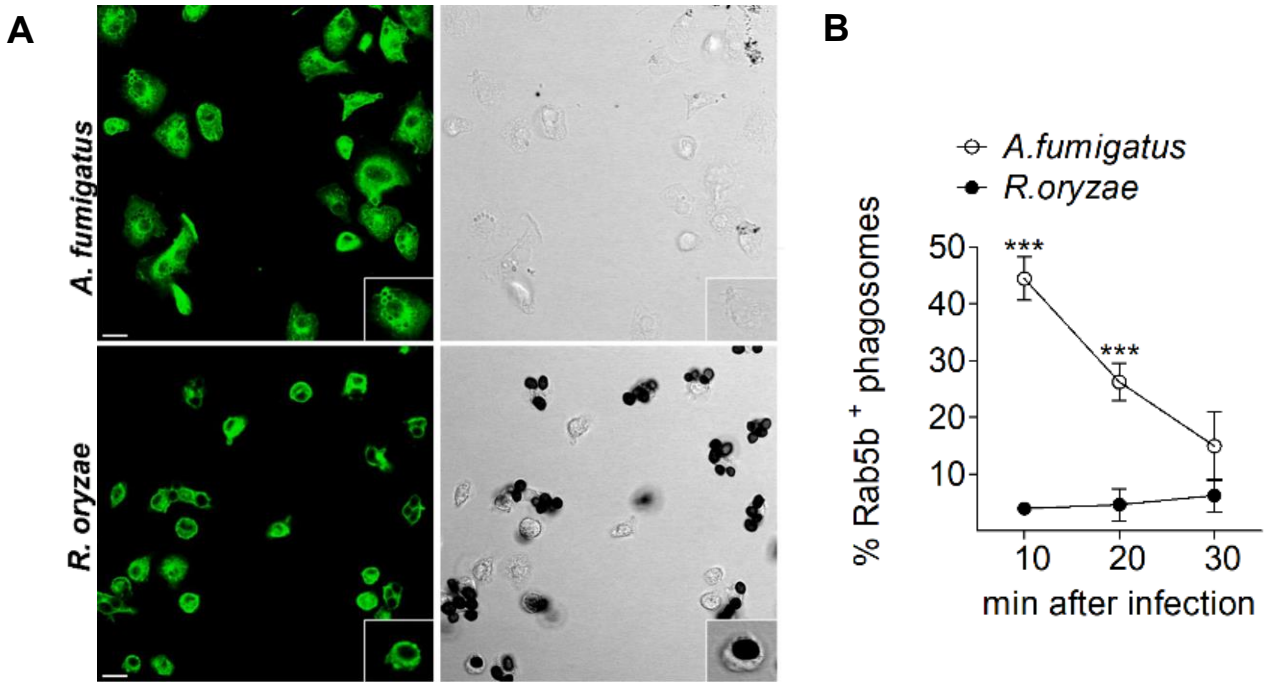

Figure 17. Rab5 is not recruited in *Rhizopus* containing phagosomes. **A.** BMDMs were infected with conidia of *Rhizopus* or *A. fumigatus* conidia, fixed at 10 min of infection, stained for Rab5 and assessed by confocal imaging. Representative fluorescence images taken from an experiment out of three are shown. Rab5 recruitment is evident only in *A. fumigatus* phagosomes (inset). Bar, 5 μm. **B.** Data on quantification of Rab5+ phagosomes are presented as mean ± SEM of three independent experiments. ***P < 0.0001, Mann–Whitney test. Bar 5μm

Next, we monitored phagolysosomal (P–L) fusion upon BMDMs infection with *A. fumigatus* vs. *R. oryzae* with the use of fluorescein isothiocyanate-labeled dextran (FITC-Dextran) assay. FITC-Dextran has the ability to be phagocytosed and reside inside lysosomes, being an exceptional marker for the P-L fusion. BMDMs were pre-loaded for 16 hours with FITC-Dextran for labeling of lysosomes and P–L fusion upon fungal infection was assessed based on accumulation of FITC-Dextran in the phagosomes with confocal imaging. BMDMs were infected with live *A.fumigatus*

and *R.oryzae* conidia at MOI 1:5 and 1:2 respectively (effector: fungal cells). Of interest, in contrast to the accumulation of FITC-Dextran in *A. fumigatus* containing phagosomes over time (Fig. 18 A,B), there was no evidence of FITC-Dextran recruitment in *R.oryzae* phagosomes. Concordant with these results, recruitment of Cathepsin D, a lysosomal hydrolase, in phagosomes was significantly impaired at 4 hours of BMDM infection with *R. oryzae* as compared to *A. fumigatus* (Fig. 18 C,D). Further, these findings were confirmed by electron microscopy studies on fusion of acid phosphatase-stained lysosomes with *A. fumigatus* vs. *R. oryzae* phagosomes. Notably, while P–L fusion was evidenced as intense acid phosphatase staining in *A. fumigatus* phagosomes at 4 hours of infection, there was no lysosomal association with *R. oryzae* phagosomes (Fig. 18E). These results were supported by in vivo studies in AMs of immunocompetent mice. GFP-LC3 or B6 mice were intratracheally infected with 5×10^6 conidia of either live *R. oryzae* or *A. fumigatus* conidia. AMs were obtained by BAL 2 and 4 hours post-infection, fixed, stained with anti-GFP or Cathepsin D antibodies respectively, and assessed by confocal imaging. The absence of LC3 and Cathespin D recruitment in *Rhizopus* containing phagosomes revealed the ability of Mucorales conidia to block P–L fusion by inhibiting LAP (Fig. 19A–D). Collectively, these studies confirm that *Rhizopus* conidia block LAP and induce phagosome maturation arrest to establish intracellular persistence inside the macrophage.

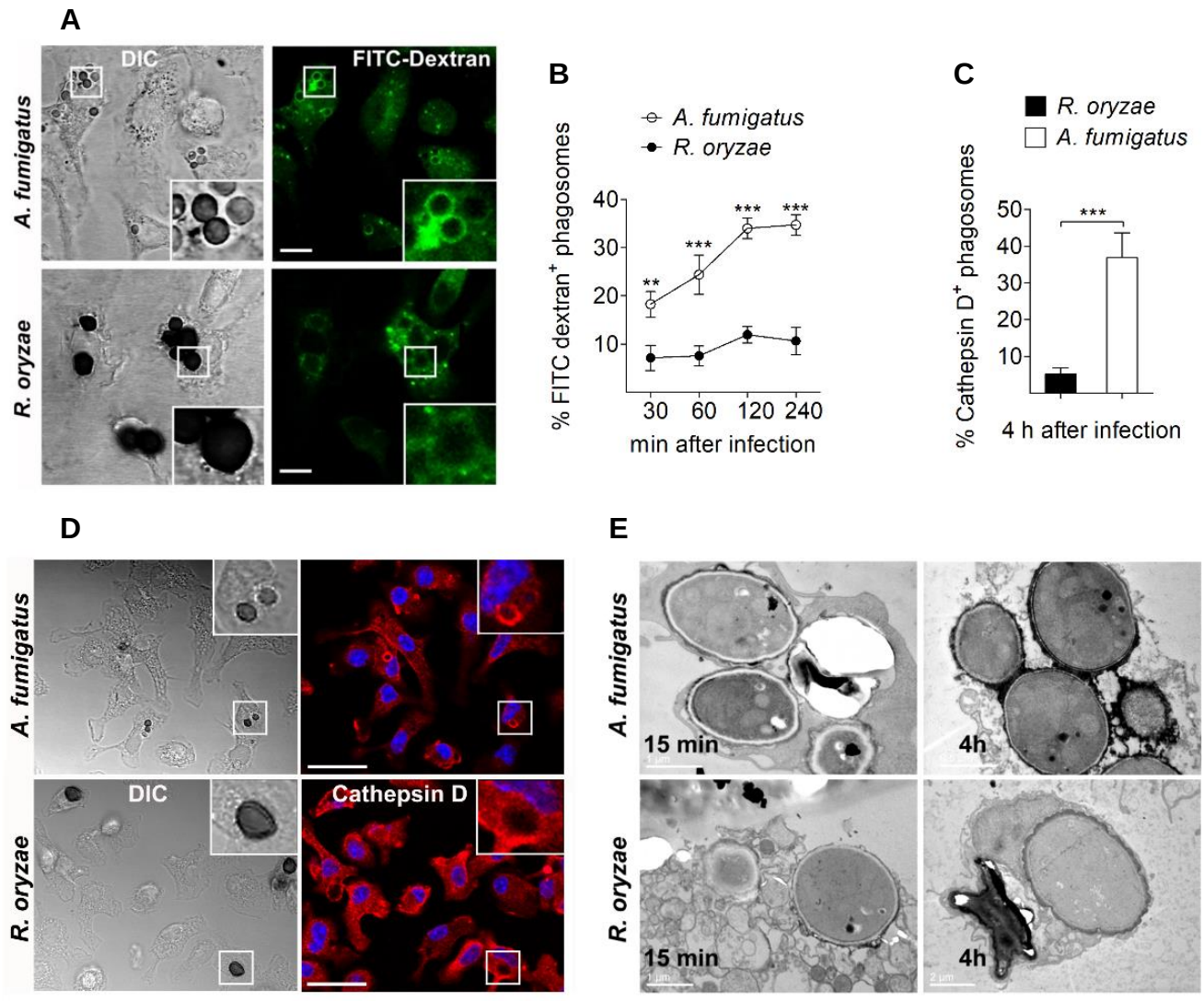

Figure 18. Mucorales conidia to block phagolysosomal fusion by inhibiting LAP. A, B. BMDMs were pre-loaded with FITCDextran, infected with live *A.fumigatus* and *R.oryzae* conidia (at MOI 1:5 and 1:2 respectively) and phagolysosomal fusion was assessed at 4 hours post-infection based on acquisition of FITC-Dextran in the phagosome. Representative fluorescence images are shown in **A**. Bar, 5 μm. Data on quantification of FITC-Dextran+ phagosomes are presented in **B** as mean ± SEM of three independent experiments. **C, D.** BMDMs were stimulated as in a, cells were fixed and stained for the lysosomal protein marker Cathepsin D. Data on quantification of Cathepsin D+ phagosomes are presented as mean ± SEM of three independent experiments in **C**, while representative fluorescence images are shown in **D**. Bar, 5 μm. **E.** Representative electron microscopy of acid phosphatase, a lysosomal enzyme marker of phagolysosomal fusion (shown as dark color on the phagosome membrane) in 15 min and 4 h phagosomes containing *A.*

fumigatus or *R. oryzae conidia*. ***P < 0.0001, **P < 0.01, Mann–Whitney test. Bar, left upper and lower panels, 1 μm; right upper panel, 0.5 μm; right lower panel, 2 μm

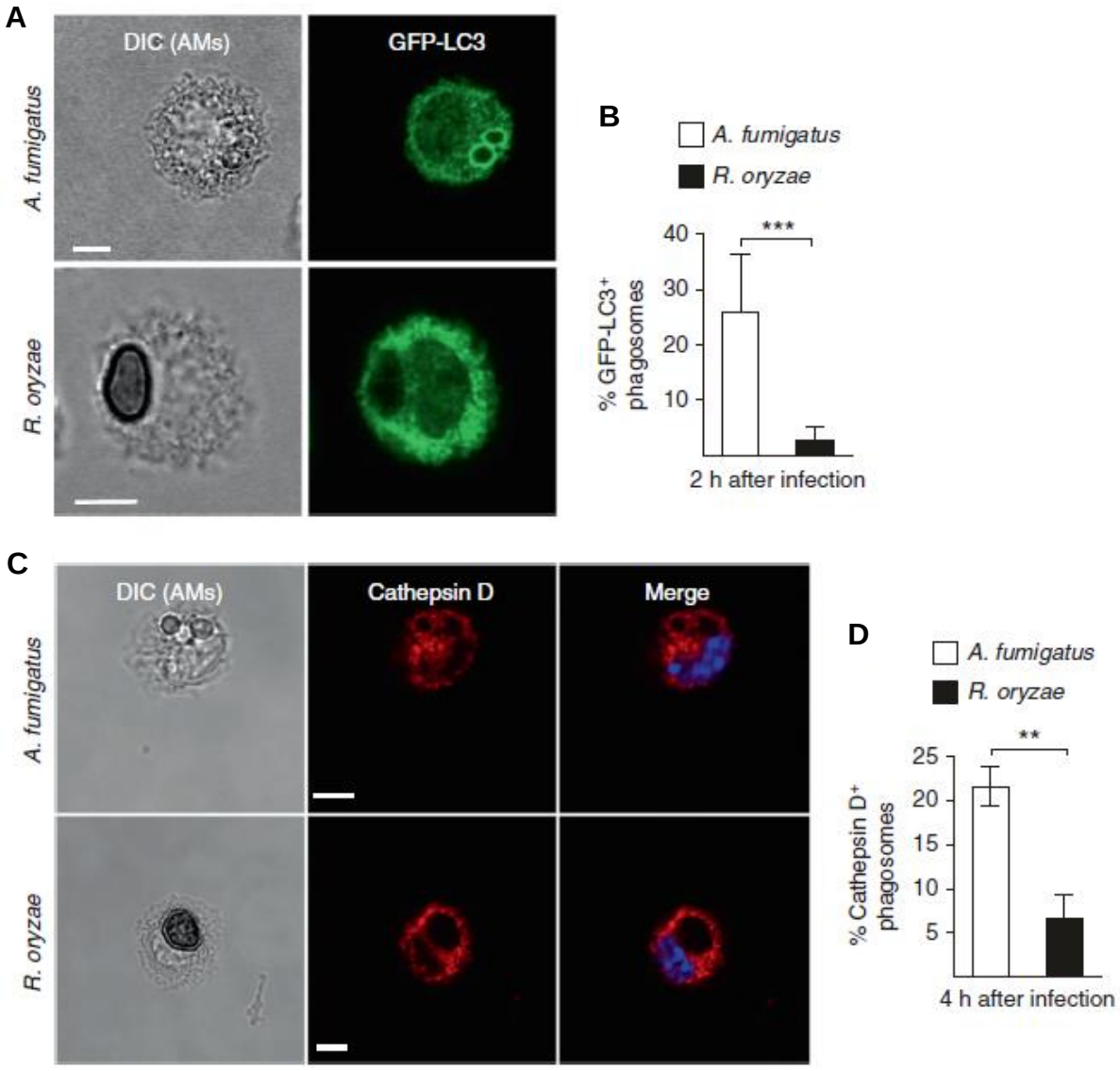

Figure 19. *Rhizopus* inhibits phagosome biogenesis in AMs during in vivo infection. GFP-LC3 (A, B) or C57BL/6 (B6) (C, D) mice were infected intratracheally with either *R. oryzae* or *A. fumigatus*. AMs were obtained by BAL at the indicated time point, fixed, stained with anti-GFP or Cathepsin D antibodies, and assessed by confocal imaging. Representative fluorescence images are shown (A, C). Data on quantification of GFP-LC3+ (B) and Cathepsin D+ (D) phagosomes are presented as mean ± SEM of three independent experiments. ***P < 0.0001, **P < 0.001 Mann–Whitney test. Scale bar, 5 μm

D4. Mucorales cell wall melanin induces phagosome maturation arrest

Recent work from our lab showed that cell wall melanin on dormant conidia of *A. fumigatus* blocks LAP to inhibit phagosome biogenesis and promote fungal pathogenicity. In addition, we revealed that removal of melanin during intracellular swelling of *A. fumigatus* conidia is a fundamental requirement for activation of LAP and efficient killing of the fungus by monocytes/macrophages (1). Thus, we assessed whether a similar mechanism is responsible for the phagosome maturation arrest seen with *R. oryzae* conidia. GFP-LC3 BMDMs were infected at 1 or 24 hours with live conidia of *A. fumigatus* or *R. oryzae* at an MOI 1:1. Cells were fixed and the conidial diameters of intracellular conidia were measured by confocal microscopy. Intriguingly, unlike *A. fumigatus* conidia, *Rhizopus* conidia remained dormant without evidence of cell wall swelling at 24 hours of infection in BMDMs (Fig. 20 A, B).

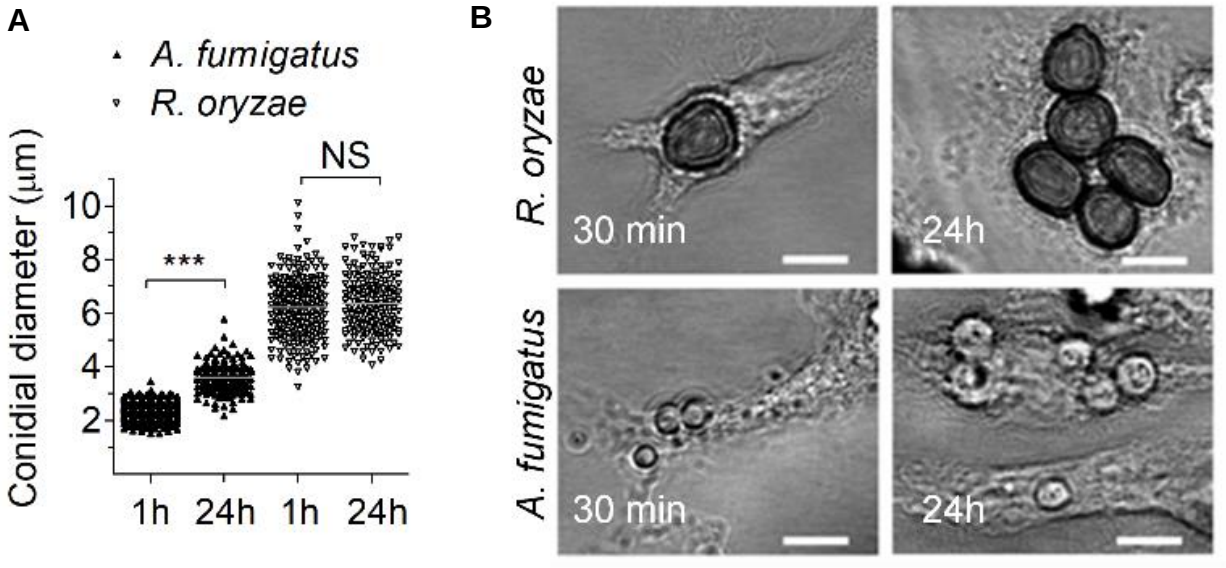

Figure 20. *Rhizopus* conidia remain dormant inside BMDMs. A. GFP-LC3 BMDMs were infected at 1 or 24 h with live conidia of *A. fumigatus* or *R. oryzae*. The conidial diameters of intracellular conidia were measured by confocal microscopy. Data on quantification of conidial diameter are presented from one out

of three independent experiments. Each symbol represents the value of maximum diameter of individual fungal cell and horizontal bars represent the mean diameter. ***P < 0.0001, Mann–Whitney test. **B.** Representative DIC images from A are shown. Scale bar, 10 μm

These results were confirmed in vivo, after intratracheal infection of GFP-LC3 immunocompetent mice with 5 X 10^6 conidia of either *A. fumigatus* or *R. oryzae*. AMs were obtained by BAL at 2 and 24 hours of infection. At the indicated time point cells were fixed, stained with anti-GFP and the conidial diameters of intracellular conidia was measured by confocal microscopy. As shown in Figure 21 (A, B) in sharp contrast to *A.fumigatus*, *R.oryzae* conidia remained dormant inside AMs.

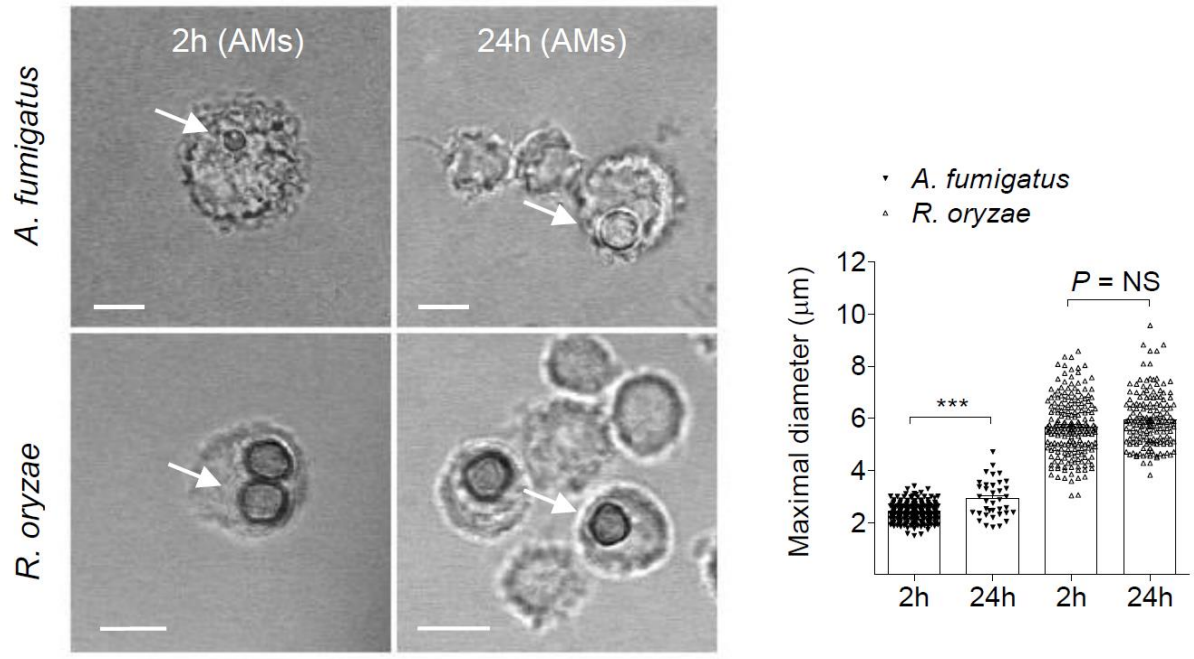

Figure 21. *In vivo* assessment of the size of conidia of *A. fumigatus*vs. Mucorales inside AMs.

A. Representative DIC images from B are shown. **B.** Data on quantification of conidial diameter are presented from one out of three independent experiments. Each symbol represents the value of maximum diameter of individual fungal cell and horizontal bars represent the mean diameter. *** P < 0.0001, Mann Whitney test. Scale bar, 10 μm

This finding corroborates the lack of apparent germination of *R. oryzae* conidia in the lungs of immunocompetent mice. Therefore, in all likelihood, lack of cell wall remodeling in Mucorales conidia results in surface retention of cell wall inhibitory molecule(s) to block phagosome responses and establish intracellular persistence. To test this hypothesis, we infected BMDMs preloaded overnight with FITC-dextran with live conidia or ultraviolet (UV) killed conidia of *Rhizopus* or A. fumigatus conidia at a MOI of 2:1. Cells were fixed at 4h of infection and assessed by confocal imaging. We found that UV-inactivated conidia of Mucorales induce phagosome maturation arrest in BMDMs to a similar degree of live conidia (Fig. 22), implying the presence of an inhibitory molecule on the fungal cell wall surface.

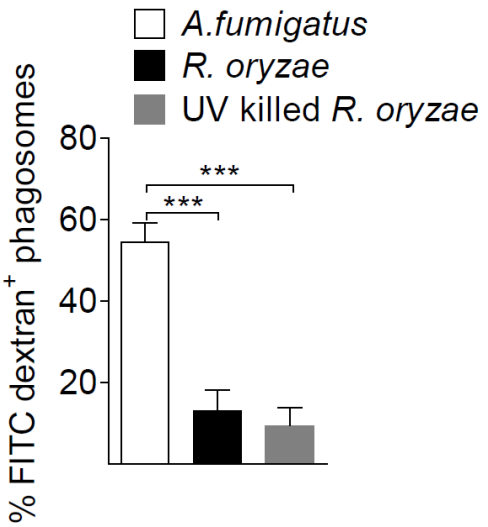

Figure 22. UV killed conidia of *Rhizopus* retain the ability to block phagosome maturation. Data on quantification of FITC-Dextran+ phagosomes are presented as mean ± SEM of three independent experiments. *** P < 0.0001, one-way ANOVA and Dunnett's multiple comparisons post-hoc test.

Despite the differences in cell wall composition of filamentous fungi, melanin is a common cell wall molecule in conidia of many filamentous fungi including *Aspergillus* (107, 141). Therefore, we purified melanin from conidial cell wall of *Rhizopus* spp. and performed comparative characterization with *A. fumigatus* 1, 8-dihydroxynaphthalene (DHN) melanin. Notably, we found that *Rhizopus* melanin exhibited all the classic characteristics of melanin pigments (Table 2). However, UV spectrophotometry (Fig. 23A), EPR (Fig. 23B), IR spectroscopy (Fig. 23C), and chemical degradation followed by LC- MS studies of the degradation

Experiment	Result
Solubility in water	Insoluble
Solubility in organic solvents (chloroform, methanol, ether, acetone, ethyl acetate and DMSO)	Insoluble
Color	Blackish brown
Solubility in 1 N (5%) KOH	Soluble
Precipitation in 0.1 -4N HCL	precipitated
Reaction for polyphenols with $FeCl_3$ test	Brown flocculent precipitate

Table 2. Solubility of *R. delemar* pigment in different solvents.

products (Fig. 23 D, E) revealed that *Rhizopus* melanin is different than DHN melanin of *A. fumigatus*. In particular, *Rhizopus* melanin has chemical composition consistent of eumelanin, and requires a biosynthetic pathway, which likely involves activity of a copper-dependent tyrosinase/ laccase. Indeed, growth in copper-free media resulted in the production of albino conidia of *Rhizopus*.

To shed light into the importance of cell wall melanin regarding the phagosome maturation arrest, BMDMs were pre-loaded with FITC-Dextran for 16 hours, stimulated with conidia of *A. fumigatus* or *R. oryzae* or purified melanin particles (melanin ghosts) obtained from conidia of the indicated *A. fumigatus* or *R. oryzae* strains at an MOI of 1:5 and 1:2 (effector:fungal conidia) respectively. Cells were removed at 4 h and assessed by confocal imaging. Our results demonstrated that both types of melanin induced complete phagosome maturation arrest (Fig. 24A).

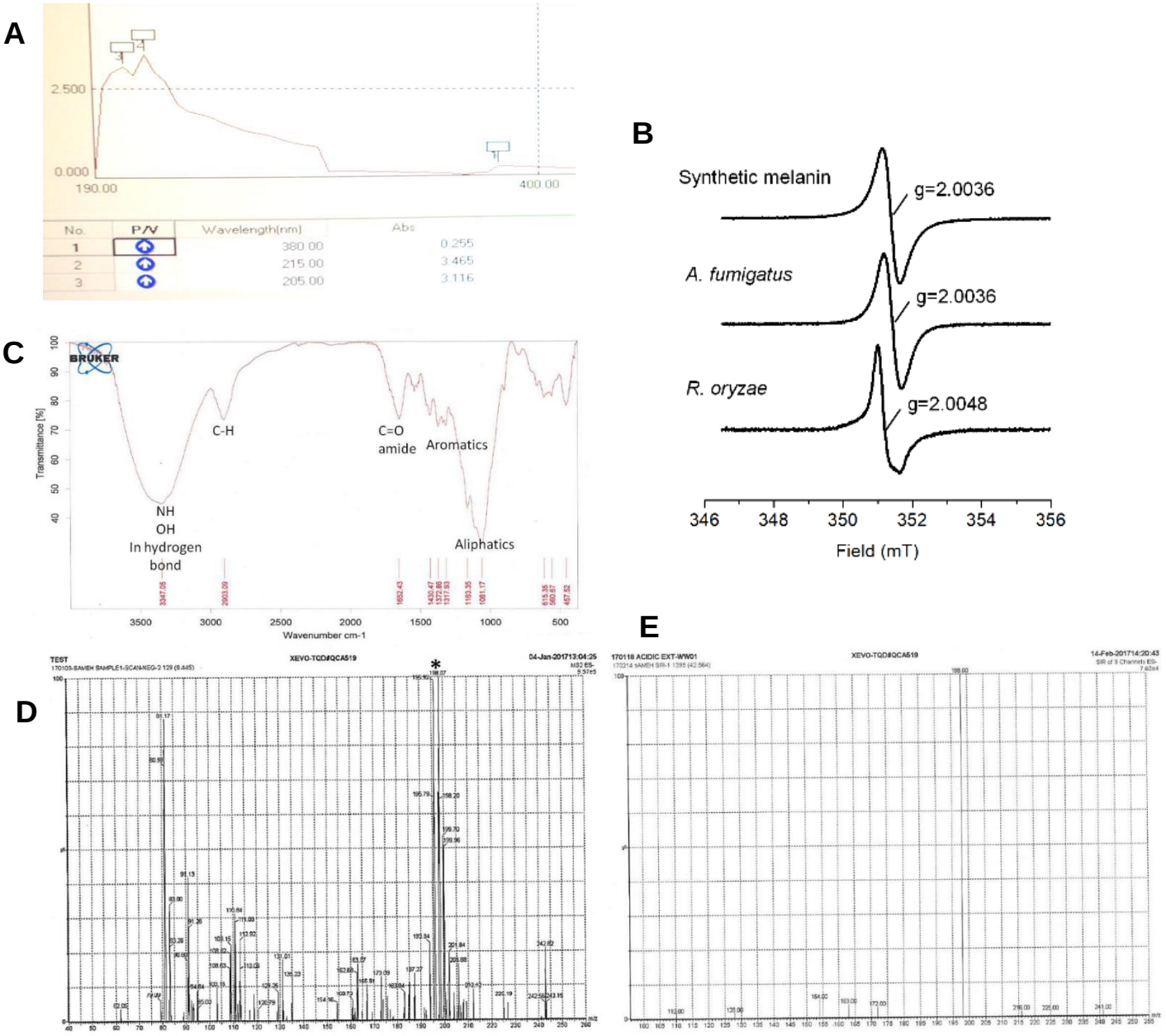

Figure 23. Characterization of *Rhizopus* melanin. A. UV absorbance of extracted pigment in 5% KOH. Two major peaks at 215 and 205 nm indicative of melanin pigment-like substance. **B.** X-band room temperature EPR spectra of purified melanin obtained from *A. fumigatus*, *R. oryzae*, or synthetic melanin are shown. **C.** IR spectroscopy of the pigment in KBrdisc. The signals in the 3600-2800 cm^{-1} area are attributed to the stretching vibrations of (O-H and N-H) of the carboxylic acid. Phenolic and aromatic amino functions present in the indolicand pyrrolic systems. 1750 and 1550 cm^{-1} the bending vibrations of the C=O double bond (COOH) can be found as well as the ones of the carbon-carbon double bond, the carbon-

nitrogen bond of the aromatic system and of the carbon-oxygen double bond of those carboxylic functions that are interested in the bond formation with the metal ions. The OH bending of the phenolic and carboxylic groups were present in the 1400-1300 cm^{-1}area. The out-of-plane bending of the aromatic carbon hydrogen bond can be found in the 700-600 cm^{-1}area. **D-E.** LC-MS analysis of the alkaline hydrolyses product. **(D)** LC-MS scan for major peaks of the pigment hydrolyses products. (**E)** Mass fragmentation pattern of the M/Z 198 peak.

As a further proof of the melanin-dependent induction of phagosome maturation arrest by intracellular conidia of *Rhizopus*, we assessed LAPosome formation and Cathepsin D recruitment upon chemical degradation of *Rhizopus* melanin via H_2O_2 bleaching, as described in (142). Briefly, $5x10^6$ *Rhizopus* conidia were incubated with 1ml H_20_2 10% for 1 hour in 65^0C. Macroscopically after the treatment the conidia were depigmented. The chemical removal of melanin from conidia of *Rhizopus* resulted in reversal of phagosome maturation arrest as evidenced by the significant increase in recruitment of LC3 II (Fig. 24B, D) and Cathepsin D (Fig. 24C, E) to the phagosomes containing melanin-deficient (albino) *Rhizopus*. To further support of the ex vivo experiments, immunocompetent B6 mice were infected intratracheally with 10^6 conidia of either *R. delemar* grown in regular media (WT *Rhizopus*) or under conditions of copper starvation to inhibit melanization (albino *Rhizopus*) (Fig. 24F). The albino *Rhizopus* conidia were rapidly cleared from the lungs, when compared to infection with WT (control) melanized *Rhizopus* conidia (Fig. 24G). Collectively, these findings demonstrate that surface retention of melanin in dormant conidia of *Rhizopus* inside macrophages is the mechanism that accounts for prolonged intracellular persistence.

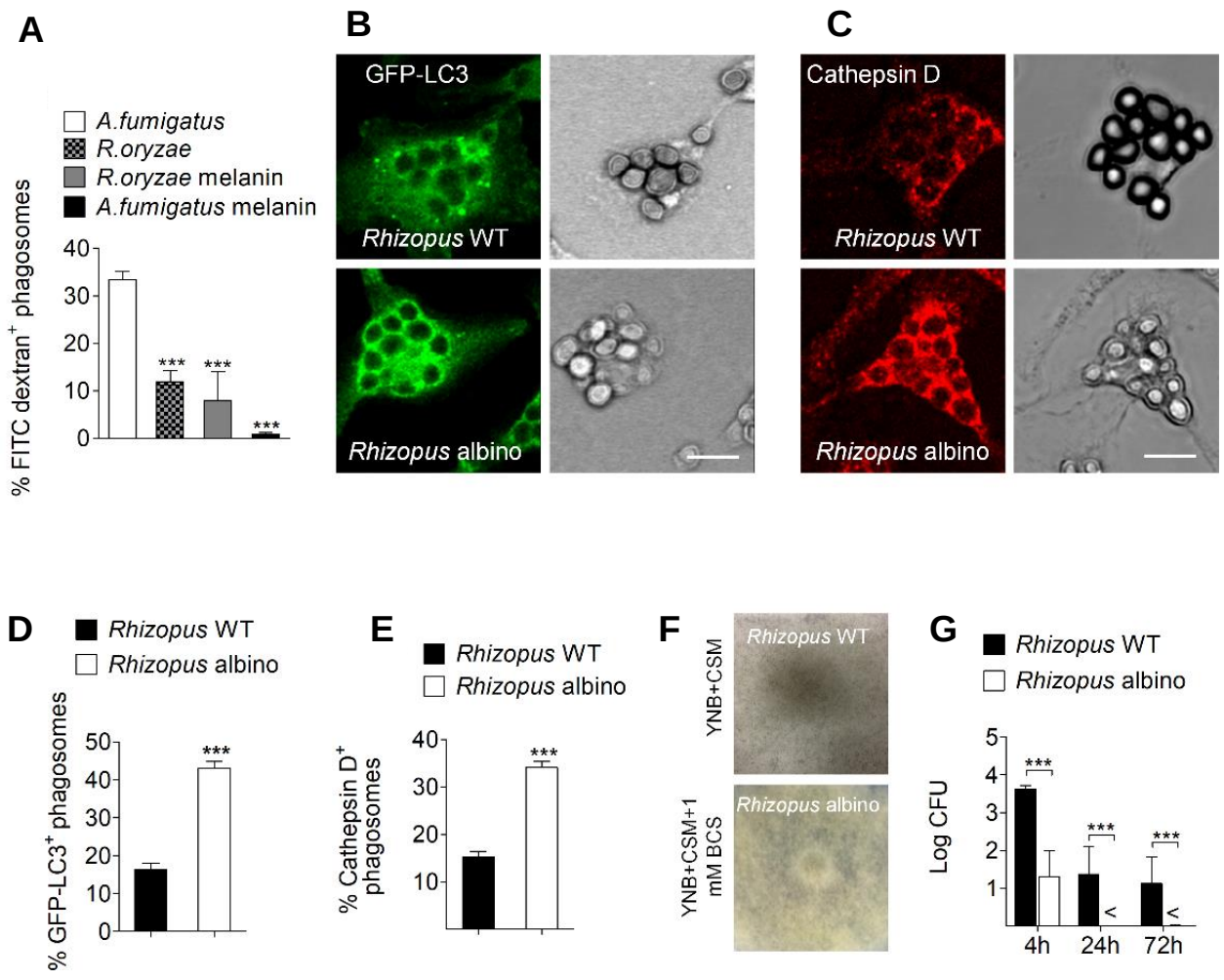

Figure 24. Melanin removal from conidia of *Rhizopus* resulted in reversal of phagosome maturation arrest. A. BMDMs pre-loaded with FITC-Dextran were stimulated with conidia of *A. fumigatus* or *R. oryzae* or melanin ghosts (purified melanin particles) obtained from conidia of the indicated *A. fumigatus* or *R. oryzae* strains at an MOI of 1:5 and 1:2 (effector: fungal conidia) respectively. Cells were removed at 4 hours and assessed by confocal imaging. Data on quantification of FITC-Dextran+ phagosomes are presented as mean ± SEM of three independent experiments. **B-E.** BMDMs from GFP-LC3 (**B, D**) or C57BL/6 (B6) (**C, E**) mice were infected with *R. oryzae* conidia (WT conidia) or *R. oryzae* conidia following chemical degradation of melanin with H_2O_2 bleaching (albino conidia) at an MOI of 1:2 (effector: fungal cells). Cells were removed at 1 hour of infection, fixed, stained, and analyzed by confocal imaging. Data on quantification of GFP-LC3+ (**D**) or Cathepsin D+ (**E**) phagosomes are presented as mean ± SEM of three independent experiments. **B, C.** Representative fluorescent images from experiments on **D** and **E** are shown. **F, G**. Fungal loads from lungs of immunocompetent mice (n = 9 per experimental group) infected with 10^6 conidia of *R. delemar* grown in regular media (WT *Rhizopus*) or under conditions of

copper starvation to inhibit melanization (albino *Rhizopus*) (**F**). Mice (n = 3 per condition) were sacrificed at the indicated time points (4, 24 and 72 hours), lungs were homogenized, and fungal loads were assessed by CFU plating (**G**). ***P < 0.0001, **P < 0.001 Mann–Whitney test. Scale bar, 10 μm

D5. Non-redundant role of macrophages in lung host defense against Mucorales

Despite the inability of macrophages to kill *Rhizopus*, inhibition of growth of phagocytosed conidia could be an important host defense mechanism. To test this hypothesis, we initially assessed differences in phagocytosis of dormant vs. germinating (swollen) conidia. To achieve a synchronized growth 10^6/ml *Rhizopus* conidia were incubated in 4ml RPMI-MOPS-2% Glucose, pH=7.2 for 4 hours at 28^0C in 6-well plates. Notably, we found a significant ≈5-fold reduction in phagocytosis of swollen as compared to dormant conidia by macrophages (Fig. 25A). Then, we infected immunocompetent mice via intratracheal administration of the same inoculum of dormant vs. swollen conidia of *Rhizopus* (5×10^6 conidia/mice), and assessed differences in the infection outcome. Surprisingly, while all mice recovered from infection with dormant *Rhizopus* conidia, infection of immunocompetent mice with swollen conidia of *Rhizopus* resulted in 100% mortality within 4 days (Fig. 25B). Histopathological examination of the lungs at 16 hours of infection with swollen *Rhizopus* conidia revealed dense neutrophil infiltrates along with extensive tissue necrosis and angioinvasive fungal growth (Fig. 25 C, D). Notably, we found no evidence of *Rhizopus* inside AMs or other phagocytes following infection of mice with swollen conidia (Fig. 25 C, D), a finding consistent with the results of ex vivo studies.

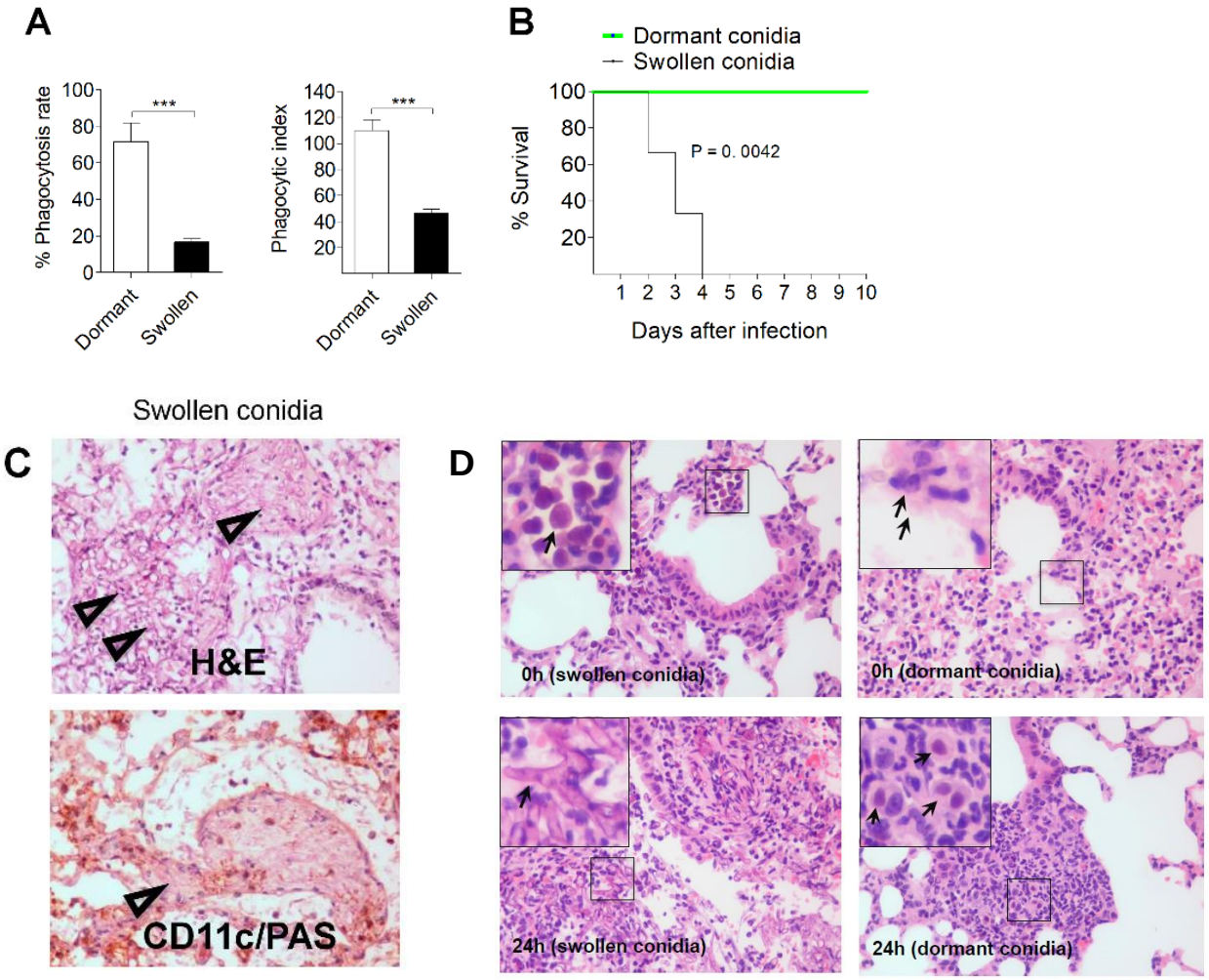

Figure 25. Swollen *Rhizopus* conidia are not sufficiently phagocytosed and cause fatal pulmonary infection. A. GFP-LC3 BMDMs were infected with dormant or swollen conidia of *R. oryzae* at an MOI of 1:2 (effector:fungal cells) and phagocytosis was assessed at 4 hours. Data on quantification of phagocytosis of *Rhizopus* conidia are presented as mean ± SEM of three independent experiments. ***P < 0.0001, Mann–Whitney test. **B.** Survival of immunocompetent C57BL/6 (B6) mice (n = 8 per group) infected via intratracheal administration of a standardized inoculum (5×10^6 conidia per mice) of dormant or swollen conidia of *R. oryzae*. **C.** Representative photomicrographs of the lungs from mice infected with 5×10^6 swollen conidia of *R. oryzae* at 24 hours of infection. Lungs were stained by H&E or IHC for CD11 and counterstaining with hematoxylin and PAS. **D.** Representative photomicrographs of the lungs from C57BL/6 (B6) mice infected intratracheally with 5 x 10^6 dormant or swollen conidia (incubated in media for 4 hours) of *R. oryzae* at 0 hour at 24 hours of infection. Lungs were removed, fixed and stained by H&E. The size of swollen as compared to dormant conidia at the time of infection (0h) is shown in insets. At 24h

of infection there is evidence of extensive *R. oryzae* hyphal growth in the lungs of the mice infected only with swollen conidia. Notably, there is no evidence of germination of dormant conidia, which predominately reside inside lung macrophages. Original magnification x400. Arrows indicate fungal cells. ***P < 0.0001, Mann–Whitney test

In order to directly evaluate the role of macrophages in physiological immune response to Mucorales, we performed AM depletion via intratracheal administration of clodronate liposomes. Liposomes are artificially prepared lipid vesicles, consisting of concentric phospholipid bilayers entrapping aqueous compartments. Clodronate are non-toxic bisphosphonate hydropihilic molecules, strongly solved in aqueous solutions, which at a certain intracellular concentration have the ability to induce apoptosis of the macrophages. Due to their strong hydrophilic properties, upon interaction with liposomes, they are rapidly encapsulated by them. After injection, liposomes are used as Trojan horses; they will be ingested and digested by macrophages followed by intracellular release and accumulation of clodronate, inducing apoptosis of the macrophages. In our experiments, 3 days after the intratracheal administration of clodronate liposomes the mice were infected with Rhizopus dormant conidia. Interestingly, survival, histopathology, and fungal load experiments demonstrate that liposome depletion resulted in significant increase in susceptibility of mice to mucormycosis as compared to treatment with control liposomes (Fig. 26A–C). In order to further validate the role of AMs in mucormycosis, we depleted CD11c transgenic mice with the intranasal administration of diphtheria toxin (DT). Firstly, via FACS analysis, we verified the successful selective depletion of CD11c+ cells (Fig. 26 D, Fig. 27). Then we assessed the effect on survival following *Rhizopus* infection. Importantly, we found a dramatic increase in susceptibility of CD11c-depleted mice to mucormycosis with 100% mortality at 5 days of infection (Fig. 26E). Collectively, these findings

demonstrate a nonredundant role of CD11c+ cells in the lungs, including AMs and DCs, in antifungal immunity against *Rhizopus*.

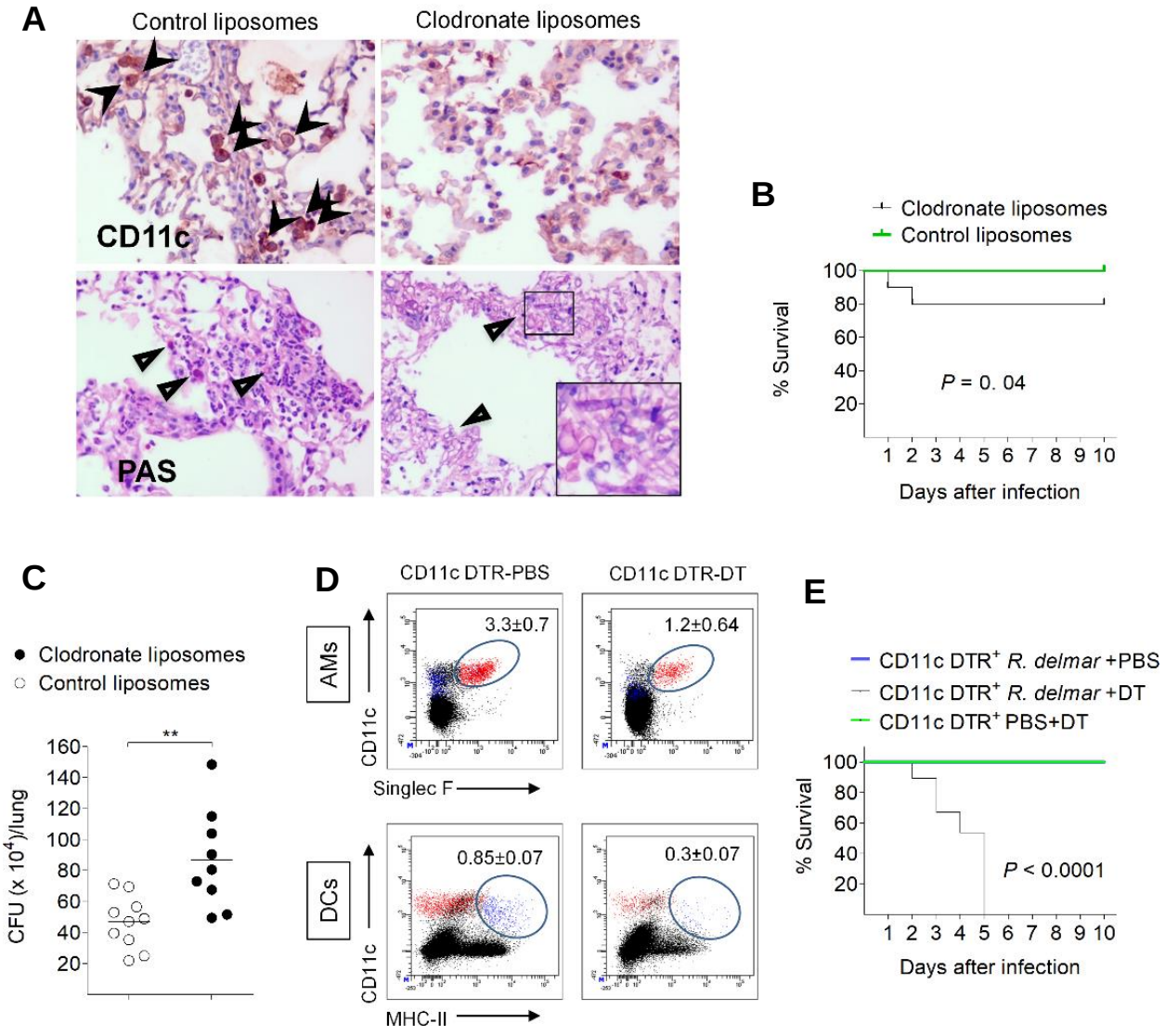

Figure 26. AMs have a non-redundant role in immunity against *Rhizopus*. A. Representative histopathology from lungs of C57BL/6 (B6) mice following intratracheal administration of 100 µl of clodronate liposomes or control liposomes and 48 hours later infection with 10^7 R. oryzae conidia. Invasive hyphal growth is present in the lungs of clodronate liposome group of mice. Original magnification ×400. **B.** Survival of C57BL/6 (B6) mice treated with clodronate liposomes (n = 10) or control liposomes (n = 15)

and infected as in A. **C.** Fungal loads in the lungs of C57BL/6 (B6) mice treated with clodronate liposomes or control liposomes and infected as in A. Lungs were removed on day 2 of infection and fungal loads were assessed by CFU plating. **P < 0.001, Mann–Whitney test. **D.** CD11c-DTR mice were intranasally inoculated with 40 µl PBS or with 20 ng/g of body weight of diphtheria toxin in 40 µl PBS and analyzed for the presence of CD11c+ cells (AMs and DCs) at 24 hours. Results represent two to three experiments with two to three mice per group per experiment. **E.** Survival of CD11c-DTR mice (n = 5 per group) treated with DT (20 ng/kg of mice) or PBS (control) and infected 48 h later with 5×10^6 conidia of *R. delemar*. The nonparametric log-rank test was used to determine differences in survival times.

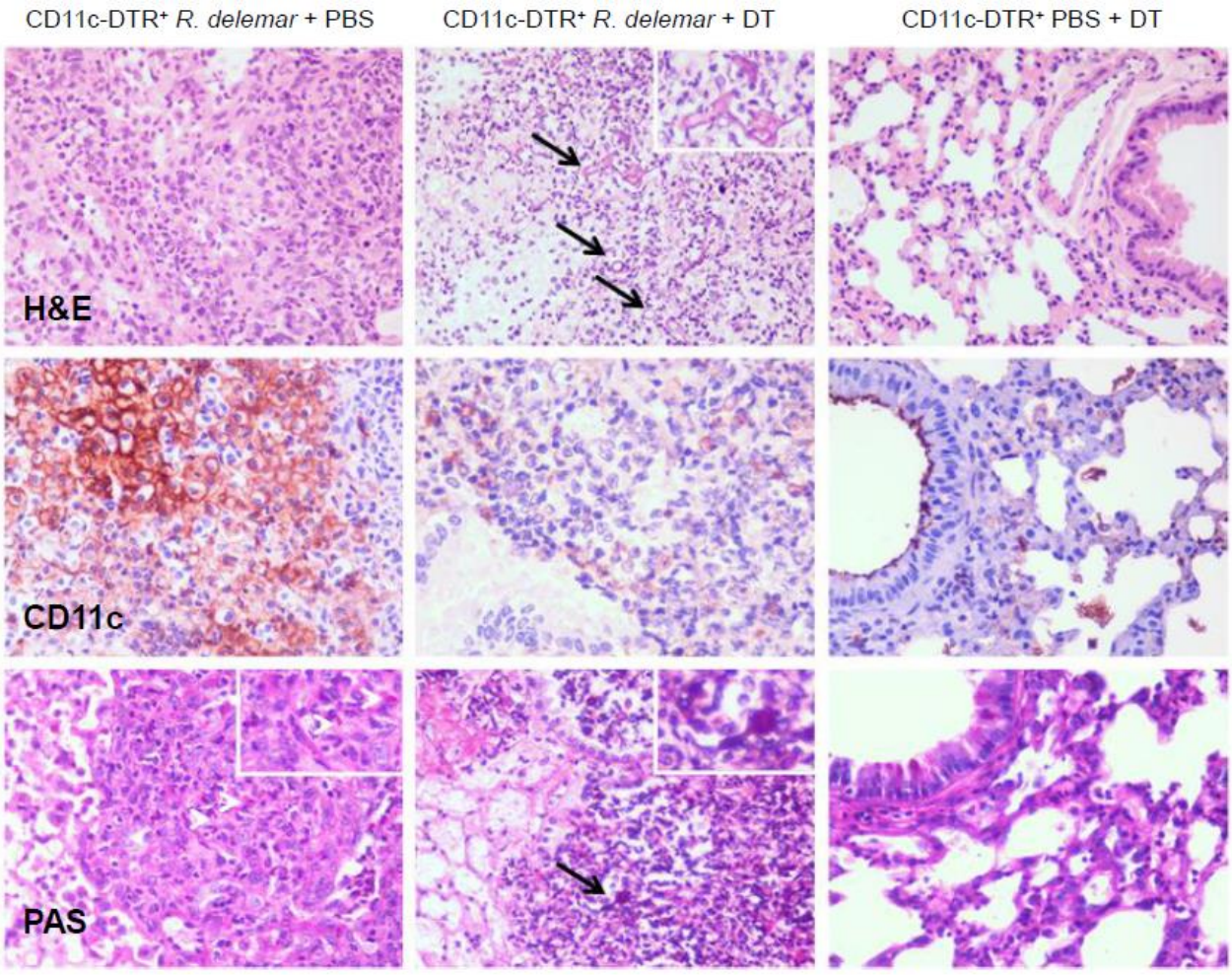

Figure 27. Histopathology of lungs from CD11c-DTR mice. Representative photomicrographs of the lungs from CD11c-DTR+mice intranasally inoculated with 40 µL PBS or 20 ng/g bwt of diphtheria toxin (DT) in 40 µL PBS and 48 hours after infected with 5 x 10^6 swollen conidia of *R. oryzae* or treated with

PBS at 24 hours of infection. Lungs were stained by H&E or PAS or IHC for CD11c. There is evidence of extensive *R. oryzae* hyphal growth with angioinvasion, intense neutrophil infiltration and necrosis, consistent with fungal pneumonia in the lungs of mice following CD11c+ cell depletion. White arrowheads: spores; Black arrows: hyphae; H&E: eosin and hematoxylin stain; PAS: Periodic-acid Shift stain; hematoxylin as counterstain; original magnifications X200, X400

D6. Iron starvation governs *Rhizopus*–macrophages interplay

Because of the blockade in P-L fusion induced by *Rhizopus*, we reasoned that nutritional immunity is the main effector mechanism to inhibit fungal growth inside macrophages. In view of the central role of iron in Mucorales growth, we performed transcriptomic analysis of host and pathogen genes to explore whether an iron restriction mechanism accounts for inhibition of conidial growth inside macrophages. Specifically, we performed RNA-seq on poly(A)-enriched RNA isolated from BMDMs infected with *R. delemar* (strain 99- 880) at different time points (1, 4, or 18 hours). The RNA preparations contained a mixture of messenger RNAs (mRNAs) expressed by the *Rhizopus* spp., as well as by the host cells. To ensure that the observed fungal gene expression changes were due to the interaction with the host cell and not simply a response to the medium, we performed RNA-seq on control *Rhizopus* conidia incubated for 5 minutes in culture medium in the absence of host cells. Similarly, we performed RNA-seq on control, uninfected BMDMs.

From the pathogen perspective, the majority of genes previously implicated in iron acquisition were regulated during infections (Fig. 28A). In particular, we identified Fet3 and Ftr1 as the most highly upregulated genes during intracellular persistence of *R.delemar* inside BMDMs. Notably, Fet3, a multicopper ferroxidase required for ferrous iron uptake and its interacting partner, the high affinity iron permease Ftr1p,

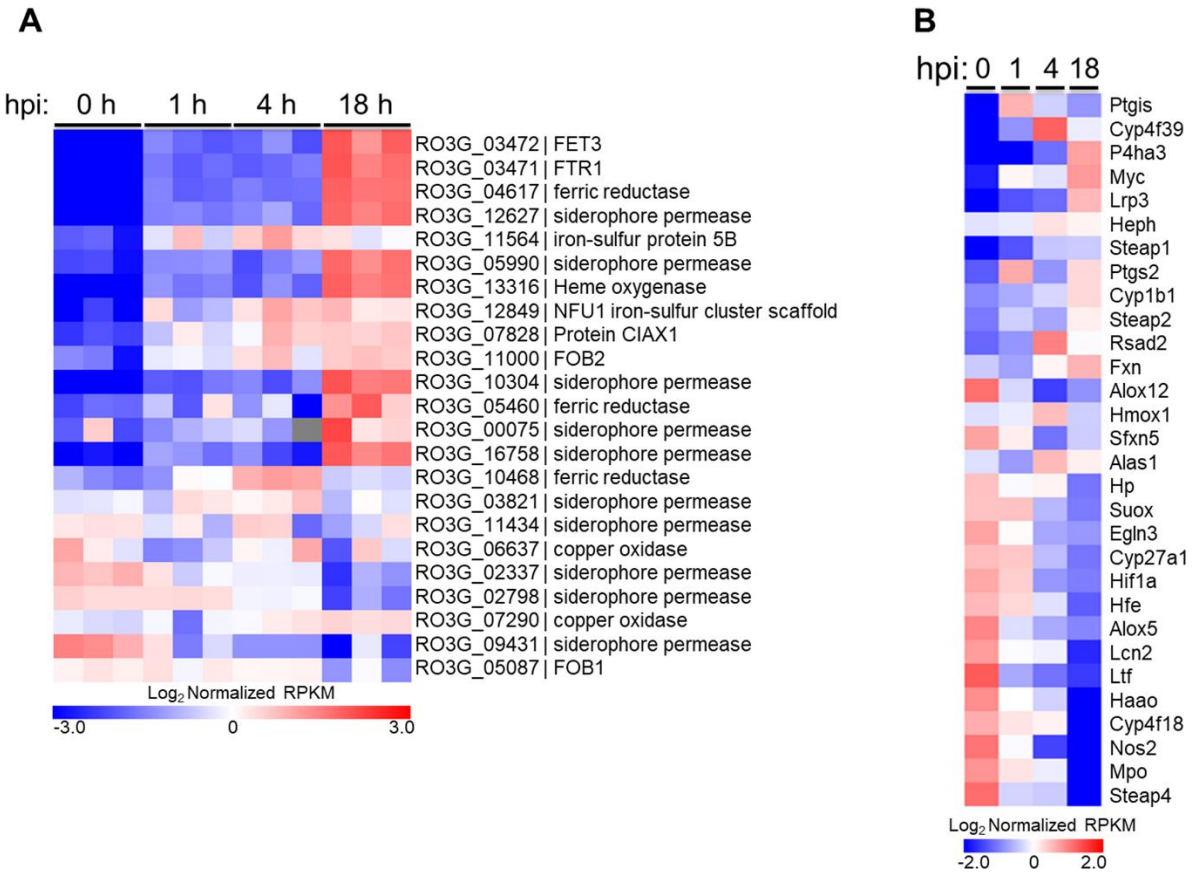

Figure 28. Global analysis of differential gene expression during infection. RNA-seq-based expression analysis of iron-related **A** *R. delemar* genes and **B** mouse genes following in vitro infection of BMDMs. **A.** Each column represents an individual sample (biological triplicates of four different conditions; n =12). Logtrans formed absolute expression normalized across all samples. Red indicates high gene expression. Blue indicates low gene expression. For the 0 h column, *R. delemar* was incubated in tissue culture media without BMDMs for 1 min. **B.** Values are presented as in A and represent the average of three biological replicates for each condition. For the 0 h columns, BMDMs were incubated in culture media in the absence of *R. delemar* spores for 1 hr.

comprise the major iron assimilation pathway of *Rhizopus* that is induced under iron-limited conditions and has a major pathogenetic role during in vivo infection.

In BMDMs, a significant number of iron metabolism-related genes identified in previous transcriptomic studies were differentially expressed over the course of

Rhizopus infection, with an expression pattern consistent with activation of an M2-alternative program (Fig. 28B). Specifically, there was evidence of downregulation of typical M1-related genes (Nos2, Mpo, Hif1a, Egln3) and upregulation of M2-related genes (Myc, fxn, Cyp1b1, Alas1). Additionally, several genes directly linked to trafficking and intracellular distribution of iron inside macrophages (heph, fxn, bdh2, hfe, ltf, lcn2, Steap 1, Steap 2, Steap 4) were differentially expressed during Mucorales infection. On the other hand, *Rhizopus* infection induced downregulation of hemochromatosis (hfe) and Ptgs2 genes, which are both upregulated during alternative activation in macrophages. Collectively, dual RNA-seq revealed the induction of an iron restriction response during the course of *Rhizopus* infection in BMDMs.

D7. Iron restriction inhibits *Rhizopus* growth inside macrophages

The results of dual RNA-seq provided a strong indirect indication of the importance of iron restriction during the course of *Rhizopus* infection in BMDMs. Next, we tested directly whether iron restriction is the primary mechanism of inhibition of fungal growth in macrophages. BMDMs from GFP-LC3 mice were infected with WT *Rhizopus delemar* strain at an MOI of 1:2 (effector:fungal cells) in regular culture media or media containing DFO (100 μM), iron (FeCl3; 100 μM), or DFO plus iron. At 1 hour after the infection, cells were extensively washed to remove non-phagocytosed conidia, media were replaced, and intracellular germination was assessed at 12 hours by confocal imaging. Notably, whereas there was minimal evidence of germination of *Rhizopus* conidia in control untreated BMDMs, ex vivo supplementation of media with iron, DFO, or both resulted in a significant increase

in germination of intracellular conidia (Fig. 29A, B) and subsequent lysis of macrophages.

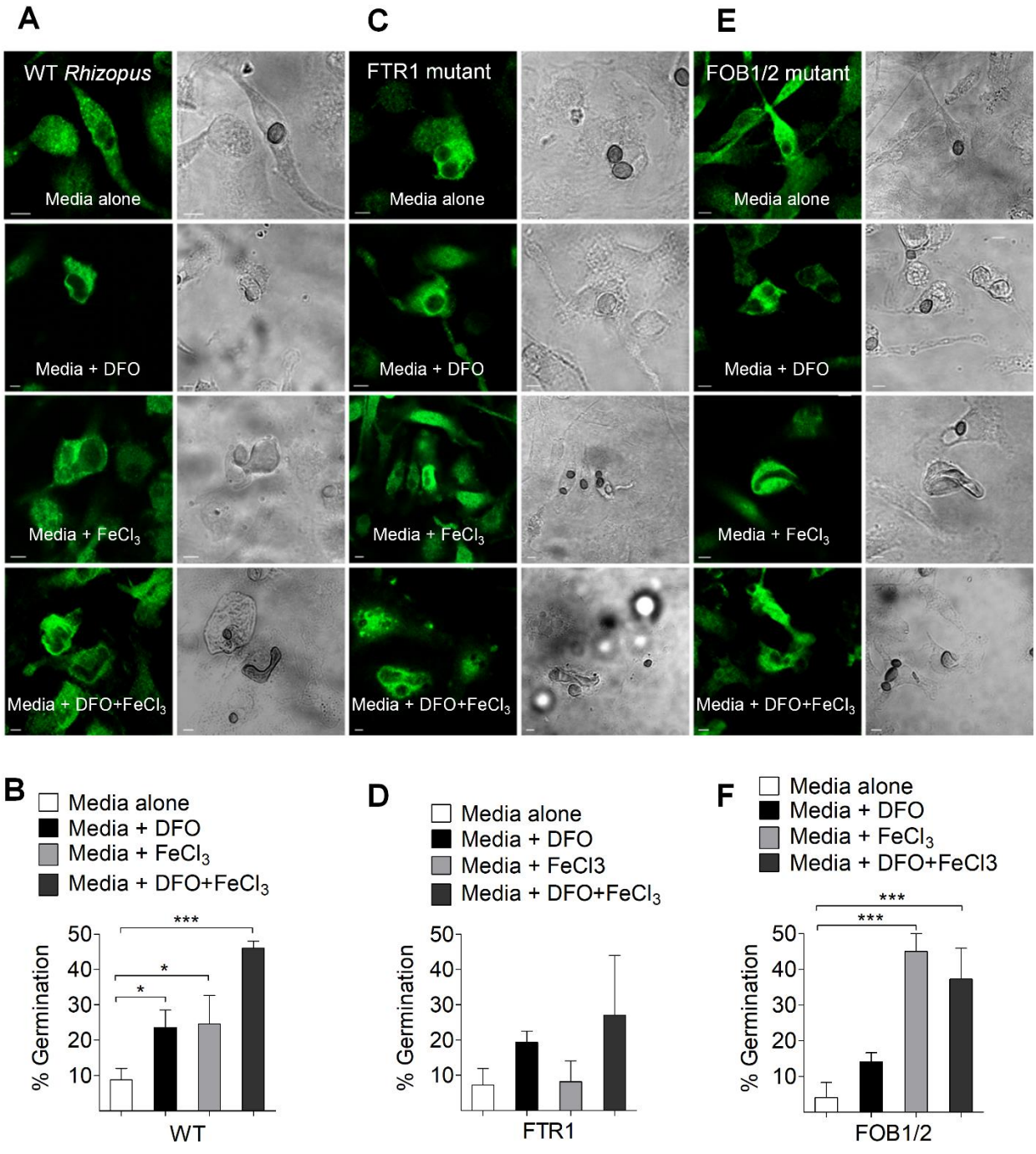

Figure 29. Macrophages inhibit intracellular growth of Rhizopus via iron starvation. **A, B** BMDMs from GFP-LC3 mice were infected with WT *Rhizopus delemar* strain at an MOI of 1:2 (effector:fungal

cells) in regular culture media or media containing DFO (100 μM), iron (FeCl3; 100 μM), or DFO plus iron. At 1 h of infection, cells were extensively washed to remove non-phagocytosed conidia, media were replaced, and intracellular germination was assessed at 12 h by confocal imaging. BMDMs from GFP-LC3 mice were also infected with *R. delemar*-attenuated mutants for FTR1 (c, d) or FOB1/2 (**E, F**), which are defective in the high affinity iron permease expression regulating iron assimilation under conditions of limited iron availability and DFO receptor FOB1/2 mediating fungal iron uptake from DFO, respectively, as in **A**. Representative immunofluorescence images are shown in **A, C** and **F**. Data on quantification of germination of intracellular conidia of the indicated Rhizopus strain are presented as mean ± SEM of three independent experiments. ***P < 0.0001, *P < 0.01, Mann–Whitney test. Bar, 5 μm

As an extra proof of the important role of iron restriction in Mucorales inhibition by macrophages, we tested the ability of Rhizopus mutants defective in pathways of iron assimilation, with attenuated in virulence in mouse models of mucormycosis of diabetic ketoacidosis and neutropenia, to germinate intracellularly following iron supplementation. In particular, we evaluated interaction of macrophages with ftr1 attenuated mutant of *Rhizopus* spp., which is compromised in virulence because of its diminished capacity to grow under iron limiting conditions and was highly induced in transcriptomics analysis. Although *Rhizopus* mutant with reduced FTR1 copies was not killed by macrophages, it displayed major defects in germination following iron supplementation by FeCl3, DFO, or both (Fig. 29C, D). Notably, infection of BMDMs with the *Rhizopus* fob1/2 mutant with defect in DFO uptake displayed impaired germination following supplementation of culture media with DFO, which was by-passed in the presence of exogenous iron (Fig. 29E, F). The attenuated mutants were derived from the wild-type strain used by RNAi (36, 37) and kindly provided to us for the afferomentioned experiments. Collectively, these findings clearly reveal the essential role of iron restriction inside the phagosome of macrophages on inhibition of intracellular growth of Mucorales conidia.

D8. Persistence of fungal conidia inside macrophages in human mucormycosis

In order to explore the physiological relevance of our studies in humans, we performed histopathological analysis of surgical specimens obtained from a 60-year-old patient with relapsed acute myelogenous leukemia who developed disseminated mucormycosis under chemotherapy with fludarabine and high-hose cytarabine (FLAG). The patient developed febrile neutropenia, left-sided chest pain and evidence of necrotizing pneumonia with chest wall myositis in computer tomography of the chest (Fig. 30A). Despite neutrophil recovery and the treatment with broad-spectrum antibiotics and anidulafungin, the infection progressed with infiltration of the abdominal wall and the spleen. In histopathology, there was evidence of necrotizing angioinvasive growth of Mucorales hyphae along with areas of granulomatous inflammation in the spleen that contained intracellular Mucorales conidia inside macrophages (Fig. 30B–E). The patient was comenced on liposomal amphotericin B and underwent radical surgery including splenectomy. Collectively, these findings are consistent with a pathogenetic model of mucormycosis highlighting the central role of Mucorales–macrophage interplay in disease development (Fig. 31).

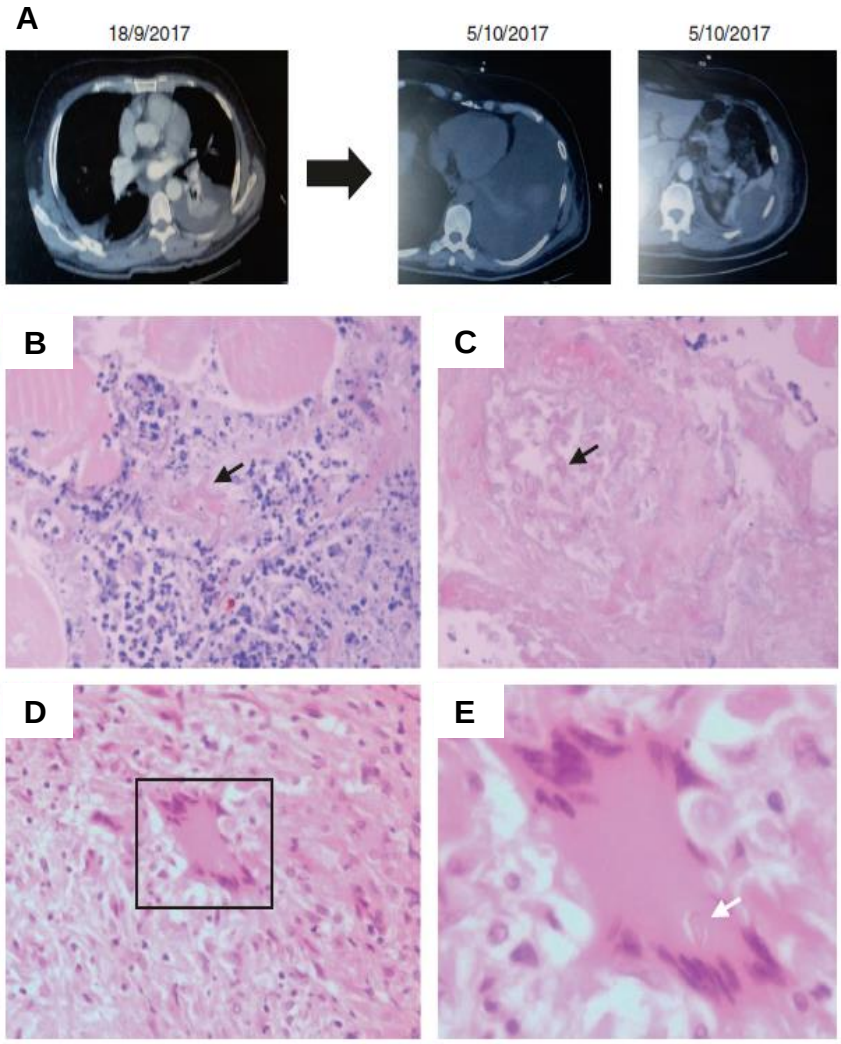

Figure 30. Invasive pulmonary mucormycosis in a patient with intracellular persistence. A. 60-year-old white male with relapsed acute myelogenous leukemia received salvage chemotherapy with fludarabine and high-hose cytarabine (FLAG) in August 2017. On September 2017, the patient developed febrile neutropenia and evidence of necrotizing pneumonia with chest wall myositis in computer tomography of the chest. **B. C.** In tissue biopsy mucormycosis was diagnosed based on characteristic histopathological findings, despite neutophil recovery. The patient was started on liposomal amphotericin B and underwent radical surgery with splenectomy in November 2017. In histopathological analysis of muscle biopsy, there is evidence of extensive tissue necrosis and growth of Mucorales hyphae inside blood vessels. **D.** In spleen histopathology there are areas of granulomatous lesions containing macrophages and multinucleated giant cells. **E**. In higher magnification (**D**, inset), there is evidence of a Mucorales conidium (spore) inside a giant cell (arrow). Original magnifications ×200, ×800. Eosin and hematoxylin stain; white arrows: spores; black arrows: hyphae

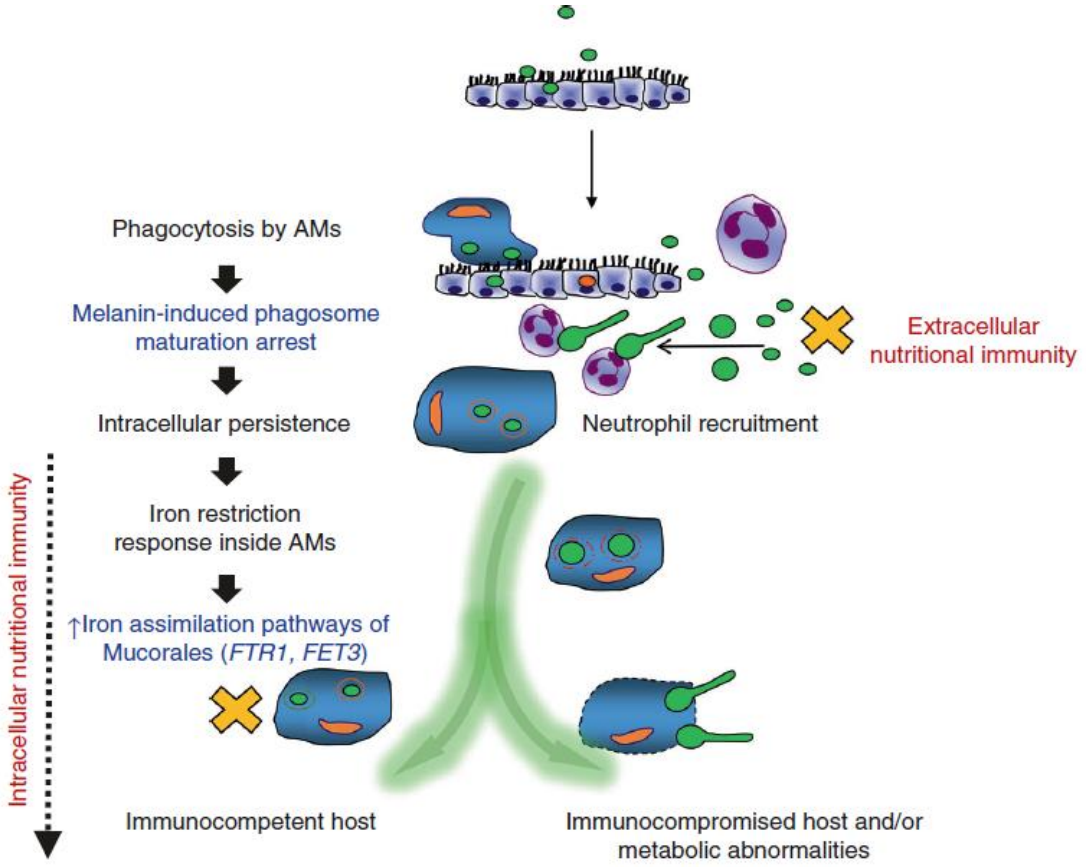

Figure 31. Proposed model of nutritional immunity inside macrophages against Mucorales.

Following inhalation, Mucorales conidia are predominantly phagocytosed by AMs. Intracellular conidia of Mucorales remain dormant and establish prolonged persistence inside the nascent phagosome of AMs. Surface retention of cell wall melanin in intracellular conidia of Mucorales blocks phagosome biogenesis and LAP, impedes killing, and induces anti-apoptotic signaling in macrophages to establish persistence. Inhibition of intracellular germination of Mucorales conidia via iron restriction is a central host defense mechanism against mucormycosis. In addition, incompletely understood nutritional immunity mechanisms, including transferrin-mediated restriction of free iron availability in serum, inhibit germination of extracellular conidia. In parallel, rapid recruitment of neutrophils results in clearance of extracellular conidia of Mucorales. Quantitative and qualitative defects in innate immunity associated with prolonged chemotherapy-induced neutropenia, and/or corticosteroid-induced immunosuppression compromise the ability of phagocytes to inhibit germination of intracellular or extracellular conidia and result in invasive fungal growth. On the other site, failure of nutritional immunity mechanisms in patients with abnormalities on iron metabolism (e.g., diabetic acidosis) allow germination of intracellular or extracellular conidia and promote invasive tissue growth. Mucorales responses inside AMs are highlighted in blue. Nutritional immunity responses are highlighted in red.

E. Discussion

E1. Intracellular persistence of Mucorales conidia inside macrophages

Our findings on prolonged persistence of *Rhizopus* in the lungs of immunocompetent mice are in sharp contrast to the rapid clearance of *Aspergillus* (1, 143) and in line with the increased pathogenicity of Mucorales. Our experiments clearly demonstrate that *Rhizopus* conidia are sufficiently phagocytosed, display a tropism and establish prolonged intracellular survival inside AMs. The failure to eradicate the dormant *Rhizopus* conidia inside the phagosomes leads to a paradigm shift in pathogenesis of mucormycosis and emphasizes the importance of AMs in disease pathogenesis. Specifically, the ability of a classic extracellular pathogen to remain in intracellular dormancy could attribute to the notable resistance of Mucorales to antifungals, analog to what has already been proven for *Staphylococcus aureus* (144). In addition, this fact might also explain clinical observations on relapse of mucormycosis years following cessation of secondary antifungal prophylaxis (145).

E2. Mechanism of phagosome maturation arrest induced by Mucorales

Our studies on biogenesis of *Rhizopus* phagosome identified for the first time that the inability of macrophages to kill *Rhizopus* is due to inhibition of LAP, a specialized pathway of phagosome biogenesis with central role in regulation of immune homeostasis and antifungal host defense,as demonstrated in previous studies from our lab (1, 84). A fundamental difference in biogenesis of *Rhizopus* vs. *Aspergillus* phagosomes that emerged from our study is the lack of intracellular swelling of *Rhizopus* conidia, which accounts for prolonged surface retention of cell

wall melanin and subsequent inhibition of LAP. These novel findings provide the rationale for targeted therapeutic strategies aiming to (i) restore phagosome blockade by harnessing the LAP pathway and (ii) target fungal melanin biosynthesis.

E3. The emerging role of nutritional immunity inside macrophages against Mucorales.

The unique susceptibility of patients suffering from diabetic ketoacidosis and treated with DFO to mucormycosis (21, 25, 43), conditions characterized from elevated available serum iron (130, 133), hinted towards the importance of iron metabolism for the pathogenesis of mucormycosis. Our studies demonstrate for the first time the essential role of iron limitation as the last and most critical line of host defense. In addition, the remarkable susceptibility of immunocompetent mice infected with dormant vs. swollen conidia indicates that the inhibition of conidial germination is of outmost importance for the control of mucormycosis.

Despite being extracellular pathogens, the prolonged intracellular life cycle of Mucorales makes them unique to study the regulation of macrophage iron homeostasis inside macrophages. Thus, further experiments on this field should be a top research priority to dissect precise mechanisms of immunopathogenesis of mucormycosis with the development of targeted iron chelation therapies inside macrophages being the ultimate goal. Our transcriptomics studies of host and fungal iron regulated genes during the course of infection have already identified potential targets for further exploitation.

E4. Final conclusions: Unresolved questions and future perspectives in immunopathogenesis of mucormycosis

Our findings shed light to the mechanisms of immunopathogenesis of mucormycosis, paving the way for further, more thorough study of the disease, which will ultimately lead to more effective therapeutic strategies.

Firstly, the disease reactivation as a consequence of the intracellular germination of conidia needs to be demonstrated in the setting of iron deregulation in vivo. This requires establishment of animal models of diabetic ketoacidosis, DFO treatment, iron overload and steroid treatment. Furthermore, the mechanisms of fungal clearance following prolonged intracellular persistence are currently unknown. A possible cross-talk of AMs with another immune cell type (from innate or adaptive immune system) contributing to the fungal clearance should be studied.

Although our study elucidates the pivotal role of macrophages to the control of mucormycosis, the role of neutrophils in pathogenesis of the disease is currently unknown. Moreover, their effector mechanisms against Mucorales are completely uncharacterized. Therefore, future studies should focus on developing animal models with depleted neutrophils to test the infection outcome. Lastly, a very intriguing field of research is the hypothesis that the intracellular persistence of conidia leads to Mucorales resistance to antifungals.

Bibliography

1. Akoumianaki T, Kyrmizi I, Valsecchi I, Gresnigt MS, Samonis G, Drakos E, et al. Aspergillus Cell Wall Melanin Blocks LC3-Associated Phagocytosis to Promote Pathogenicity. Cell Host Microbe. 2016;19(1):79-90.

2. Voelz K, Gratacap RL, Wheeler RT. A zebrafish larval model reveals early tissue-specific innate immune responses to Mucor circinelloides. Disease models & mechanisms. 2015;8(11):1375-88.

3. Woese CR, Fox GE. Phylogenetic structure of the prokaryotic domain: the primary kingdoms. Proceedings of the National Academy of Sciences of the United States of America. 1977;74(11):5088-90.

4. J.W. D. Fungal Biology. 4th Edition ed. Oxford, UK: Blackwell Publishing; 2006.

5. Blackwell M. The fungi: 1, 2, 3 ... 5.1 million species? American journal of botany. 2011;98(3):426-38.

6. Hawksworth DL, Lucking R. Fungal Diversity Revisited: 2.2 to 3.8 Million Species. Microbiology spectrum. 2017;5(4).

7. Spatafora JW, Aime MC, Grigoriev IV, Martin F, Stajich JE, Blackwell M. The Fungal Tree of Life: from Molecular Systematics to Genome-Scale Phylogenies. Microbiology spectrum. 2017;5(5).

8. Joanne Willey LSaCW. Prescott, Harley, and Klein's Microbiology. 7th ed: McGraw-Hill Publishing Company; 2008.

9. Erwig LP, Gow NA. Interactions of fungal pathogens with phagocytes. Nature reviews Microbiology. 2016;14(3):163-76.

10. Christopher CK, Richard B, Neil ARG, Susan H, Donna MM, Rohini JM, et al. Fungal cell structure and organization
Oxford Textbook of Medical Mycology. Oxford, UK.

11. Sproson EL, Thomas KM, Lau LC, Harries PG, Howarth PH, Salib RJ. Common airborne fungi induce species-specific effects on upper airway inflammatory and remodelling responses. Rhinology. 2016;54(1):51-5.

12. Yates MV, Nakatsu CH, Miller RV, Pillai SD. Manual of Environmental Microbiology, Fourth Edition: American Society of Microbiology; 2016.

13. Walsh TJ, Hiemenz JW, Anaissie E. Recent progress and current problems in treatment of invasive fungal infections in neutropenic patients. Infect Dis Clin North Am. 1996;10(2):365-400.

14. McNeil MM, Nash SL, Hajjeh RA, Phelan MA, Conn LA, Plikaytis BD, et al. Trends in mortality due to invasive mycotic diseases in the United States, 1980-1997. Clin Infect Dis. 2001;33(5):641-7.

15. Groll AH, Walsh TJ. Uncommon opportunistic fungi: new nosocomial threats. Clinical Microbiology and Infection. 2001;7:8-24.

16. Chamilos G, Luna M, Lewis RE, Bodey GP, Chemaly R, Tarrand JJ, et al. Invasive fungal infections in patients with hematologic malignancies in a tertiary care cancer center: an autopsy study over a 15-year period (1989-2003). Haematologica. 2006;91(7):986-9.

17. Maschmeyer G, Calandra T, Singh N, Wiley J, Perfect J. Invasive mould infections: a multi-disciplinary update. Med Mycol. 2009;47(6):571-83.

18. Mendoza L, Vilela R, Voelz K, Ibrahim AS, Voigt K, Lee SC. Human Fungal Pathogens of Mucorales and Entomophthorales. Cold Spring Harbor perspectives in medicine. 2014;5(4).

19. Park HR, Voigt K. Interaction of Zygomycetes with innate immune cells reconsidered with respect to ecology, morphology, evolution and infection biology: a mini-review. Mycoses. 2014;57 Suppl 3:31-9.

20. Hibbett DS, Binder M, Bischoff JF, Blackwell M, Cannon PF, Eriksson OE, et al. A higher-level phylogenetic classification of the Fungi. Mycological research. 2007;111(Pt 5):509-47.

21. Roden MM, Zaoutis TE, Buchanan WL, Knudsen TA, Sarkisova TA, Schaufele RL, et al. Epidemiology and outcome of zygomycosis: a review of 929 reported cases. Clin Infect Dis. 2005;41(5):634-53.

22. Kontoyiannis DP, Lewis RE. How I treat mucormycosis. Blood. 2011;118(5):1216.

23. Farmakiotis D, Kontoyiannis DP. Mucormycoses. Infectious Disease Clinics of North America. 2016;30(1):143-63.

24. Andresen D, Donaldson A, Choo L, Knox A, Klaassen M, Ursic C, et al. Multifocal cutaneous mucormycosis complicating polymicrobial wound infections in a tsunami survivor from Sri Lanka. Lancet (London, England). 2005;365(9462):876-8.

25. Ibrahim AS, Spellberg B, Walsh TJ, Kontoyiannis DP. Pathogenesis of mucormycosis. Clinical infectious diseases : an official publication of the Infectious Diseases Society of America. 2012;54 Suppl 1(Suppl 1):S16-S22.

26. Ribes JA, Vanover-Sams CL, Baker DJ. Zygomycetes in human disease. Clinical microbiology reviews. 2000;13(2):236-301.

27. Larone DH. Medically Important Fungi: A Guide to Identification. 5th ed: ASM Press; 2011 September 7, 2011.

28. St-Germain G, and R. Summerbell. Identifying Fungi: A Clinical Laboratory Handbook. 2nd ed. Belmont, CA, United States: Star Publishing Company (Belmont, CA); 2010 01 Aug 2010.

29. Bouza E, Muñoz P, Guinea J. Mucormycosis: an emerging disease? Clinical Microbiology and Infection. 2006;12:7-23.

30. Goodill JJ, Abuelo JG. Mucormycosis--a new risk of deferoxamine therapy in dialysis patients with aluminum or iron overload? The New England journal of medicine. 1987;317(1):54.

31. Veis JH, Contiguglia R, Klein M, Mishell J, Alfrey AC, Shapiro JI. Mucormycosis in deferoxamine-treated patients on dialysis. Annals of internal medicine. 1987;107(2):258.

32. Diamond RD, Krzesicki R, Epstein B, Jao W. Damage to hyphal forms of fungi by human leukocytes in vitro. A possible host defense mechanism in aspergillosis and mucormycosis. The American journal of pathology. 1978;91(2):313-28.

33. Waldorf AR, Ruderman N, Diamond RD. Specific susceptibility to mucormycosis in murine diabetes and bronchoalveolar macrophage defense against Rhizopus. The Journal of clinical investigation. 1984;74(1):150-60.

34. Hassan MIA, Voigt K. Pathogenicity patterns of mucormycosis: epidemiology, interaction with immune cells and virulence factors. Medical mycology. 2019;57(Supplement_2):S245-S56.

35. Ibrahim AS, Gebermariam T, Fu Y, Lin L, Husseiny MI, French SW, et al. The iron chelator deferasirox protects mice from mucormycosis through iron starvation. J Clin Invest. 2007;117(9):2649-57.

36. Ibrahim AS, Gebremariam T, Lin L, Luo G, Husseiny MI, Skory CD, et al. The high affinity iron permease is a key virulence factor required for Rhizopus oryzae pathogenesis. Molecular microbiology. 2010;77(3):587-604.

37. Liu M, Lin L, Gebremariam T, Luo G, Skory CD, French SW, et al. Fob1 and Fob2 Proteins Are Virulence Determinants of Rhizopus oryzae via Facilitating Iron Uptake from Ferrioxamine. PLOS Pathogens. 2015;11(5):e1004842.

38. Gebremariam T, Liu M, Luo G, Bruno V, Phan QT, Waring AJ, et al. CotH3 mediates fungal invasion of host cells during mucormycosis. J Clin Invest. 2014;124(1):237-50.

39. Chamilos G, Lewis RE, Kontoyiannis DP. Multidrug-resistant endosymbiotic bacteria account for the emergence of zygomycosis: A hypothesis. Fungal genetics and biology : FG & B. 2007;44(2):88-92.

40. Ibrahim AS, Gebremariam T, Liu M, Chamilos G, Kontoyiannis D, Mink R, et al. Bacterial endosymbiosis is widely present among zygomycetes but does not contribute to the pathogenesis of mucormycosis. The Journal of infectious diseases. 2008;198(7):1083-90.

41. Partida-Martinez LP, Hertweck C. Pathogenic fungus harbours endosymbiotic bacteria for toxin production. Nature. 2005;437(7060):884-8.

42. Jeong W, Keighley C, Wolfe R, Lee WL, Slavin MA, Kong DCM, et al. The epidemiology and clinical manifestations of mucormycosis: a systematic review and meta-analysis of case reports. Clinical microbiology and infection : the official publication of the European Society of Clinical Microbiology and Infectious Diseases. 2019;25(1):26-34.

43. Spellberg B, Edwards J, Jr., Ibrahim A. Novel perspectives on mucormycosis: pathophysiology, presentation, and management. Clinical microbiology reviews. 2005;18(3):556-69.

44. Lionakis MS, Kontoyiannis DP. Glucocorticoids and invasive fungal infections. The Lancet. 2003;362(9398):1828-38.

45. Charles A. Janeway JR PT, Mark Walport, Mark J. Shlomchik. Immunobiology : the immune system in health and disease. 5th ed. New York Garland Publishing, New York 2001.

46. GM. C. The Cell: A Molecular Approach. 2nd edition ed: Sunderland (MA): Sinauer Associates; 2000.

47. Serbina NV, Jia T, Hohl TM, Pamer EG. Monocyte-mediated defense against microbial pathogens. Annu Rev Immunol. 2008;26:421-52.

48. Sallusto F, Lanzavecchia A. The instructive role of dendritic cells on T-cell responses. Arthritis Res. 2002;4 Suppl 3(Suppl 3):S127-S32.

49. Nathan C. Neutrophils and immunity: challenges and opportunities. Nature Reviews Immunology. 2006;6(3):173-82.

50. Rosales C. Neutrophil: A Cell with Many Roles in Inflammation or Several Cell Types? Front Physiol. 2018;9:113-.

51. Bonilla FA, Oettgen HC. Adaptive immunity. The Journal of allergy and clinical immunology. 2010;125(2 Suppl 2):S33-40.

52. Zhu J, Paul WE. CD4 T cells: fates, functions, and faults. Blood. 2008;112(5):1557-69.

53. Romani L. Immunity to fungal infections. Nature Reviews Immunology. 2004;4(1):11-24.

54. Shen P, Fillatreau S. Antibody-independent functions of B cells: a focus on cytokines. Nature reviews Immunology. 2015;15(7):441-51.

55. Lionakis MS, Iliev ID, Hohl TM. Immunity against fungi. JCI Insight. 2017;2(11).

56. Bruns S, Kniemeyer O, Hasenberg M, Aimanianda V, Nietzsche S, Thywissen A, et al. Production of extracellular traps against Aspergillus fumigatus in vitro and in infected lung tissue is dependent on invading neutrophils and influenced by hydrophobin RodA. PLoS pathogens. 2010;6(4):e1000873-e.

57. Wynn TA, Chawla A, Pollard JW. Macrophage biology in development, homeostasis and disease. Nature. 2013;496(7446):445-55.

58. Ren Y, Khan FA, Pandupuspitasari NS, Zhang S. Immune Evasion Strategies of Pathogens in Macrophages: the Potential for Limiting Pathogen Transmission. Current issues in molecular biology. 2017;21:21-40.

59. Sica A, Mantovani A. Macrophage plasticity and polarization: in vivo veritas. The Journal of clinical investigation. 2012;122(3):787-95.

60. Mills C. M1 and M2 Macrophages: Oracles of Health and Disease. 2012;32(6):463-88.

61. Gordon S. Alternative activation of macrophages. Nature reviews Immunology. 2003;3(1):23-35.

62. Benoit M, Desnues B, Mege JL. Macrophage polarization in bacterial infections. Journal of immunology (Baltimore, Md : 1950). 2008;181(6):3733-9.

63. Xu S, Shinohara ML. Tissue-Resident Macrophages in Fungal Infections. Frontiers in immunology. 2017;8:1798-.

64. Philippe B, Ibrahim-Granet O, Prévost MC, Gougerot-Pocidalo MA, Sanchez Perez M, Van der Meeren A, et al. Killing of Aspergillus fumigatus by alveolar macrophages is mediated by reactive oxidant intermediates. Infection and immunity. 2003;71(6):3034-42.

65. Ibrahim-Granet O, Philippe B, Boleti H, Boisvieux-Ulrich E, Grenet D, Stern M, et al. Phagocytosis and intracellular fate of Aspergillus fumigatus conidia in alveolar macrophages. Infection and immunity. 2003;71(2):891-903.

66. Gersuk GM, Underhill DM, Zhu L, Marr KA. Dectin-1 and TLRs permit macrophages to distinguish between different Aspergillus fumigatus cellular states. Journal of immunology (Baltimore, Md : 1950). 2006;176(6):3717-24.

67. McQuiston TJ, Williamson PR. Paradoxical roles of alveolar macrophages in the host response to Cryptococcus neoformans. J Infect Chemother. 2012;18(1):1-9.
68. Osterholzer JJ, Milam JE, Chen G-H, Toews GB, Huffnagle GB, Olszewski MA. Role of dendritic cells and alveolar macrophages in regulating early host defense against pulmonary infection with Cryptococcus neoformans. Infection and immunity. 2009;77(9):3749-58.

69. Duclos S, Diez R, Garin J, Papadopoulou B, Descoteaux A, Stenmark H, et al. Rab5 regulates the kiss and run fusion between phagosomes and endosomes and the acquisition of phagosome leishmanicidal properties in RAW 264.7 macrophages. Journal of cell science. 2000;113 Pt 19:3531-41.

70. Canton J. Phagosome maturation in polarized macrophages. Journal of leukocyte biology. 2014;96(5):729-38.

71. Pauwels A-M, Trost M, Beyaert R, Hoffmann E. Patterns, Receptors, and Signals: Regulation of Phagosome Maturation. Trends Immunol. 2017;38(6):407-22.

72. Fairn GD, Grinstein S. How nascent phagosomes mature to become phagolysosomes. Trends Immunol. 2012;33(8):397-405.

73. Levin R, Grinstein S, Canton J. The life cycle of phagosomes: formation, maturation, and resolution. Immunological reviews. 2016;273(1):156-79.

74. Sanjuan MA, Dillon CP, Tait SWG, Moshiach S, Dorsey F, Connell S, et al. Toll-like receptor signalling in macrophages links the autophagy pathway to phagocytosis. Nature. 2007;450:1253.

75. Mehta P, Henault J, Kolbeck R, Sanjuan MA. Noncanonical autophagy: one small step for LC3, one giant leap for immunity. Current opinion in immunology. 2014;26:69-75.

76. Herb M, Gluschko A, Schramm M. LC3-associated phagocytosis - The highway to hell for phagocytosed microbes. Seminars in cell & developmental biology. 2019.

77. Martinez J, Malireddi RK, Lu Q, Cunha LD, Pelletier S, Gingras S, et al. Molecular characterization of LC3-associated phagocytosis reveals distinct roles for Rubicon, NOX2 and autophagy proteins. Nature cell biology. 2015;17(7):893-906.

78. Huang J, Canadien V, Lam GY, Steinberg BE, Dinauer MC, Magalhaes MA, et al. Activation of antibacterial autophagy by NADPH oxidases. Proc Natl Acad Sci U S A. 2009;106(15):6226-31.

79. Kyrmizi I, Ferreira H, Carvalho A, Figueroa JAL, Zarmpas P, Cunha C, et al. Calcium sequestration by fungal melanin inhibits calcium-calmodulin signalling to prevent LC3-associated phagocytosis. Nature microbiology. 2018;3(7):791-803.

80. Yang C-S, Lee J-S, Rodgers M, Min C-K, Lee J-Y, Kim Hee J, et al. Autophagy Protein Rubicon Mediates Phagocytic NADPH Oxidase Activation in Response to Microbial Infection or TLR Stimulation. Cell Host & Microbe. 2012;11(3):264-76.

81. Brown GD. Dectin-1: a signalling non-TLR pattern-recognition receptor. Nature reviews Immunology. 2006;6(1):33-43.

82. Ma J, Becker C, Lowell CA, Underhill DM. Dectin-1-triggered Recruitment of Light Chain 3 Protein to Phagosomes Facilitates Major Histocompatibility Complex Class II Presentation of Fungal-derived Antigens. Journal of Biological Chemistry. 2012;287(41):34149-56.

83. Cunha C, Di Ianni M, Bozza S, Giovannini G, Zagarella S, Zelante T, et al. Dectin-1 Y238X polymorphism associates with susceptibility to invasive aspergillosis in hematopoietic transplantation through impairment of both recipient- and donor-dependent mechanisms of antifungal immunity. Blood. 2010;116(24):5394-402.

84. Kyrmizi I, Gresnigt MS, Akoumianaki T, Samonis G, Sidiropoulos P, Boumpas D, et al. Corticosteroids block autophagy protein recruitment in Aspergillus fumigatus phagosomes via targeting dectin-1/Syk kinase signaling. Journal of immunology (Baltimore, Md : 1950). 2013;191(3):1287-99.

85. Tam JM, Mansour MK, Khan NS, Seward M, Puranam S, Tanne A, et al. Dectin-1-dependent LC3 recruitment to phagosomes enhances fungicidal activity in macrophages. The Journal of infectious diseases. 2014;210(11):1844-54.

86. Nicola AM, Albuquerque P, Martinez LR, Dal-Rosso RA, Saylor C, De Jesus M, et al. Macrophage Autophagy in Immunity to *Cryptococcus neoformans* and *Candida albicans*. Infection and Immunity. 2012;80(9):3065-76.

87. Gluschko A, Herb M, Wiegmann K, Krut O, Neiss WF, Utermohlen O, et al. The beta2 Integrin Mac-1 Induces Protective LC3-Associated Phagocytosis of Listeria monocytogenes. Cell Host Microbe. 2018;23(3):324-37.e5.

88. Koster S, Upadhyay S, Chandra P, Papavinasasundaram K, Yang G, Hassan A, et al. Mycobacterium tuberculosis is protected from NADPH oxidase and LC3-associated phagocytosis by the LCP protein CpsA. Proc Natl Acad Sci U S A. 2017;114(41):E8711-e20.

89. Sprenkeler EG, Gresnigt MS, van de Veerdonk FL. LC3-associated phagocytosis: a crucial mechanism for antifungal host defence against Aspergillus fumigatus. Cellular microbiology. 2016;18(9):1208-16.

90. Diamond RD, Clark RA. Damage to Aspergillus fumigatus and Rhizopus oryzae hyphae by oxidative and nonoxidative microbicidal products of human neutrophils in vitro. Infect Immun. 1982;38(2):487-95.

91. Diamond RD, Haudenschild CC, Erickson NF, 3rd. Monocyte-mediated damage to Rhizopus oryzae hyphae in vitro. Infect Immun. 1982;38(1):292-7.

92. Marchevsky AM, Bottone EJ, Geller SA, Giger DK. The changing spectrum of disease, etiology, and diagnosis of mucormycosis. Human pathology. 1980;11(5):457-64.

93. Waldorf AR, Levitz SM, Diamond RD. In vivo bronchoalveolar macrophage defense against Rhizopus oryzae and Aspergillus fumigatus. The Journal of infectious diseases. 1984;150(5):752-60.

94. Levitz SM, Selsted ME, Ganz T, Lehrer RI, Diamond RD. In vitro killing of spores and hyphae of Aspergillus fumigatus and Rhizopus oryzae by rabbit neutrophil cationic peptides and bronchoalveolar macrophages. The Journal of infectious diseases. 1986;154(3):483-9.

95. Chinn RY, Diamond RD. Generation of chemotactic factors by Rhizopus oryzae in the presence and absence of serum: relationship to hyphal damage mediated by human neutrophils and effects of hyperglycemia and ketoacidosis. Infect Immun. 1982;38(3):1123-9.

96. Ibrahim AS, Kontoyiannis DP. Update on mucormycosis pathogenesis. Current opinion in infectious diseases. 2013;26(6):508-15.

97. Zarember KA, Sugui JA, Chang YC, Kwon-Chung KJ, Gallin JI. Human polymorphonuclear leukocytes inhibit Aspergillus fumigatus conidial growth by lactoferrin-mediated iron depletion. Journal of immunology (Baltimore, Md : 1950). 2007;178(10):6367-73.

98. Lemaitre B, Hoffmann J. The host defense of Drosophila melanogaster. Annu Rev Immunol. 2007;25:697-743.

99. Chamilos G, Lewis RE, Hu J, Xiao L, Zal T, Gilliet M, et al. Drosophila melanogaster as a model host to dissect the immunopathogenesis of zygomycosis. Proc Natl Acad Sci U S A. 2008;105(27):9367-72.

100. Chamilos G, Lewis RE, Lamaris G, Walsh TJ, Kontoyiannis DP. Zygomycetes hyphae trigger an early, robust proinflammatory response in human polymorphonuclear neutrophils through toll-like receptor 2 induction but display relative resistance to oxidative damage. Antimicrobial agents and chemotherapy. 2008;52(2):722-4.

101. Chamilos G, Ganguly D, Lande R, Gregorio J, Meller S, Goldman WE, et al. Generation of IL-23 producing dendritic cells (DCs) by airborne fungi regulates fungal pathogenicity via the induction of T(H)-17 responses. PloS one. 2010;5(9):e12955.

102. Schmidt S, Tramsen L, Perkhofer S, Lass-Florl C, Roger F, Schubert R, et al. Characterization of the cellular immune responses to Rhizopus oryzae with potential impact on immunotherapeutic strategies in hematopoietic stem cell transplantation. The Journal of infectious diseases. 2012;206(1):135-9.

103. Ben-Ami R, Luna M, Lewis RE, Walsh TJ, Kontoyiannis DP. A clinicopathological study of pulmonary mucormycosis in cancer patients: extensive angioinvasion but limited inflammatory response. The Journal of infection. 2009;59(2):134-8.

104. Ibrahim AS, Spellberg B, Avanessian V, Fu Y, Edwards JE, Jr. Rhizopus oryzae adheres to, is phagocytosed by, and damages endothelial cells in vitro. Infect Immun. 2005;73(2):778-83.

105. Liu M, Spellberg B, Phan QT, Fu Y, Fu Y, Lee AS, et al. The endothelial cell receptor GRP78 is required for mucormycosis pathogenesis in diabetic mice. The Journal of clinical investigation. 2010;120(6):1914-24.

106. Gebremariam T, Lin L, Liu M, Kontoyiannis DP, French S, Edwards JE, Jr., et al. Bicarbonate correction of ketoacidosis alters host-pathogen interactions and alleviates mucormycosis. The Journal of Clinical Investigation. 2016;126(6):2280-94.

107. Latge JP. The cell wall: a carbohydrate armour for the fungal cell. Mol Microbiol. 2007;66(2):279-90.

108. Gow NAR, Latge JP, Munro CA. The Fungal Cell Wall: Structure, Biosynthesis, and Function. Microbiology spectrum. 2017;5(3).

109. Sucher AJ, Chahine EB, Balcer HE. Echinocandins: the newest class of antifungals. The Annals of pharmacotherapy. 2009;43(10):1647-57.

110. Latgé J-P, Beauvais A, Chamilos G. The Cell Wall of the Human Fungal Pathogen Aspergillus fumigatus: Biosynthesis, Organization, Immune Response, and Virulence. Annual Review of Microbiology. 2017;71(1):99-116.

111. Aimanianda V, Bayry J, Bozza S, Kniemeyer O, Perruccio K, Elluru SR, et al. Surface hydrophobin prevents immune recognition of airborne fungal spores. Nature. 2009;460(7259):1117-21.

112. Toledo AV, Franco MEE, Yanil Lopez SM, Troncozo MI, Saparrat MCN, Balatti PA. Melanins in fungi: Types, localization and putative biological roles. Physiological and Molecular Plant Pathology. 2017;99:2-6.

113. Chamilos G, Akoumianaki T, Kyrmizi I, Brakhage A, Beauvais A, Latge J-P. Melanin targets LC3-associated phagocytosis (LAP): A novel pathogenetic mechanism in fungal disease. Autophagy. 2016;12(5):888-9.

114. Lecointe K, Cornu M, Leroy J, Coulon P, Sendid B. Polysaccharides Cell Wall Architecture of Mucorales. Frontiers in microbiology. 2019;10(469).

115. Jones D, Bacon JS, Farmer VC, Webley DM. Lysis of cell walls of Mucor ramannianus Moller by a Streptomyces sp. Antonie van Leeuwenhoek. 1968;34(2):173-82.

116. Bartnicki-Garcia S, Reyes E. CHEMISTRY OF SPORE WALL DIFFERENTIATION IN MUCOR ROUXII. Archives of biochemistry and biophysics. 1964;108:125-33.

117. Wurster S, Thielen V, Weis P, Walther P, Elias J, Waaga-Gasser AM, et al. Mucorales spores induce a proinflammatory cytokine response in human mononuclear phagocytes and harbor no rodlet hydrophobins. Virulence. 2017;8(8):1708-18.

118. Nairz M, Dichtl S, Schroll A, Haschka D, Tymoszuk P, Theurl I, et al. Iron and innate antimicrobial immunity-Depriving the pathogen, defending the host. Journal of trace elements in medicine and biology : organ of the Society for Minerals and Trace Elements (GMS). 2018;48:118-33.

119. Poss KD, Tonegawa S. Heme oxygenase 1 is required for mammalian iron reutilization. Proc Natl Acad Sci U S A. 1997;94(20):10919-24.

120. Rogers JT. Ferritin translation by interleukin-1and interleukin-6: the role of sequences upstream of the start codons of the heavy and light subunit genes. Blood. 1996;87(6):2525-37.

121. Stefanova D, Raychev A, Arezes J, Ruchala P, Gabayan V, Skurnik M, et al. Endogenous hepcidin and its agonist mediate resistance to selected infections by clearing non-transferrin-bound iron. Blood. 2017;130(3):245-57.

122. Bachman MA, Lenio S, Schmidt L, Oyler JE, Weiser JN. Interaction of lipocalin 2, transferrin, and siderophores determines the replicative niche of Klebsiella pneumoniae during pneumonia. mBio. 2012;3(6).

123. Skaar EP, Humayun M, Bae T, DeBord KL, Schneewind O. Iron-source preference of Staphylococcus aureus infections. Science (New York, NY). 2004;305(5690):1626-8.

124. Nairz M, Haschka D, Demetz E, Weiss G. Iron at the interface of immunity and infection. Frontiers in pharmacology. 2014;5:152.

125. Bellmann-Weiler R, Schroll A, Engl S, Nairz M, Talasz H, Seifert M, et al. Neutrophil gelatinase-associated lipocalin and interleukin-10 regulate intramacrophage Chlamydia pneumoniae replication by modulating intracellular iron homeostasis. Immunobiology. 2013;218(7):969-78.

126. Haschka D, Nairz M, Demetz E, Wienerroither S, Decker T, Weiss G. Contrasting regulation of macrophage iron homeostasis in response to infection with Listeria monocytogenes depending on localization of bacteria. Metallomics : integrated biometal science. 2015;7(6):1036-45.

127. Nairz M, Theurl I, Ludwiczek S, Theurl M, Mair SM, Fritsche G, et al. The co-ordinated regulation of iron homeostasis in murine macrophages limits the availability of iron for intracellular Salmonella typhimurium. Cellular microbiology. 2007;9(9):2126-40.

128. Willemetz A, Beatty S, Richer E, Rubio A, Auriac A, Milkereit RJ, et al. Iron- and Hepcidin-Independent Downregulation of the Iron Exporter Ferroportin in Macrophages during Salmonella Infection. Frontiers in immunology. 2017;8:498.

129. Howard DH. Acquisition, transport, and storage of iron by pathogenic fungi. Clinical microbiology reviews. 1999;12(3):394-404.

130. Artis WM, Fountain JA, Delcher HK, Jones HE. A mechanism of susceptibility to mucormycosis in diabetic ketoacidosis: transferrin and iron availability. Diabetes. 1982;31(12):1109-14.

131. Petrikkos G, Tsioutis C. Recent Advances in the Pathogenesis of Mucormycoses. Clinical Therapeutics. 2018;40(6):894-902.

132. de Locht M, Boelaert JR, Schneider YJ. Iron uptake from ferrioxamine and from ferrirhizoferrin by germinating spores of Rhizopus microsporus. Biochemical pharmacology. 1994;47(10):1843-50.

133. Boelaert JR, de Locht M, Van Cutsem J, Kerrels V, Cantinieaux B, Verdonck A, et al. Mucormycosis during deferoxamine therapy is a siderophore-mediated infection. In vitro and in vivo animal studies. The Journal of clinical investigation. 1993;91(5):1979-86.

134. Ibrahim AS, Edwards JE, Jr, Fu Y, Spellberg B. Deferiprone iron chelation as a novel therapy for experimental mucormycosis. Journal of Antimicrobial Chemotherapy. 2006;58(5):1070-3.

135. Spellberg B, Ibrahim AS, Chin-Hong PV, Kontoyiannis DP, Morris MI, Perfect JR, et al. The Deferasirox-AmBisome Therapy for Mucormycosis (DEFEAT Mucor) study: a randomized, double-blinded, placebo-controlled trial. The Journal of antimicrobial chemotherapy. 2012;67(3):715-22.

136. Skory CD, Ibrahim AS. Native and modified lactate dehydrogenase expression in a fumaric acid producing isolate Rhizopus oryzae 99-880. Current genetics. 2007;52(1):23-33.

137. Ardrey RE. Liquid Chromatography – Mass Spectrometry: An Introduction.: John Wiley & Sons, Ltd; 2003.

138. Bedoret D, Wallemacq H, Marichal T, Desmet C, Quesada Calvo F, Henry E, et al. Lung interstitial macrophages alter dendritic cell functions to prevent airway allergy in mice. J Clin Invest. 2009;119(12):3723-38.

139. Kim D, Pertea G, Trapnell C, Pimentel H, Kelley R, Salzberg SL. TopHat2: accurate alignment of transcriptomes in the presence of insertions, deletions and gene fusions. Genome biology. 2013;14(4):R36.

140. Anders S, Huber W. Differential expression analysis for sequence count data. Genome biology. 2010;11(10):R106.

141. Nosanchuk JD, Stark RE, Casadevall A. Fungal Melanin: What do We Know About Structure? Frontiers in microbiology. 2015;6:1463.

142. Manicam C, Pitz S, Brochhausen C, Grus FH, Pfeiffer N, Gericke A. Effective Melanin Depigmentation of Human and Murine Ocular Tissues: An Improved Method for Paraffin and Frozen Sections. PloS one. 2014;9(7):e102512.

143. Mircescu MM, Lipuma L, van Rooijen N, Pamer EG, Hohl TM. Essential role for neutrophils but not alveolar macrophages at early time points following Aspergillus fumigatus infection. The Journal of infectious diseases. 2009;200(4):647-56.

144. Lehar SM, Pillow T, Xu M, Staben L, Kajihara KK, Vandlen R, et al. Novel antibody–antibiotic conjugate eliminates intracellular S. aureus. Nature. 2015;527:323.

145. Davoudi S, Anderlini P, Fuller GN, Kontoyiannis DP. A long-term survivor of disseminated Aspergillus and mucorales infection: an instructive case. Mycopathologia. 2014;178(5-6):465-70.

Appendix

nature COMMUNICATIONS

Corrected: Author correction

ARTICLE

DOI: 10.1038/s41467-018-05820-2 OPEN

Iron restriction inside macrophages regulates pulmonary host defense against *Rhizopus* species

Angeliki M. Andrianaki[1], Irene Kyrmizi[1,2], Kalliopi Thanopoulou[3], Clara Baldin[4], Elias Drakos[1], Sameh S.M. Soliman[5], Amol C. Shetty[6], Carrie McCracken[6], Tonia Akoumianaki[1], Kostas Stylianou[1], Petros Ioannou[1], Charalampos Pontikoglou[1], Helen A. Papadaki[1], Maria Tzardi[1], Valerie Belle[7], Emilien Etienne[7], Anne Beauvais[8], George Samonis[1], Dimitrios P. Kontoyiannis[9], Evangelos Andreakos[3], Vincent M. Bruno[6], Ashraf S. Ibrahim[4,10] & Georgios Chamilos[1,2]

Mucormycosis is a life-threatening respiratory fungal infection predominantly caused by *Rhizopus* species. Mucormycosis has incompletely understood pathogenesis, particularly how abnormalities in iron metabolism compromise immune responses. Here we show how, as opposed to other filamentous fungi, *Rhizopus* spp. establish intracellular persistence inside alveolar macrophages (AMs). Mechanistically, lack of intracellular swelling of *Rhizopus* conidia results in surface retention of melanin, which induces phagosome maturation arrest through inhibition of LC3-associated phagocytosis. Intracellular inhibition of *Rhizopus* is an important effector mechanism, as infection of immunocompetent mice with swollen conidia, which evade phagocytosis, results in acute lethality. Concordantly, AM depletion markedly increases susceptibility to mucormycosis. Host and pathogen transcriptomics, iron supplementation studies, and genetic manipulation of iron assimilation of fungal pathways demonstrate that iron restriction inside macrophages regulates immunity against *Rhizopus*. Our findings shed light on the pathogenetic mechanisms of mucormycosis and reveal the role of macrophage-mediated nutritional immunity against filamentous fungi.

[1] Department of Medicine, University of Crete, Foundation for Research and Technology, 71300 Heraklion, Crete, Greece. [2] Institute of Molecular Biology and Biotechnology, Foundation for Research and Technology, 71300 Heraklion, Crete, Greece. [3] Laboratory of Immunobiology, Center for Clinical, Experimental Surgery, and Translational Research, Biomedical Research Foundation of the Academy of Athens, 11527 Athens, Greece. [4] Division of Infectious Diseases, Los Angeles Biomedical Research Institute, Harbor-University of California Los Angeles (UCLA) Medical Center, 1124 West Carson Street, St. John's Cardiovascular Research Center, Torrance, CA 90502, USA. [5] Sharjah Institute for Medical Research, College of Pharmacy, University of Sharjah, PO Box 27272 Sharjah, UAE. [6] Institute for Genome Sciences, University of Maryland School of Medicine, Baltimore, MD 21201, USA. [7] CNRS, BIP (UMR 7281), IMM (FR 3479), Aix-Marseille Université, 31 chemin J. Aiguier, 13402 Marseille, France. [8] Unité des Aspergillus, Institut Pasteur, 75015 Paris, France. [9] Department of Infectious Diseases, Infection Control, and Employee Health, The University of Texas MD Anderson Cancer Center, Houston, TX 77030, USA. [10] David Geffen School of Medicine at UCLA, Los Angeles, CA 90095, USA. These authors contributed equally: Angeliki M. Andrianaki, Irene Kyrmizi. Correspondence and requests for materials should be addressed to A.S.I. (email: ibrahim@labiomed.org) or to G.C. (email: hamilos@imbb.forth.gr)

Respiratory fungal infections caused by opportunistic filamentous fungi, predominantly *Aspergillus* species and Mucorales, are major causes of death in an expanding population of debilitated and immunocompromised patients[1–3]. When compared to other airborne filamentous fungi (molds), Mucorales are emerging pathogens that possess unique clinical, epidemiological, and pathogenetic characteristics[4–8]. Specifically, although acquired innate immune defects associated with myeloablative and immunosuppressive therapies are typical risk factors for mucormycosis, Mucorales frequently cause lethal infections in patients with certain metabolic disorders, and occasionally in immunocompetent individuals following trauma and burns[6–8]. In particular, patients with diabetic ketoacidosis or other forms of acidosis, and patients with elevated available serum iron are uniquely predisposed to mucormycosis[6–8]. Importantly, pulmonary mucormycosis is the most devastating invasive fungal infection, associated with mortality rates of 50% to 70% and can reach 90% upon dissemination[6–8]. This disease also has significant morbidity and frequently requires disfiguring radical surgery as the only lifesaving measure[6–8]. Because of the inherent resistance of Mucorales to most available antifungal agents[8], there is a dire need to better understand immunopathogenesis of mucormycosis and develop new therapeutic concepts for the disease.

Iron has an essential role in the life cycle of Mucorales and its utilization from the host is a critical pathogenetic mechanism of mucormycosis[7,8]. In contrast, the host-mediated iron limitation is an important defense strategy known as nutritional immunity. Recent genetic and biochemical studies in *Rhizopus*, the Mucorales causing 70% of human mucormycosis, have identified key molecular determinants of iron assimilation that are required for invasive fungal growth. Specifically, studies highlighted the role of the high affinity iron permease (Ftr1p) in iron acquisition from iron-limited environment encountered by the fungus during in vivo infection[9]. Additionally, the fungal proteins Fob1 and Fob2 act specifically as receptors for iron uptake from ferrioxamine[10]. Ferrioxamine is the iron-rich form of deferoxamine (DFO), which is utilized by the fungus as a xenosiderophore. The use of DFO for iron chelation therapy in dialysis patients with end-stage renal failure is associated with unique predisposition to mucormycosis[11,12]. Furthermore, in patients with diabetic ketoacidosis or other forms of acidosis, increased availability of free iron in the serum as a result of protonation of transferrin, is a critical pathogenetic event in the development of mucormycosis[8]. Notably, correction of diabetic acidosis with bicarbonate has been an effective adjunct treatment of mucormycosis in mice[13]. Also, abnormalities of iron metabolism and hyperglycemia facilitate interaction of CotH3 Mucorales invasin[14] with endothelial GRP78 receptor[15] and induce angioinvasive fungal growth, another hallmark of mucormycosis.

Despite the progress in identifying important iron assimilation pathways in Mucorales, the host effector mechanisms that limit iron availability to these pathogens are incompletely characterized. Furthermore, there is no pathogenetic model to explain whether and how abnormalities in iron metabolism compromise physiological immune responses leading to development of mucormycosis.

It is known that professional phagocytes, including neutrophils and macrophages, have a central role in host defense against airborne filamentous fungi[1,16]. However, there is a significant gap of knowledge on physiological immune responses against Mucorales. In fact, current evidence on the role of cellular immunity against Mucorales is extrapolated from studies on *Aspergillus*[16]. Similarly, at the molecular level, little is known about the mechanisms of intracellular killing of Mucorales conidia inside phagocytes. From the pathogen perspective, the presence of putative virulence mechanisms that protect Mucorales conidia from killing by phagocytes remain elusive.

Herein, we analyze physiological immune responses in the lungs of immunocompetent mice during *Rhizopus* infection and identify an essential role of macrophages during host–*Rhizopus* interplay. In particular, we demonstrate that *Rhizopus* spp. subvert physiological killing mechanisms of macrophages and establish prolonged intracellular dormancy via melanin-induced phagosome maturation arrest. Furthermore, we discover that inhibition of *Rhizopus* growth inside macrophages is a central host defense mechanism that depends on nutritional immunity via iron starvation. Finally, dual RNA-sequencing (RNA-seq) and functional studies identify critical host and fungal modulators of iron homeostasis inside macrophages that promote invasive fungal growth. Our findings shed light on pathogenesis of mucormycosis with potential therapeutic implications in the management of this devastating disease, and provide a mechanistic link between iron homeostasis inside macrophages and immune responses to Mucorales.

Results

***Rhizopus* conidia persist inside alveolar macrophages**. In order to understand general aspects of the physiological immune response against Mucorales, we infected immunocompetent mice with conidia of either *Aspergillus fumigatus* or two clinical isolates of *Rhizopus* (*Rhizopus oryzae* and *Rhizopus delemar*) and compared fungal clearance by CFU (colony-forming unit) counts and histopathological studies of total lung homogenates at different time points of infection (0, 2, 5, and 10 days). We found that opposite to *A. fumigatus* conidia, a significant proportion of each *Rhizopus* isolate conidia remained viable in the lungs of immunocompetent mice as late as 10 days post infection (Fig. 1a), despite the lack of mortality of the infected animals (Fig. 1b). Histopathology of lung tissue sections collected on day 5 post infecting immunocompetent mice with *R. oryzae* confirmed the presence of abundant conidia in the lungs, which resulted in considerable tissue edema and neutrophil infiltration (Fig. 1c). Interestingly, there was no apparent evidence of *R. oryzae* germination in infected lungs (Fig. 1c). Furthermore, immunohistochemistry studies revealed that *R. oryzae* conidia predominantly resided inside CD11c+/CD68+cells consistent with alveolar macrophages (AMs), while there was evidence of extracellular conidia associated with areas of intensive neutrophil infiltration (Fig. 1d).

We next assessed kinetics of recruitment and degree of association of myeloid cells in the lungs of immunocompetent mice following infection with fluorescence-labeled conidia of *R. oryzae*. Although we found a significant influx of neutrophils (identified as CD45+/CD11b+/Ly6G+/Ly6C− cells; Supplementary Fig. 1) and Ly6C^{high} inflammatory monocytes (identified as CD45+/CD11b+/Ly6G−/CD11c−/Ly6C+ cells; Supplementary Fig. 1) in the lungs on days 1 and 5 of infection (Fig. 1e), most *R. oryzae* conidia were associated with AMs (identified as CD45+/F4/80+/CD11c+/MHCII^{low} cells), interstitial macrophages (IMs; identified as CD45+/F4/80+/CD11c−/MHCII+), and dendritic cells (DCs; identified as CD45+/F4/80−/CD11c+/MHCII+) in the lungs of immunocompetent mice (Fig. 1f). Confocal imaging in sorted neutrophils, AMs, and IMs on day 5 post infection (Supplementary Fig. 2) confirmed that *R. oryzae* conidia were predominantly phagocytosed by AMs (Fig. 1g, h). Collectively, these studies demonstrate that a significant proportion of *Rhizopus* conidia remain viable inside AMs for several days following infection of immunocompetent mice.

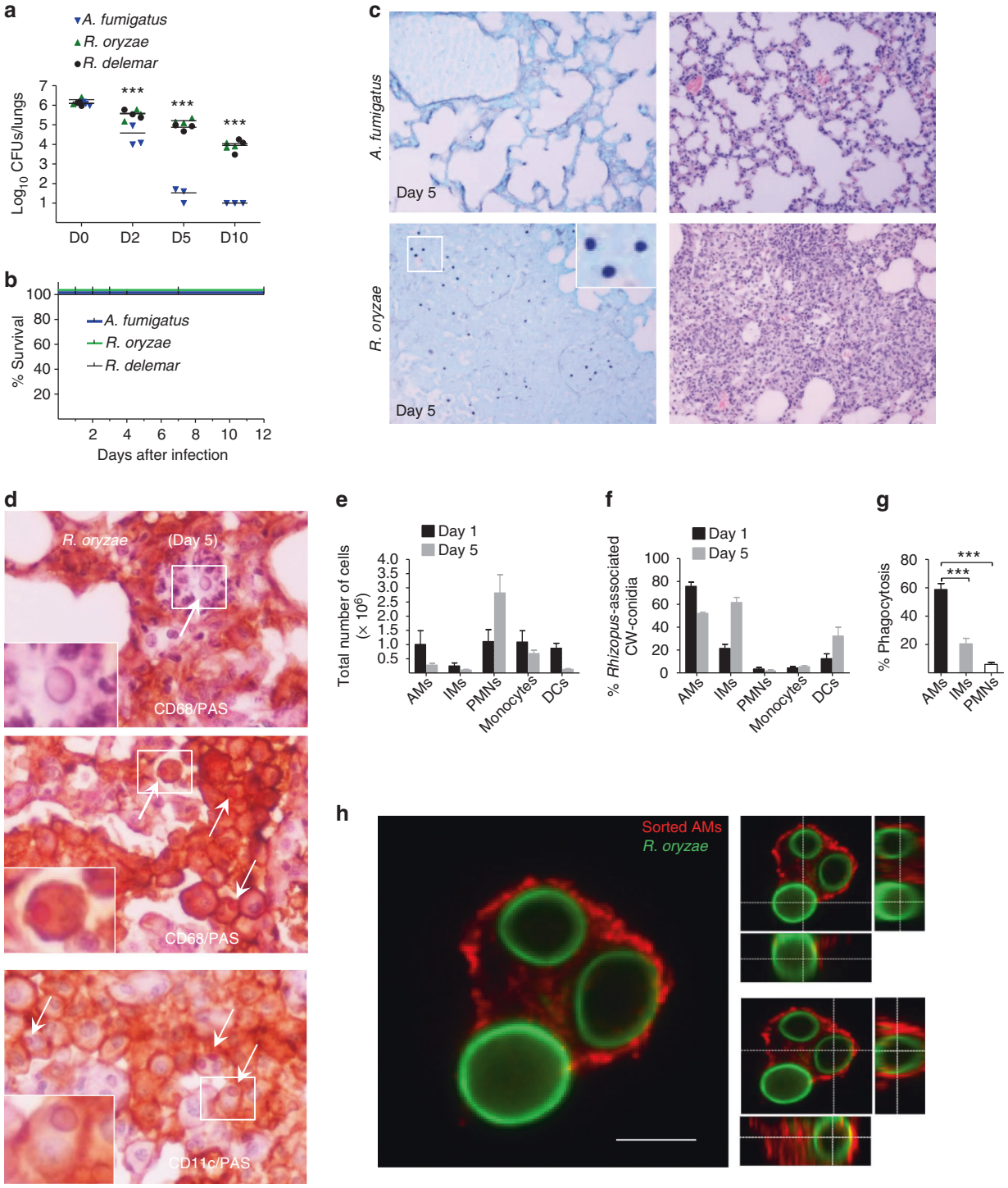

***Rhizopus* conidia are resistant to killing by macrophages**. In order to shed light on the mechanisms of intracellular persistence of *Rhizopus*, we studied interactions of bone marrow-derived macrophages (BMDMs) and neutrophils with conidia of *A. fumigatus* or *R. oryzae*. In contrast to conidia of *A. fumigatus*, which were phagocytosed comparably by BMDMs and neutrophils, conidia of *R. oryzae* were almost exclusively phagocytosed by BMDMs (Fig. 2a–c). In addition, despite their larger size, *Rhizopus* conidia were phagocytosed by BMDMs at a higher index rate than *A. fumigatus* conidia. Next, we compared killing rates of *A. fumigatus* vs. *R. oryzae* conidia by BMDMs. We found that unlike *A. fumigatus* (Fig. 2d, Supplementary Fig. 3), different clinical isolates of *Rhizopus* were resistant to killing by BMDMs (Fig. 2d, e, Supplementary Fig. 3). These studies corroborate the results of in vivo studies on selective tropism and prolonged intracellular persistence of *Rhizopus* conidia inside AMs.

In order to evaluate the mechanism of *Rhizopus* persistence inside macrophages, we tested whether fungal conidia are resistant to damage by phagocyte effector mechanisms[4,7,8]. Therefore, we compared susceptibility of *A. fumigatus* vs. *R. oryzae* conidia to (i) oxidative damage induced by hydrogen peroxide (H_2O_2) and (ii) non-oxidative damage mediated by

Fig. 1 Persistence of *Rhizopus* conidia inside alveolar macrophages (AMs). **a** Fungal loads in lungs of immunocompetent C57BL/6 (B6) mice ($n = 3$ per group) infected via intratracheal administration of a standardized inoculum (5×10^6 conidia per mice) of *A. fumigatus*, *R. oryzae*, or *R. delemar*. ***$P < 0.0001$, Mann–Whitney test. **b** Survival of immunocompetent C57BL/6 (B6) mice ($n = 8$ per group) infected as in **a**, with either *A. fumigatus*, *R. oryzae*, or *R. delemar*. **c** Representative photomicrographs of the lungs from mice infected as in **b** with either *A. fumigatus* or *R. oryzae* and sacrificed on day 5. Histopathological sections were stained with Grocott methenamine silver (GMS; left panels) or hematoxylin and eosin (H&E; right panels). The presence of *R. oryzae* conidia (black color) in the lungs is shown by GME stain. Original magnification ×400. **d** Representative photomicrographs of the lungs from mice infected as in **b**, sacrificed on day 5. Lungs were stained by IHC for CD68 or CD11 and counterstained with hematoxylin and PAS. There is evidence of extracellular *R. oryzae* conidia surrounded by neutrophils (top panel), and intracellular *R. oryzae* conidia inside AMs. **e** FACS analysis of total number of professional phagocytes in the lungs of immunocompetent mice ($n = 3$ per group) infected with *R. oryzae* as in **a**, assessed on days 1 and 5. The gating strategy for identification of neutrophils, monocytes, AMs, interstitial macrophages (IMs), and dendritic cells (DCs) is shown in Supplementary Fig. 1. **f** FACS analysis of association of labeled (Fluorescent Brightener 28; CW) conidia of *R. oryzae* with professional phagocytes of mice infected as in **a**, assessed on days 1 and 5. **g** In vivo phagocytosis rates of *R. oryzae* conidia on day 5 of infection of mice infected as in **a**. ***$P < 0.0001$ Mann–Whitney test. **h** Representative confocal image of sorted AM from mice infected as in **a** with fluorescent-labeled, live conidia of *R. oryzae* (day 1), fixed and stained with Cathepsin D. Cross-section analysis was performed to discriminate intracellular conidia from conidia associated/bound to the cell surface of AM

lysosomal hydrolases. Importantly, conidia of both fungi displayed comparable degree of susceptibility to killing by increasing concentrations of either H_2O_2 (Fig. 2f) or crude lysosomal extracts (Fig. 2g, h). Therefore, both fungi displayed comparable degree of susceptibility to macrophage effector killing mechanisms and the inability of BMDMs to kill *Rhizopus* could not be explained by resistance of the conidia to oxidative or non-oxidative damage.

During interaction of human fungal pathogens with macrophages, the induction of different forms of host cell death is a survival strategy that allows the fungus to escape host defense[17–19]. In addition, studies on *Mucor circinelloides* demonstrated that fungal sporangiospores germinate and induce killing of a murine macrophage cell line[20]. Therefore, we investigated if *A. fumigatus* and *R. oryzae* vary in their ability to induce host cell apoptosis or necrosis. We found no difference between the two fungi in induction of either form of host cell death during interaction with murine BMDMs (Fig. 2i). Collectively, these data demonstrate that Mucorales survive inside macrophages by avoiding phagocyte-mediated killing.

Conidia induce phagosome maturation arrest via targeting LAP. To understand the mechanism of establishment of *Rhizopus* intracellular persistence, we performed comparative phagosome biogenesis studies following phagocytosis of *A. fumigatus* or *R. oryzae* by BMDMs. Because LC3-associated phagocytosis (LAP) is a major antifungal pathway regulating early events in biogenesis of *A. fumigatus* phagosome[21,22], we initially analyzed $LC3^+$ phagosome (LAPosome) formation at different time points of infection by confocal imaging. In sharp contrast to the robust activation of LAP pathway upon infection with *A. fumigatus*, we found no evidence of LAPosome formation during infection of BMDMs with *R. oryzae* (Fig. 3a, b). Similarly, Rab5 recruitment to the phagosome, an early event in phagosome maturation process[23], selectively and transiently occurred at early time points of BMDM infection with *A. fumigatus*, while there was no evidence of Rab5 localization in *R. oryzae*-containing phagosomes (Fig. 3c, Supplementary Fig. 4).

Next, we monitored phagolysosomal (P–L) fusion upon BMDM infection with *A. fumigatus* vs. *R. oryzae* with the use of fluorescein isothiocyanate-labeled dextran (FITC-Dextran) assay. Briefly, BMDMs were pre-loaded with FITC-Dextran for labeling of lysosomes and P–L fusion upon fungal infection was assessed based on accumulation of FITC-Dextran in the phagosomes. In contrast to the accumulation of FITC-Dextran in A. *fumigatus* containing phagosomes over time (Fig. 3d, e), there was no evidence of FITC-Dextran recruitment in Mucorales phagosomes. Concordant with these results, recruitment of Cathepsin D, a lysosomal hydrolase, in phagosomes was significantly impaired at 4 h of BMDM infection with *R. oryzae* as compared to *A. fumigatus* (Fig. 3f, g). Further, these findings were confirmed by electron microscopy studies on fusion of acid phosphatase-stained lysosomes with *A. fumigatus* vs. *R. oryzae* phagosomes. Notably, while P–L fusion was evidenced as intense acid phosphatase staining in *A. fumigatus* phagosomes at 4 h of infection, there was no lysosomal association with *R. oryzae* phagosomes (Fig. 3h). Similarly, in vivo studies in AMs of immunocompetent mice following infection with *R. oryzae* revealed the ability of Mucorales conidia to block P–L fusion by inhibiting LAP (Fig. 4a–d). Collectively, these studies confirm that *Rhizopus* conidia block LAP and induce phagosome maturation arrest to establish intracellular persistence inside the macrophage.

Cell wall melanin induces phagosome maturation arrest. We have recently demonstrated that cell wall melanin on dormant conidia of *A. fumigatus* blocks LAP to inhibit phagosome biogenesis and promote fungal pathogenicity[22]. In addition, we revealed that removal of melanin during intracellular swelling of *A. fumigatus* conidia is a fundamental requirement for activation of LAP and efficient killing of the fungus by monocytes/macrophages[21,22]. Thus, we assessed whether a similar mechanism is responsible for the phagosome maturation arrest seen with *R. oryzae* conidia. Intriguingly, in sharp contrast to *A. fumigatus* conidia, *Rhizopus* conidia remained dormant without evidence of cell wall swelling at 24 h of infection in macrophages ex vivo (Fig. 5a, b) and in vivo, inside AMs (Supplementary Fig. 5). This finding corroborates the lack of apparent germination of *R. oryzae* conidia in the lungs of immunocompetent mice. Therefore, in all likelihood, lack of cell wall remodeling in Mucorales conidia results in surface retention of cell wall inhibitory molecule(s) to block phagosome responses and establish intracellular persistence. Consistent with this hypothesis, we found that ultraviolet (UV)-inactivated conidia of Mucorales induce phagosome maturation arrest in macrophages to a similar degree of live conidia (Supplementary Fig. 6), implying the presence of an inhibitory molecule on the fungal cell wall surface.

Despite the differences in cell wall composition of filamentous fungi, melanin is a common cell wall molecule in conidia of many filamentous fungi including *Aspergillus*[24,25]. Therefore, we purified melanin from conidial cell wall of *Rhizopus* spp. and performed comparative characterization with *A. fumigatus* 1, 8-dihydroxynaphthalene (DHN) melanin. Notably, we found that *Rhizopus* melanin exhibited all the classic characteristics of melanin pigments (Supplementary Table 1). However, electron paramagnetic resonance (EPR) spectra (Fig. 5c), UV spectrophotometry (Supplementary Fig. 7), infrared (IR) spectroscopy (Supplementary Fig. 8), and chemical degradation followed by

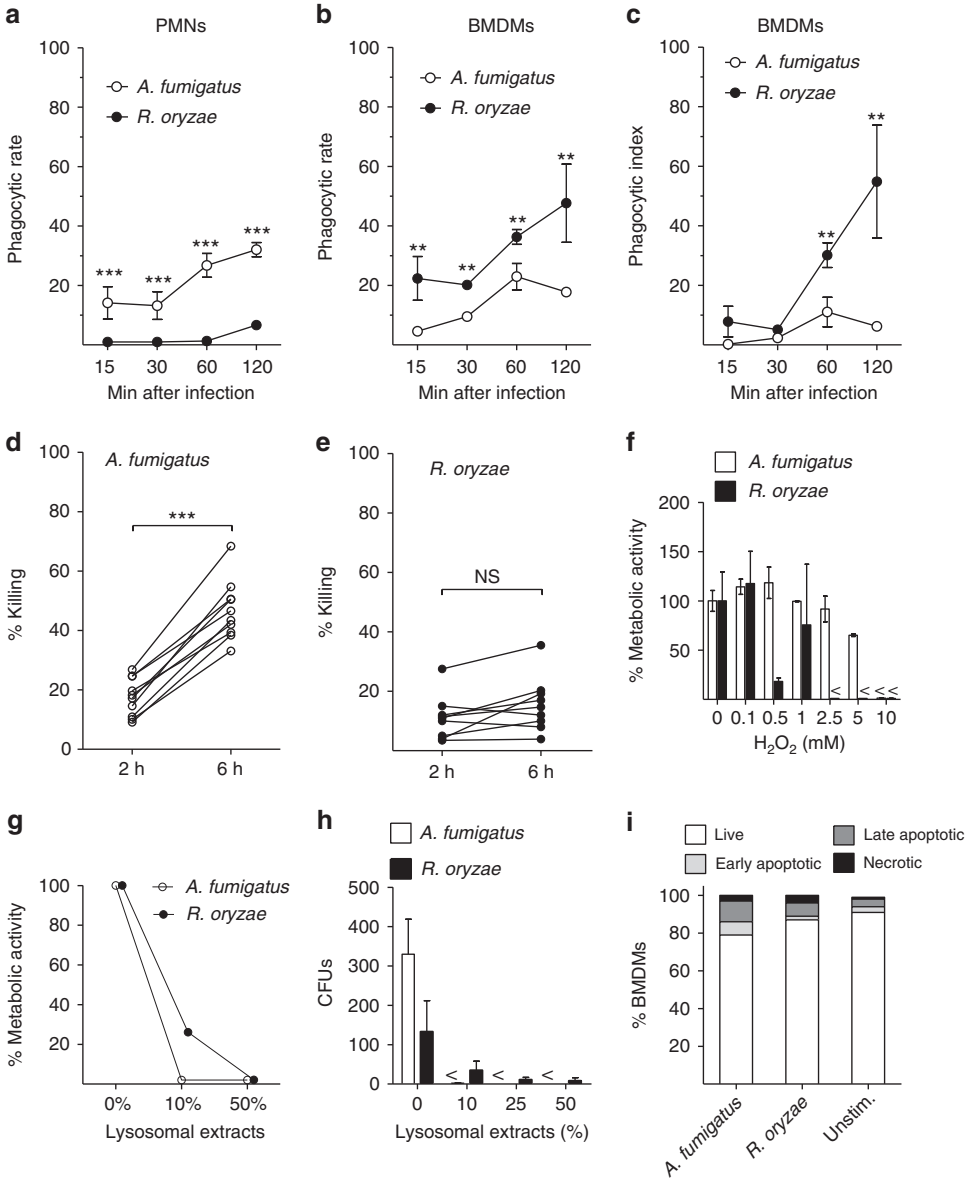

Fig. 2 *Rhizopus* conidia display resistance to ex vivo killing by macrophages. **a**–**c** Comparative studies on phagocytosis of *A. fumigatus* and *R. oryzae* conidia by BMDMs and neutrophils (PMNs) assessed by confocal imaging. Data on quantification of phagocytosis are presented as mean ± SEM of five independent experiments ***$P < 0.0001$, **$P < 0.001$, Mann–Whitney test. **d**, **e** Intracellular killing of *A. fumigatus* and *R. oryzae* (Mucorales) conidia by BMDMs. Symbols connected with a line represent time points of the same independent experiment ($n = 9$ per group). ***$P < 0.0001$, Mann–Whitney test. **f**, **g** Assessment of in vitro susceptibility of *A. fumigatus* and *R. oryzae* conidia to **f** oxidative damage induced by increasing concentrations of H_2O_2 or **g** to damage induced by enzymatic activity of increasing concentrations of lysosomal extracts of BMDMs, assessed by measurement of fungal metabolic activity using the XTT assay at 24 h. **h** In vitro fungicidal activity of increasing concentrations of lysosomal extracts against conidia of *A. fumigatus* or *R. oryzae* assessed by CFU plating. **i** Induction of apoptosis in unstimulated BMDMs or BMDMs infected with *A. fumigatus* or *R. oryzae* at an MOI of 3:1 (effector:fungal cells) for 6 h. Apoptotic BMDMs were assessed by FACS analysis following Annexin V/PI staining. Data are representative of one out of three independent experiments. *NS* not significant

liquid chromatography-mass spectrometry (LC-MS) studies of the degradation products (Supplementary Fig. 9) revealed that *Rhizopus* melanin is different than DHN melanin of *A. fumigatus*. In particular, *Rhizopus* melanin has chemical composition consistent of eumelanin, and requires a biosynthetic pathway, which likely involves activity of a copper-dependent tyrosinase/laccase (Supplementary Figs. 7, 8 and 9). Indeed, growth in copper-free media resulted in the production of albino conidia of *Rhizopus*.

Importantly, functional studies on phagosome responses in macrophages stimulated with purified melanin of either *Aspergillus* or *Rhizopus* demonstrated that both types of melanin induced complete phagosome maturation arrest (Fig. 5d). As a further proof of the melanin-dependent induction of phagosome maturation arrest by intracellular conidia of *Rhizopus*, we assessed LAPosome formation and Cathepsin D recruitment upon chemical degradation of *Rhizopus* melanin via H_2O_2 bleaching, as previously described[22]. Importantly, chemical removal of melanin from conidia of *Rhizopus* resulted in reversal of phagosome maturation arrest as evidenced by the significant increase in recruitment of LC3 II (Fig. 5e, f) and Cathepsin D (Fig. 5g, h) to the phagosomes containing melanin-deficient

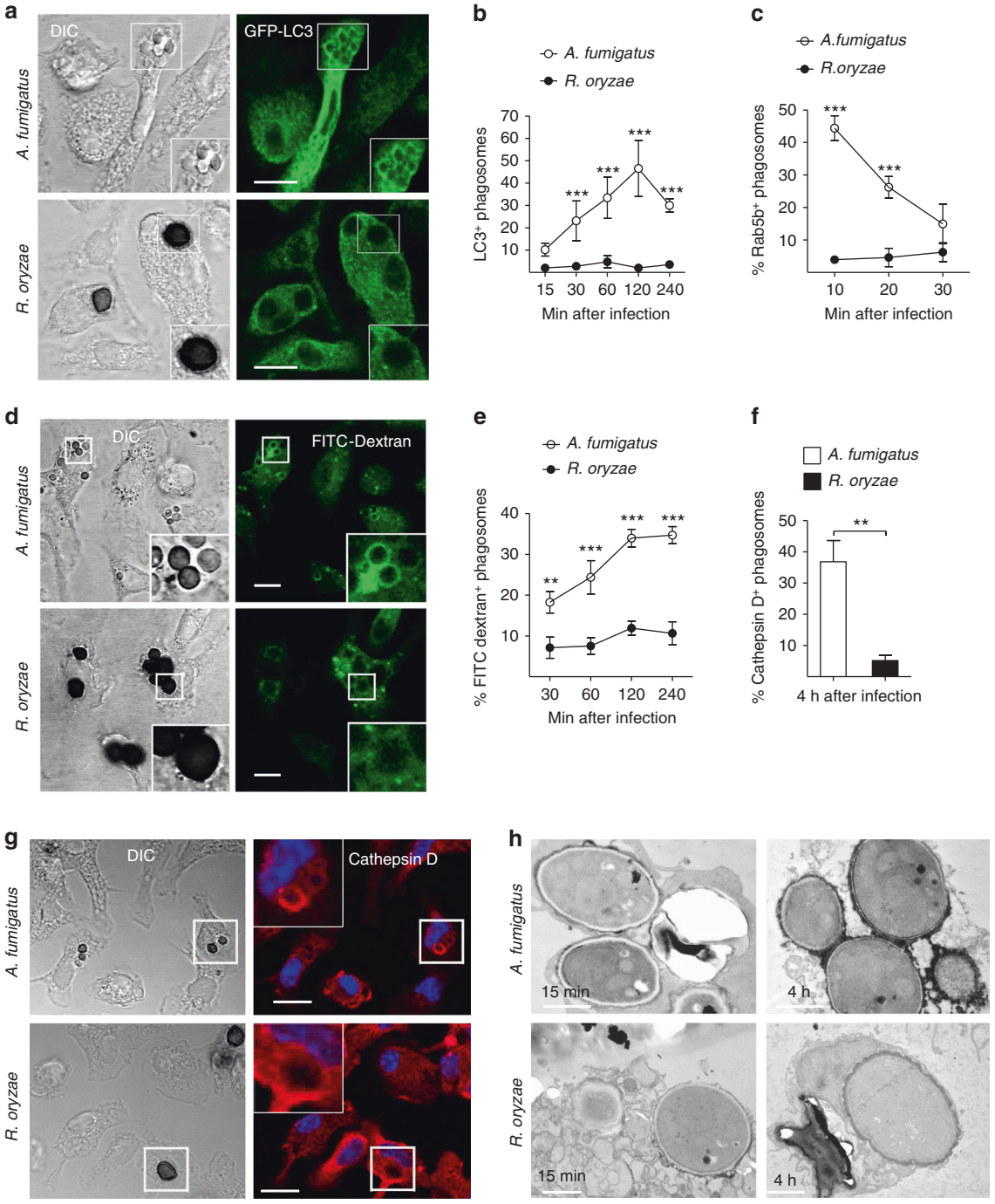

Fig. 3 *Rhizopus* conidia induce phagosome maturation arrest in BMDMs. **a**, **b** BMDMs from GFP-LC3 mice were infected at different time points with live conidia of *A. fumigatus* or *R. oryzae* at an MOI 3:1 (effector:fungal cells). At the indicated time point, cells were fixed and analyzed by confocal microscopy. Representative fluorescence images are presented in **a**. Bar, 5 µm. Data on quantification of $LC3^+$ phagosomes are presented as mean ± SEM of five independent experiments in **b**. **c** BMDMs from C57BL/6 (B6) mice were infected as in **a**. Cells were fixed at the indicated time point and stained for Rab5B. Data on quantification of $Rab5^+$ phagosomes are presented as mean ± SEM of three independent experiments. **d**, **e** BMDMs were pre-loaded with FITC-Dextran, infected as in **a**, and phagolysosomal fusion was assessed at the indicated time point based on acquisition of FITC-Dextran in the phagosome. Representative fluorescence images are shown in **d**. Bar, 5 µm. Data on quantification of FITC-$Dextran^+$ phagosomes are presented in **e** as mean ± SEM of three independent experiments. **f**, **g** BMDMs were stimulated as in **a**, cells were fixed and stained for the lysosomal protein marker Cathepsin D. Data on quantification of Cathepsin D^+ phagosomes are presented as mean ± SEM of three independent experiments in **f**, while representative fluorescence images are shown in **g**. Bar, 5 µm. **h** Representative electron microscopy of acid phosphatase, a lysosomal enzyme marker of phagolysosomal fusion (shown as dark color on the phagosome membrane) in 15 min and 4 h phagosomes containing *A. fumigatus* or *R. oryzae* conidia. $^{***}P < 0.0001$, $^{**}P < 0.01$, Mann–Whitney test. Bar, left upper and lower panels, 1 µm; right upper panel, 0.5 µm; right lower panel, 2 µm

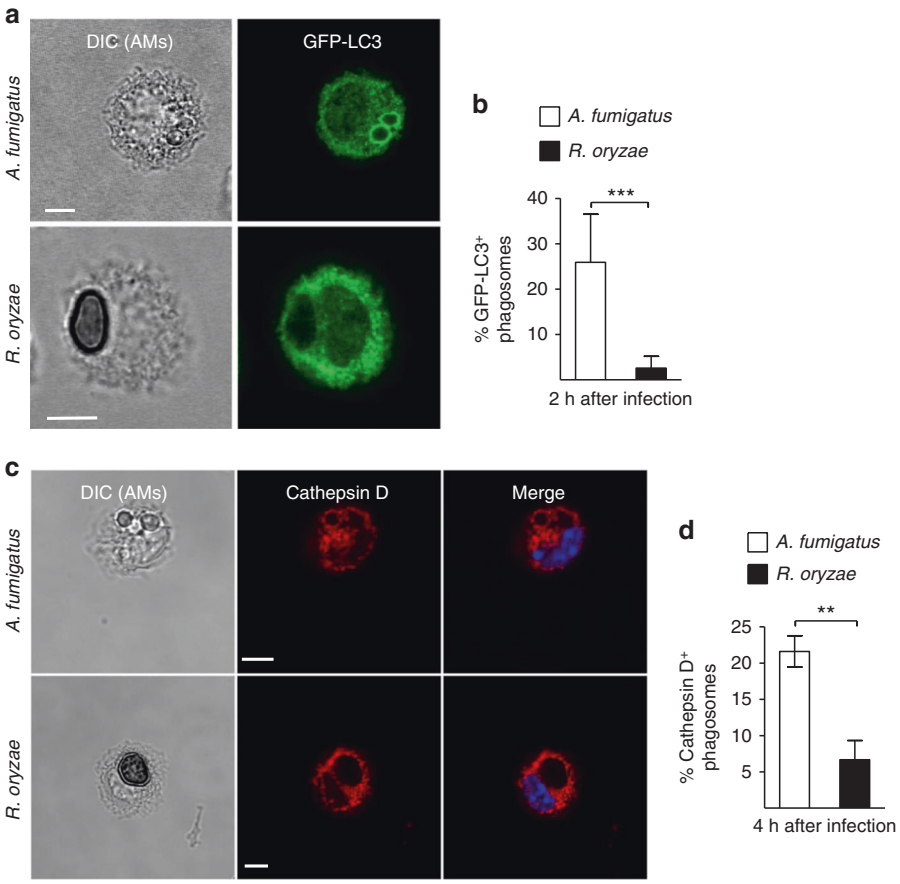

Fig. 4 *Rhizopus* inhibits phagosome biogenesis in AMs during in vivo infection. GFP-LC3 (**a**, **b**) or C57BL/6 (B6) (**c**, **d**) mice were infected intratracheally with 5×10^6 conidia of either *R. oryzae* or *A. fumigatus*. AMs were obtained by bronchoalveolar lavage at the indicated time point, fixed, stained with anti-GFP (**a**) or Cathepsin D (**b**) antibodies, and assessed by confocal imaging. Representative fluorescence images are shown (**a**, **c**). Data on quantification of GFP-LC3$^+$ (**b**) and Cathepsin D$^+$ (**d**) phagosomes are presented as mean ± SEM of three independent experiments. ***$P < 0.0001$, **$P < 0.001$ Mann–Whitney test. Scale bar, 5 µm

(albino) *Rhizopus*. Finally, infection of immunocompetent mice with melanin-deficient (albino) *Rhizopus* conidia recovered from culture in copper-free media (Fig. 5i) resulted in rapid fungal clearance from the lungs, when compared to infection with wild-type (WT) (control) melanized *Rhizopus* conidia (Fig. 5j). Collectively, these findings demonstrate that surface retention of melanin in dormant conidia of *Rhizopus* inside macrophages is the mechanism that accounts for prolonged intracellular persistence.

Non-redundant role of macrophages in pulmonary mucormycosis. Despite the inability of macrophages to kill *Rhizopus*, inhibition of growth of phagocytosed conidia could be an important host defense mechanism. To test this hypothesis, we initially assessed differences in phagocytosis of dormant vs. germinating (swollen) conidia following 4 h pre-incubation in culture media. Notably, we found a significant ≈5-fold reduction in phagocytosis of swollen as compared to dormant conidia by macrophages (Fig. 6a).

Then, we infected immunocompetent mice via intratracheal administration of the same inoculum of dormant vs. swollen conidia of *Rhizopus* (5×10^6 conidia/mice), and assessed differences in the infection outcome. Surprisingly, while all mice recovered from infection with dormant *Rhizopus* conidia, infection of immunocompetent mice with swollen conidia of *Rhizopus* resulted in 100% mortality within 4 days (Fig. 6b). Histopathological examination of the lungs at 16 h of infection with swollen *Rhizopus* conidia revealed dense neutrophil infiltrates along with extensive tissue necrosis and angioinvasive fungal growth (Fig. 6c, Supplementary Fig. 10). Notably, we found no evidence of *Rhizopus* inside AMs or other phagocytes following infection of mice with swollen conidia (Fig. 6c, Supplementary Fig. 10), a finding consistent with the results of ex vivo studies.

In order to directly evaluate the role of macrophages in physiological immune response to Mucorales, we performed AM depletion via intratracheal administration of clodronate liposomes[26,27] and 3 days latter infected mice with *Rhizopus* dormant conidia. Interestingly, survival, histopathology, and fungal load experiments demonstrate that liposome depletion resulted in significant increase in susceptibility of mice to mucormycosis as compared to treatment with control liposomes (Fig. 6d–f). In order to further validate the role of AMs in mucormycosis, we depleted CD11c transgenic mice with the administration of diphtheria toxin (DT), verified selective depletion of CD11c+ cells (Fig. 6g, Supplementary Fig. 11), and assessed the effect on survival following *Rhizopus* infection. Importantly, we found a dramatic increase in susceptibility of CD11c-depleted mice to mucormycosis with 100% mortality at 5 days of infection (Fig. 6h). Collectively, these findings demonstrate a non-redundant role of CD11c+ cells in the lungs, including AMs and DCs, in antifungal immunity against *Rhizopus*.

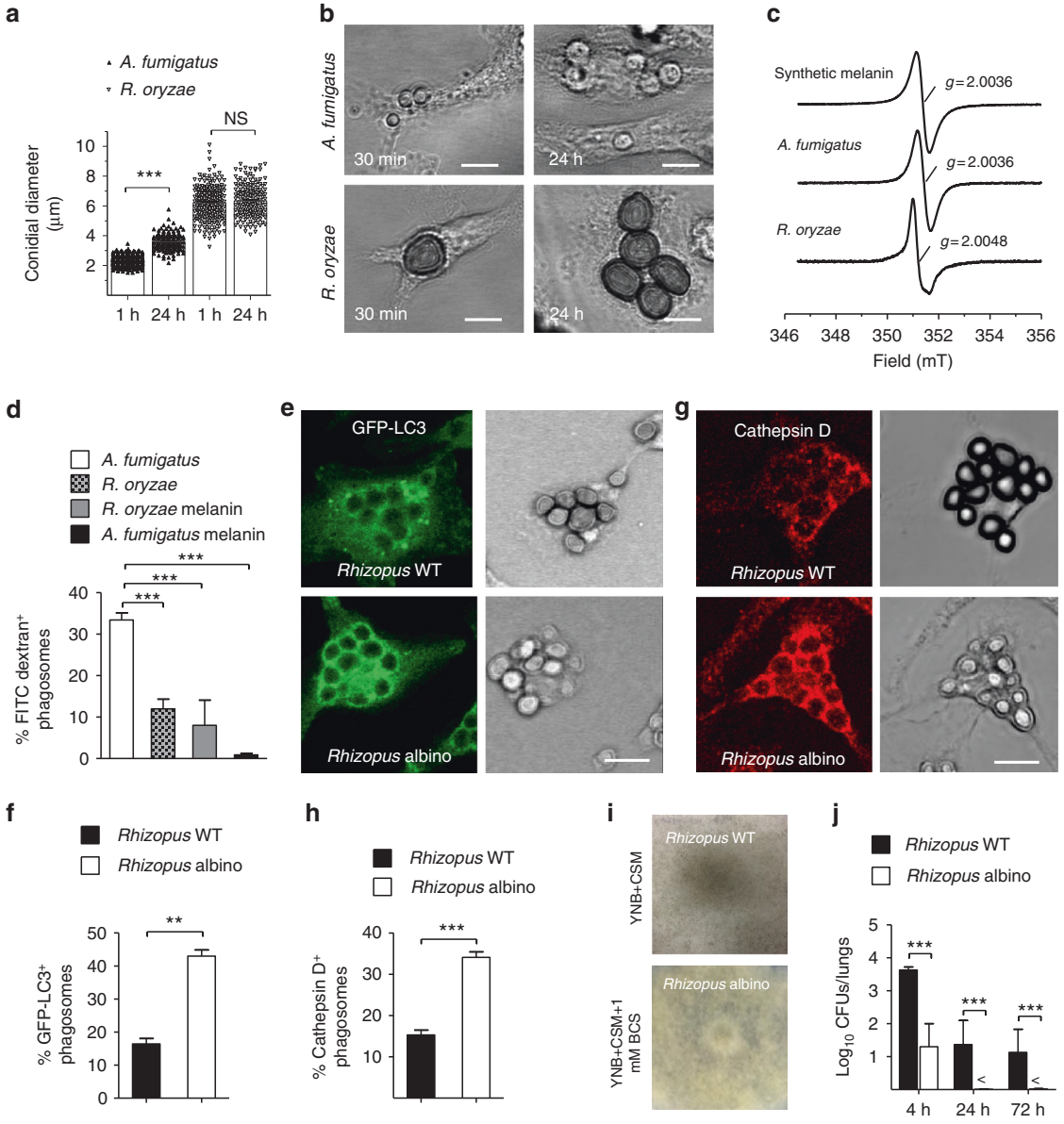

Fig. 5 *Rhizopus* melanin blocks early event in phagosome biogenesis. **a** GFP-LC3 BMDMs were infected at 1 or 24 h with live conidia of *A. fumigatus* or *R. oryzae* at an MOI 1:1. Cells were fixed and the conidial diameters of intracellular conidia was measured by confocal microscopy. Data on quantification of conidial diameter are presented from one out of three independent experiments. Each symbol represents the value of maximum diameter of individual fungal cell and horizontal bars represent the mean diameter. ***$P < 0.0001$, Mann–Whitney test. **b** Representative DIC images from **a** are shown. **c** X-band room temperature EPR spectra of purified melanin obtained from *A. fumigatus*, *R. oryzae*, or synthetic melanin are shown. **d** BMDMs pre-loaded with FITC-Dextran were stimulated with conidia of *A. fumigatus* or *R. oryzae* or melanin ghosts (purified melanin particles) obtained from conidia of the indicated *A. fumigatus* or *R. oryzae* strains at an MOI of 3:1 (effector:fungal conidia). Cells were removed at 4 h and assessed by confocal imaging. Data on quantification of FITC-Dextran$^+$ phagosomes are presented as mean ± SEM of three independent experiments. **e**, **h** BMDMs from GFP-LC3 (**e**, **f**) or C57BL/6 (B6) (**g**, **h**) mice were infected with *R. oryzae* conidia (WT conidia) or *R. oryzae* conidia following chemical degradation of melanin with H_2O_2 bleaching (albino conidia) at an MOI of 3:1 (effector:fungal cells). Cells were removed at 1 h of infection, fixed, stained, and analyzed by confocal imaging. Data on quantification of GFP-LC3$^+$ (**f**) or Cathepsin D$^+$ (**h**) phagosomes are presented as mean ± SEM of three independent experiments. **e**, **g** Representative fluorescent images from experiments on **f** and **h** are shown. **i**, **j** Fungal loads from lungs of immunocompetent mice ($n = 9$ per experimental group) infected with 10^6 conidia of *R. delemar* grown in regular media (WT *Rhizopus*) or under conditions of copper starvation to inhibit melanization (albino *Rhizopus*) (**i**). Mice ($n = 3$ per condition) were sacrificed at the indicated time points, lungs were homogenized, and fungal loads were assessed by CFU plating (**j**). ***$P < 0.0001$,
**$P < 0.001$ Mann–Whitney test. Scale bar, 10 µm

Iron starvation governs *Rhizopus*–macrophages interplay. Because of the blockade in P fusion induced by *Rhizopus*, we reasoned that nutritional immunity is the main effector mechanism to inhibit fungal growth inside macrophages. In view of the central role of iron in Mucorales growth[7,8], we performed transcriptomic analysis of host and pathogen genes to explore whether an iron restriction mechanism accounts for inhibition of conidial growth inside macrophages. Specifically, we performed RNA-seq on poly(A)-enriched RNA isolated from BMDMs infected with *R. delemar* (strain 99-880) at different time points (1, 4, or 18 h). The RNA preparations contained a mixture of messenger RNAs (mRNAs)

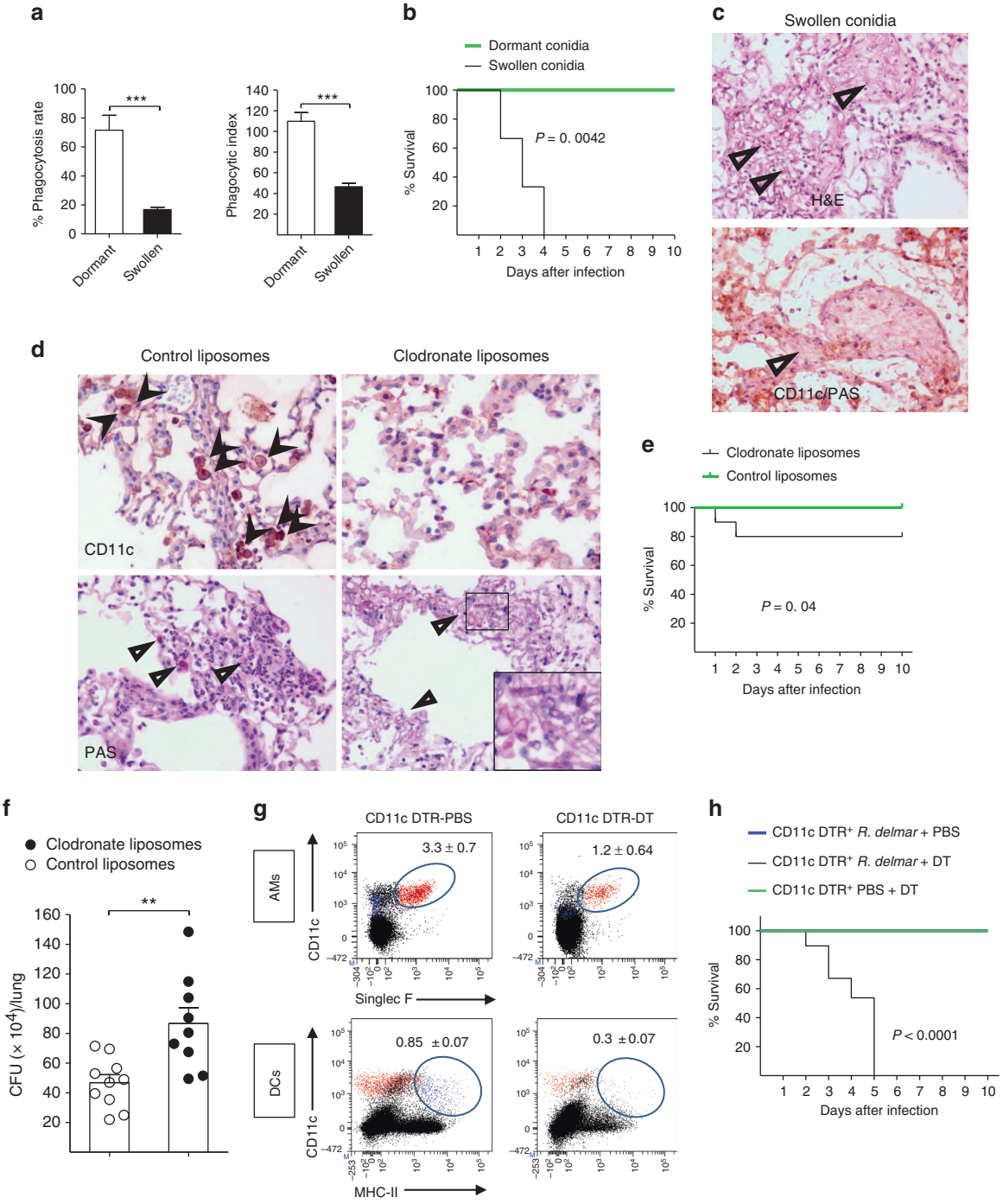

Fig. 6 AMs have a non-redundant role in immunity against *Rhizopus*. **a** GFP-LC3 BMDMs were infected with dormant or swollen conidia of *R. oryzae* at an MOI of 3:1 (effector:fungal cells) and phagocytosis was assessed at 4 h. Data on quantification of phagocytosis of *Rhizopus* conidia are presented as mean ± SEM of three independent experiments. ***$P < 0.0001$, Mann–Whitney test. **b** Survival of immunocompetent C57BL/6 (B6) mice ($n = 8$ per group) infected via intratracheal administration of a standardized inoculum (5×10^6 conidia per mice) of dormant or swollen conidia of *R. oryzae*. **c** Representative photomicrographs of the lungs from mice infected with 5×10^6 swollen conidia of *R. oryzae* at 24 h of infection. Lungs were stained by H&E or IHC for CD11 and counterstaining with hematoxylin and PAS. **d** Representative histopathology from lungs of C57BL/6 (B6) mice following intratracheal administration of 100 µl of clodronate liposomes or control liposomes and 48 h later infection with 10^7 *R. oryzae* conidia. Invasive hyphal growth is present in the lungs of clodronate liposome group of mice. **c**, **d** Original magnification ×400. **e** Survival of C57BL/6 (B6) mice treated with clodronate liposomes ($n = 10$) or control liposomes ($n = 15$) and infected as in **d**. **f** Fungal loads in the lungs of C57BL/6 (B6) mice treated with clodronate liposomes or control liposomes and infected as in **d**. Lungs were removed on day 2 of infection and fungal loads were assessed by CFU plating. **$P < 0.001$, Mann–Whitney test. **g** CD11c-DTR mice were intranasally inoculated with 40 µl PBS or with 20 ng/g of body weight of diphtheria toxin in 40 µl PBS and analyzed for the presence of $CD11c^+$ cells (AMs and DCs) at 24 h. Results represent two to three experiments with two to three mice per group per experiment. **h** Survival of CD11c-DTR mice ($n = 5$ per group) treated with DT (20 ng/kg of mice) or PBS (control) and infected 48 h later with 5×10^6 conidia of *R. delemar*. The nonparametric log-rank test was used to determine differences in survival times

expressed by the *Rhizopus* spp., as well as by the host cells. To ensure that the observed fungal gene expression changes were due to the interaction with the host cell and not simply a response to the medium, we performed RNA-seq on control *Rhizopus* conidia incubated for 5 min in culture medium in the absence of host cells. Similarly, we performed RNA-seq on control, uninfected BMDMs.

From the pathogen perspective, the majority of genes previously implicated in iron acquisition were regulated during infections (Fig. 7a). In particular, we identified *Fet3* and *Ftr1* as the most highly upregulated genes during intracellular persistence of *R. delemar* inside BMDMs. Notably, Fet3, a multicopper ferroxidase required for ferrous iron uptake and its interacting partner, the high affinity iron permease Ftr1p, comprise the major iron assimilation pathway of *Rhizopus* that is induced under iron-limited conditions and has a major pathogenetic role during in vivo infection[9].

In BMDMs, a significant number of iron metabolism-related genes identified in previous transcriptomic studies were differentially expressed over the course of *Rhizopus* infection[28,29], with an expression pattern consistent with activation of an M2-alternative program (Fig. 7b). Specifically, there was evidence of downregulation of typical M1-related genes (*Nos2*, *Mpo*, *Hif1a*, *Egln3*) and upregulation of M2-related genes (*Myc*, *fxn*, *Cyp1b1*, *Alas1*). Additionally, several genes directly linked to trafficking and intracellular distribution of iron inside macrophages (*heph*, *fxn*, *bdh2*, *hfe*, *ltf*, *lcn2*, *Steap 1*, *Steap 2*, *Steap 4*) were differentially expressed during Mucorales infection. On the other hand, *Rhizopus* infection induced downregulation of hemochromatosis (*hfe*) and *Ptgs2* genes, which are both upregulated during alternative activation in macrophages[28–30]. Collectively, dual RNA-seq revealed the induction of an iron restriction response during the course of *Rhizopus* infection in BMDMs.

Iron restriction inhibits *Rhizopus* growth inside macrophages. Next, we tested directly whether iron restriction is the primary mechanism of inhibition of fungal growth in macrophages. Importantly, BMDMs were infected with *Rhizopus* with or without the presence of iron, DFO, or iron plus DFO in culture media and germination of intracellular conidia was assessed at different time points of infection. Notably, whereas there was minimal evidence of germination of *Rhizopus* conidia in control-untreated BMDMs, ex vivo supplementation of media with iron, DFO, or both resulted in a significant increase in germination of intracellular conidia that was apparent at 12 h of infection (Fig. 8a, b) and subsequent lysis of macrophages.

As an extra proof of the important role of iron restriction in Mucorales inhibition by macrophages, we tested the ability of *Rhizopus* mutants defective in pathways of iron assimilation, which have been shown to be attenuated in virulence in mouse models of mucormycosis of diabetic ketoacidosis and neutropenia, to germinate intracellularly following iron supplementation[9,10]. In particular, we evaluated interaction of macrophages with *ftr1* attenuated mutant of *Rhizopus* spp., which is compromised in virulence because of its diminished capacity to grow under iron-limiting conditions and was highly induced in transcriptomics analysis[9]. Although *Rhizopus* mutant with reduced *FTR1* copies was not killed by macrophages, it displayed major defects in germination following iron supplementation by either $FeCl_3$, DFO, or both (Fig. 8c, d). Notably, infection of BMDMs with the *Rhizopus fob1/2* mutant with defect in DFO uptake[10] displayed impaired germination following supplementation of culture media with DFO, which was by-passed in the presence of exogenous iron (Fig. 8e, f). Collectively, these findings clearly reveal the essential role of iron restriction inside the phagosome of macrophages on inhibition of intracellular growth of Mucorales conidia.

Persister conidia inside macrophages in human mucormycosis. In order to explore the physiological relevance of our studies in humans, we performed histopathological analysis of surgical specimens obtained from a patient with acute myelogenous leukemia who developed disseminated mucormycosis. The patient underwent radical surgery including splenectomy because of worsening necrotizing pneumonia with infiltration of the chest wall and the spleen (Fig. 9a). In histopathology, there was evidence of necrotizing angioinvasive growth of Mucorales hyphae along with areas of granulomatous inflammation in the spleen that contained intracellular Mucorales conidia inside macrophages (Fig. 9b–e). Collectively, these findings are consistent with a pathogenetic model of mucormycosis highlighting the central role of Mucorales–macrophage interplay in disease development (Fig. 10).

Discussion

Mucorales are successful pathogens of a range of phylogenetically disparate hosts, from plants to invertebrates and humans[7,8,31–33]. The emergence of mucormycosis in patients with acquired innate immune defects illustrates the important role of professional phagocytic cells in Mucorales host defense[8]. In contrast, the rarity of mucormycosis in patients with primary immunodeficiencies, who are prone to infections caused by other filamentous fungi[34–36], implies that distinct immune pathways are important to restrict Mucorales growth. For example, *Aspergillus* is the primary pulmonary pathogen in patients with genetic defects in NADPH oxidase (chronic granulomatous disease; CGD)[1,16]. In contrast, mucormycosis is a rare infection in CGD patients and occurs only upon administration of corticosteroids[36].

Herein, we reveal the essential role of *Rhizopus*–macrophage interplay for infection outcome and introduce evidence that a central pathogenetic event in development of mucormycosis is related to the prolonged intracellular survival of the fungus inside these immune cells. In addition, we dissect the molecular mechanisms that allow *Rhizopus* to persist inside macrophages via melanin-induced phagosome maturation arrest. Finally, we identify nutritional immunity via iron restriction inside the phagosome as an important host defense mechanism during pulmonary mucormycosis. These findings lead to a pathogenetic model of mucormycosis that links abnormalities in iron metabolism with nutritional immunity inside macrophages and has important implications in future design of therapeutics against mucormycosis.

Our findings on prolonged persistence of *Rhizopus* in the lungs of immunocompetent mice are in sharp contrast to the rapid clearance of *Aspergillus* (this study and refs.[22,26]) and in line with the increased pathogenicity of Mucorales. Previous studies describe the fungistatic activity of macrophages and other professional phagocytes against *Rhizopus* as a possible link to their increased virulence[32,33,37–40]. The present work extends on these findings by providing mechanistic insight on the molecular aspects of macrophages–Mucorales interplay. Specifically, our in vivo studies clearly demonstrate that *Rhizopus* conidia display a tropism and establish prolonged intracellular survival inside AMs that accounts for persistence in the lungs of immunocompetent mice. Importantly, definitive evidence on the non-redundant role of macrophages and other CD11c+ cells of the lungs in immunity against *Rhizopus* was shown by in vivo studies following targeted depletion with the use of clodronate liposomes and CD11c-DTR transgenic mice. In addition, persister conidia of Mucorales inside macrophages were found in a patient with disseminated mucormycosis. Notably, evidence of Mucorales conidia in tissue has also been reported as a characteristic histopathological finding of mucormycosis[41]. These findings have

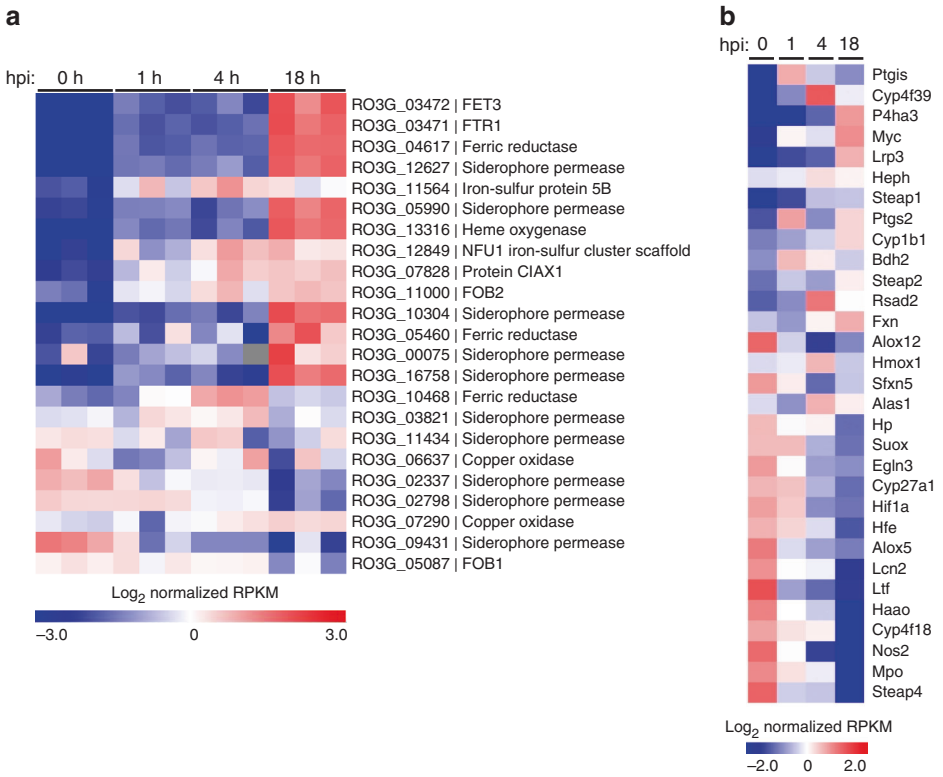

Fig. 7 Global analysis of differential gene expression during infection. RNA-seq-based expression analysis of iron-related **a** *R. delemar* genes and **b** mouse genes following in vitro infection of BMDMs. **a** Each column represents an individual sample (biological triplicates of four different conditions; $n = 12$). Log-transformed absolute expression normalized across all samples. Red indicates high gene expression. Blue indicates low gene expression. For the 0 h column, *R. delemar* was incubated in tissue culture media without BMDMs for 1 min. **b** Values are presented as in **a** and represent the average of three biological replicates for each condition. For the 0 h columns, BMDMs were incubated in culture media in the absence of *R. delemar* spores for 1 hr

important implications in pathogenesis, epidemiology, and therapeutics of mucormycosis. Specifically, the ability of a classic extracellular pathogen to remain in intracellular dormancy could provide protection from host effector mechanisms and antimicrobial therapy[42]. Notably, failure to eradicate intracellular conidia of Mucorales might also explain clinical observations on relapse of mucormycosis years following cessation of secondary antifungal prophylaxis[43].

In addition, our studies on biogenesis of *Rhizopus* phagosome identified the mechanism of resistance of conidia to killing by macrophages. Specifically, we demonstrate that *Rhizopus* conidia are fully susceptible to oxidative and non-oxidative effector mechanisms of macrophages. In contrast to recent work on macrophage cell lines showing germination and lysis of host cells by conidia of *Mucor circinelloides*[20], we show that primary macrophages completely inhibit Mucorales growth. These results are consistent with studies showing that bronchoalveolar macrophages harvested from lungs of immunocompetent mice are able to ingest and inhibit germination of *R. oryzae* spores without killing them in vitro[40]. The inability of macrophages to kill *Rhizopus* is due to inhibition of LAP, a specialized pathway of phagosome biogenesis with central role in regulation of immune homeostasis and antifungal host defense[21,22]. These early inhibition effects result in phagosome maturation arrest and account for resistance to macrophage killing.

A fundamental difference in biogenesis of *Rhizopus* vs. *Aspergillus* phagosomes that emerged from our study is the lack of intracellular swelling of *Rhizopus* conidia, which accounts for prolonged surface retention of cell wall melanin and subsequent inhibition of LAP and phagosome responses[22]. Furthermore, the ability of melanin to inhibit apoptosis in macrophages via sustained activation of Akt/PI3K signaling[44] facilitates the establishment of prolonged intracellular dormancy. In view of the critical role of melanin in intracellular survival of *Rhizopus*, further understanding of melanin biosynthesis pathway in these pathogens and harnessing activation of LAP pathway could pave the way for alternative therapeutic strategies in mucormycosis that will prevent or treat the disease with reduced risk of relapse.

In vivo studies on infection of immunocompetent mice with dormant vs. swollen conidia provided insight on the critical role of nutritional immunity mechanisms during early stages of infection by *Rhizopus*. Specifically, the inability of host related factors to inhibit *Rhizopus* growth results in failure of physiological immune responses to prevent invasive fungal growth and acute lethality, as evidenced by infection of immunocompetent mice with swollen conidia. Therefore, poorly understood intracellular and extracellular nutritional immunity mechanisms are at the first line of defense against Mucorales. One clear critical aspect of the failure of nutritional immunity responses against mucormycosis is clinically manifested by the unique susceptibility of diabetic ketoacidosis and DFO-treated patients (DFO is utilized by Mucorales as a xenosiderophore to supply iron to the fungus) to mucormycosis[6–8]. These two patient categories suffer from elevated available serum iron[11,45]. Our transcriptomic analysis of host and fungal iron regulated genes during the course of infection is consistent with activation of an iron restriction response in macrophages triggering the induction of iron starvation pathways in Mucorales, with notable example being the upregulation of the high affinity iron permease *FTR1*, its interacting partner *FET3*, and genes encoding ferric reductases[9]. Furthermore, direct evidence on the central role of iron restriction in inhibition of Mucorales growth is provided by reversal of

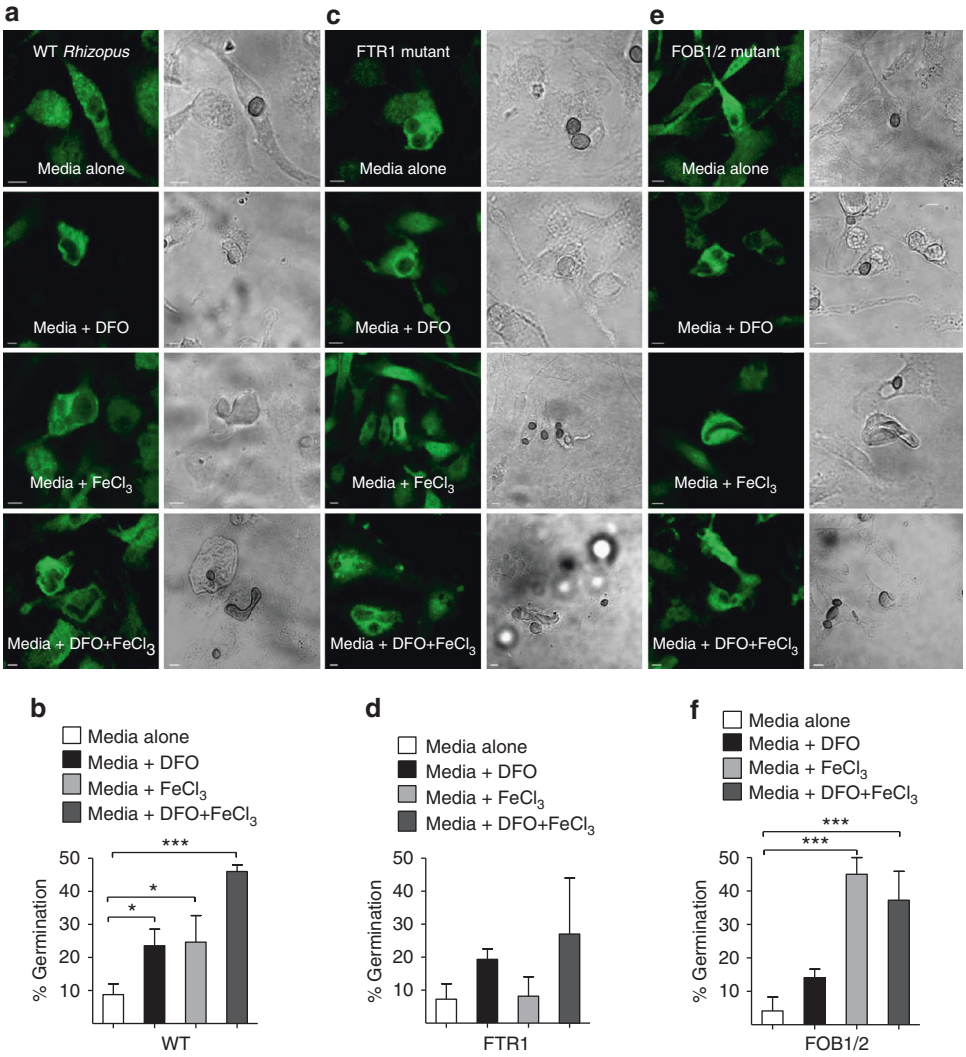

Fig. 8 Macrophages inhibit intracellular growth of *Rhizopus* via iron starvation. **a**, **b** BMDMs from GFP-LC3 mice were infected with WT *Rhizopus delemar* strain at an MOI of 1:2 (effector:fungal cells) in regular culture media or media containing DFO (100 μM), iron ($FeCl_3$; 100 μM), or DFO plus iron. At 1 h of infection, cells were extensively washed to remove non-phagocytosed conidia, media were replaced, and intracellular germination was assessed at 12 h by confocal imaging. BMDMs from GFP-LC3 mice were also infected with *R. delemar*-attenuated mutants for *FTR1* (**c**, **d**) or FOB1/2 (**e**, **f**), which are defective in the high affinity iron permease expression regulating iron assimilation under conditions of limited iron availability and DFO receptor FOB1/2 mediating fungal iron uptake from DFO, respectively, as in **a**. The attenuated mutants were derived from the wild-type strain used in **a**, **b** by RNAi[9, 10]. Representative immunofluorescence images are shown in **a**, **c**, and **f**. Data on quantification of germination of intracellular conidia of the indicated *Rhizopus* strain are presented as mean ± SEM of three independent experiments. ***$P < 0.0001$, *$P < 0.01$, Mann–Whitney test. Bar, 5 μm

the fungal growth inhibition when iron was exogenously administered in the form of $FeCl_3$, DFO, or ferrioxamine (the iron-rich form of DFO). Finally, studies utilizing *Rhizopus ftr1* mutant, which displays genetic defects in iron assimilation pathways and attenuated pathogenicity[9,10], showed inability to germinate inside the macrophages in the presence of iron supplementation. Our studies on the role of iron homeostasis inside macrophages in antifungal host defense should foster the concept of targeted iron chelation therapies inside these cells[46].

Overall, our study provides a pathogenetic model of mucormycosis, which places nutritional immunity inside macrophages in the forefront of antifungal immunity in the lung and explains how abnormalities in iron metabolism lead to development of immunodeficiency. Furthermore, these findings pave the way for future studies on host determinants of iron homeostasis in macrophages implicated in development of invasive fungal pneumonia[47,48]. Several questions on the signaling pathways, cytokine responses, and molecular components of iron homeostasis inside macrophages that maintain iron restriction inside the fungal phagosome remain unanswered. Notably, in patients with immune defects in LAP and/or other signaling pathways regulating phagolysosomal fusion, restriction of iron availability inside phagocytes could become the predominant effector mechanism to prevent invasive fungal disease. Therefore, dissecting abnormalities of iron metabolism in myeloid cells of immunocompromised patients at high risk for invasive mold infections should become a priority for development of future therapeutic strategies. Finally, the role of intracellular and extracellular nutritional immunity mechanisms related to other metals or nutrients against medically important fungi deserve further exploitation.

Methods

Reagents. The following antibodies and reagents were used for ex vivo studies in murine primary macrophages: anti-GFP polyclonal Ab (Minotech, #721-1, dilution 1:500), Cathepsin D (Santa Cruz, #sc-377299, dilution 1:100), Rab5B (clone A20,

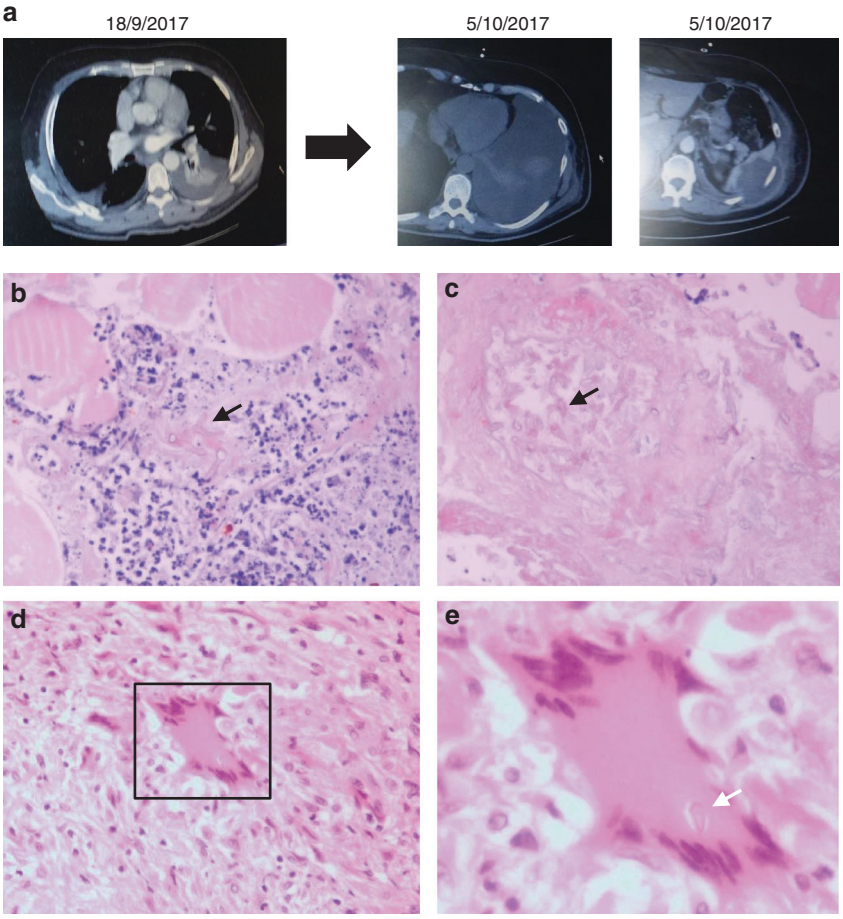

Fig. 9 Invasive pulmonary mucormycosis in a patient with intracellular persistence (**a**). A 60-year-old white male with relapsed acute myelogenous leukemia received salvage chemotherapy with fludarabine and high-hose cytarabine (FLAG) in August 2017. On September 2017, the patient developed febrile neutropenia, left-sided chest pain, and evidence of necrotizing pneumonia with chest wall myositis in computer tomography of the chest. He received treatment with broad-spectrum antibiotics and anidulafungin. Despite neutrophil recovery, the infection progressed with infiltration of the abdominal wall and the spleen. In tissue biopsy mucormycosis was diagnosed based on characteristic histopathological findings (**b**, **c**). The patient was started on liposomal amphotericin B and radical surgery with splenectomy was performed in November 2017. In histopathological analysis of muscle biopsy, there is evidence of extensive tissue necrosis and growth of Mucorales hyphae inside blood vessels (**b**, **c**). In spleen histopathology there are areas of granulomatous lesions containing macrophages and multinucleated giant cells (**d**). **e** In higher magnification (**d**, inset), there is evidence of a Mucorales conidium (spore) inside a giant cell (arrow). Original magnifications ×200, ×800. Eosin and hematoxylin stain; white arrows: spores; black arrows: hyphae

Santa Cruz, # sc-598, dilution 1:100), Alexa 555 (Life Technologies, #A21425, dilution 1:1000), Alexa 488 (CF488A, Biotium, #20012-1, dilution 1:1000), FITC Annexin V Apoptosis Detection Kit (BD Pharmingen, #556547), FITC-Dextran (Sigma, #46945), propidium iodide (Sigma, #P4170), DFO (Sigma, #D9553), $FeCl_3$ (Sigma, #157740), clodronate liposomes (http://www.clodronateliposomes.org), bathocuproinedisulfonic acid disodium salt (BCS) (Sigma-Aldrich, #B1125), and RNeasy Plant Mini Kit (Qiagen, #74903).

Microorganisms and culture conditions. *Aspergillus fumigatus* ATCC[22] and *Rhizopus* strains used (WT *R. oryzae* ATCC557969[32]; WT strain *R. delemar* 99-880, a brain isolate obtained from the University of Texas Health Science Center at San Antonio, which had its genome sequenced[9,10]) were grown on Yeast extract agar glucose agar plates for 3 days at 37 °C. *Rhizopus delemar* M16 is a *pyrf*-null mutant that is derived from *R. delemar* 99-880 and is unable to synthesize its own uracil[49], and was grown on YPD medium (MP Biomedicals) supplemented with 100 µg/ml uracil. *Rhizopus delemar* with reduced *FTR1* copy number, and *R. delemar* transformed with RNA interference (RNAi) targeting *FTR1* expression were all derived from strain M16[9]. In experiments including RNAi mutants, a chemically defined synthetic medium containing yeast nitrogen base (YNB) supplemented with complete supplemental mixture without uracil (CSM-URA) (MP Biomedicals) (i.e., YNB + CSM-URA) (formulation per liter, 17 g YNB without amino acids (YNB) (BD), 20 g dextrose, and 7.7 g complete supplemental mixture minus uracil) was used. Fungal conidia (spores) were harvested by gentle shaking in the presence of sterile 0.1% Tween-20 in phosphate-buffered saline (PBS), washed twice with PBS, filtered through a 40 µm pore size cell strainer (Falcon) to separate conidia from contaminating mycelium, counted by a hemocytometer, and suspended at a concentration of 10^7 and 10^8 spores/ml for *Rhizopus* and *Aspergillus* strains, respectively. Inactivation of *Rhizopus* conidia was done by exposure to UV light (1 h, room temperature). To achieve synchronized swelling of *Rhizopus* conidia, 10^6/ml dormant conidia were incubated at 28 °C in a 6-well plate with RPMI-MOPS supplemented with 2% glucose for 4 h. For fluorescence labeling of *Rhizopus*, 10^6 conidia were stained in 100 µl PBS containing 100 µg/ml Fluorescent Brightener 28 (Sigma-Aldrich, #475300) and 0.1 M $NaHCO_3$ for 30 min protected from light in a bench-top rotator[33]. Afterwards, conidia were washed three times with PBS and the concentration was adjusted to 10^7 or 10^8 conidia/ml.

Fungal melanin extraction. The isolation of melanin from *A. fumigatus* and *R. oryzae* conidia was performed[22]. Briefly, conidia were treated with a combination of proteolytic (proteinase K; Sigma) and glycohydrolytic (Glucanex; Novo) enzymes, denaturing guanidine thiocyanate, and hot concentrated HCl (6 M). This treatment resulted in an electron-dense layer similar in size and shape to the original conidial melanin layer without underlying cell components, for which reason these electron-dense materials were called melanin ghosts.

Chemical characterization of *R. oryzae* melanin. *Rhizopus* conidia of 1.6 g was ground with mortar and pestle under liquid nitrogen into very fine powder. The black fine powder was extracted by boiling with 5% KOH under reflux for 1 h followed by filtration. The black colored filtrate was left to cool at room temperature and then precipitated with 1 N HCl. The black precipitate was collected by filtration using filter paper. The black precipitate was left to dry on the filter paper

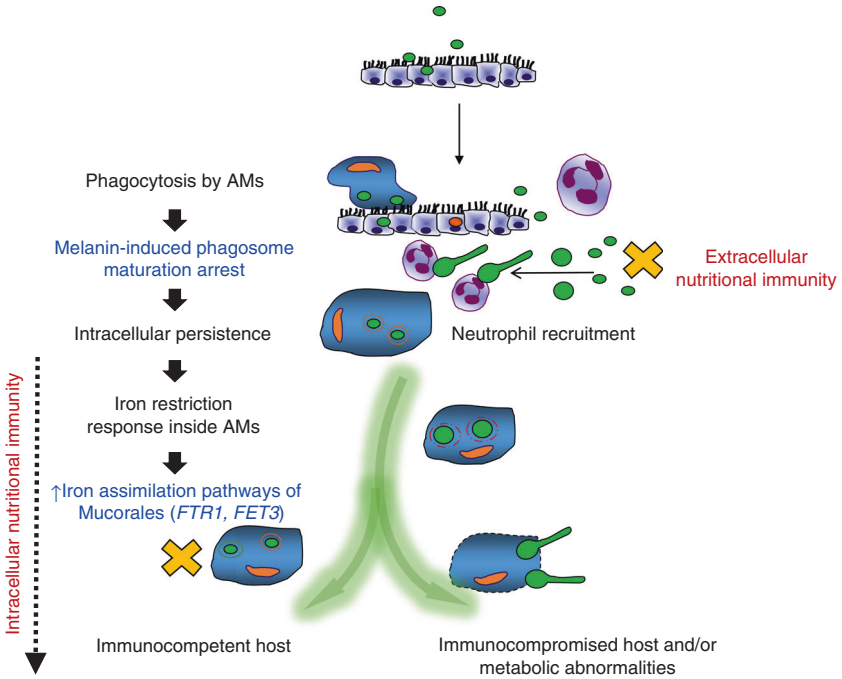

Fig. 10 Proposed model of nutritional immunity inside macrophages against Mucorales. Following inhalation, Mucorales conidia are predominantly phagocytosed by alveolar macrophages (AMs). Intracellular conidia of Mucorales remain dormant and establish prolonged persistence inside the nascent phagosome of AMs. Surface retention of cell wall melanin in intracellular conidia of Mucorales blocks phagosome biogenesis and LAP, impedes killing, and induces anti-apoptotic signaling in macrophages to establish persistence. Inhibition of intracellular germination of Mucorales conidia via iron restriction is a central host defense mechanism against mucormycosis. In addition, incompletely understood nutritional immunity mechanisms, including transferrin-mediated restriction of free iron availability in serum, inhibit germination of extracellular conidia. In parallel, rapid recruitment of neutrophils results in clearance of extracellular conidia of Mucorales. Quantitative and qualitative defects in innate immunity associated with prolonged chemotherapy-induced neutropenia, and/or corticosteroid-induced immunosuppression compromise the ability of phagocytes to inhibit germination of intracellular or extracellular conidia and result in invasive fungal growth. On the other site, failure of nutritional immunity mechanisms in patients with abnormalities on iron metabolism (e.g., diabetic acidosis) allow germination of intracellular or extracellular conidia and promote invasive tissue growth. Mucorales responses inside AMs are highlighted in blue. Nutritional immunity responses are highlighted in red

followed by washing several times with 1 N HCl, then 3 N HCl, water, and methanol. The remaining black/brown precipitate was dried at room temperature and used for further analysis.

The chemical analysis of melanin pigment was carried out by the modified method of Fava et al.[50]. Briefly, the solubility of the black pigment in distilled deionized water, 0.1 N HCl, 1 N HCl, 3 N HCl, 1 N KOH, methanol, ethanol, acetone, chloroform, benzene, and dimethyl sulfoxide (DMSO) were checked and found to be insoluble in all these solvents with the exception of 1 N KOH (Supplementary Table 1). Reactions with oxidizing agents such as 6% sodium hypochlorite and 30% H_2O_2 were determined by measuring solubility of the pigments in these reagents[50]. The precipitation of the pigments with $FeCl_3$ which reacts to polyphenols was also tested and found to be precipitated (Supplementary Table 1).

UV absorbance and IR analysis of *Rhizopus* melanin. The melanin extract in 1 N KOH was measured at 200–700 nm with the use of a SPECTRO UV–VIS spectrophotometer. One normal KOH was used as blank. For IR measurement, melanin powder was mixed with KBr and used to measure IR absorbance using a Bruker machine with KBr disc used as a blank.

Melanin alkaline H_2O_2 oxidation. To identify the production of various pyrrole acids (PTCA, PDCA, isoPTCA, and PTeCA) from melanin samples by LC-MS, alkaline H_2O_2 degradation was performed as described by Ito et al.[51]. In brief, extracted *Rhizopus* melanin was taken in a 5-ml screw-capped conical test tube, to which 500 µl of 1 mol/L K_2CO_3 and 50 µl of 30% H_2O_2 (final concentration: 1.5%) were added. The mixture was vigorously mixed and then kept on a shaker at 25 °C for 20 h. The residual H_2O_2 was decomposed by adding 100 µl 10% Na_2SO_3 and the mixture was then acidified with the addition of 200 µl of 6 M HCl. The reaction mixture was centrifuged at 4000 × *g* for 5 min and then subjected to thin linear chromatography (TLC) along with total KOH extract. The TLC developing system comprised of water:1 M HCl:chloroform:methanol (0.5:0.5:1:6).

LC-MS of melanin hydrolyses product. LC-MS analyses were carried out in negative ion mode by electrospray ionization on (Waters) ACQUITY UPLC triple Quadrupole (Xevo TQD) instrument equipped with the MassLynx software, at a flow rate of 0.3 ml/min, run time of 5 min, and the use of a solvent system containing 85% methanol, 15% water, and 0.1% formic acid. All solvents and reagents were HPLC grade and used without further purification.

EPR studies. EPR spectra were recorded at room temperature on an ELEXSYS Bruker spectrometer equipped with a Super High Q Sensitivity resonator operating at X-band (9.9 GHz). Microwave power was 1 mW for synthetic melanin and 0.1 mW for *A. fumigatus* or *R. oryzae*. Magnetic field modulation amplitude and frequency were, respectively, set to 0.2 mT and 100 kHz.

Virulence studies in mice. GFP-LC3 (obtained from RIKEN BioResource Center) and C57BL/6 (B6) mice were maintained in grouped cages in a high-efficiency particulate air-filtered environmentally controlled virus-free facility (24 °C, 12/12-h light/dark cycle), and fed by standard chow diet and water ad libitum. All experiments were approved by the local ethics committee of the University of Crete Medical School, Greece in line with the corresponding National and European Union legislation. Animal studies on virulence of albino *Rhizopus* were approved by the IACUC of the Los Angeles Biomedical Research Institute at Harbor-UCLA Medical Center, according to the NIH guidelines for animal housing and care.

For virulence studies, 8- to 12-week-old female C57BL/6 (B6) mice were challenged by intratracheal installation with a standard dose of *A. fumigatus* or *Rhizopus* conidia. Mice were euthanized at the indicated time point, lungs were homogenized, and CFU counts were assessed[21,22]. For AM depletion studies, mice received by intratracheal administration 100 µl of clodronate liposomes (containing 500 µg of clodronate; http://www.clodronateliposomes.org) or control (empty) liposomes[26]. For CD11c cell depletion, CD11c-DTR mice received by intratracheal administration 20 ng/kg of diphtheria toxin (DT). The efficiency of cell depletion was assessed by immunohistochemistry for CD11c and flow cytometry analysis of bronchoalveolar lavage (see below).

Immunocompetent CD-1 male mice were infected with 10^6 spores of *R. delemar* strain 99-880 grown in two different condition: on synthetic defined (SD) medium complete plates and on SD complete plates + 1 mM of the copper chelator, BCS. Sporulation on plates with BCS was subjected to copper deprivation and thus conidia appeared pigmentless (referred to in experiments as albino). Infection was carried out intratracheally, with 9 mice per group. Lungs were collected at three different time points: 4 h post infection, at day +1, and at day +3. At each time point, three mice per group were sacrificed. Right after infection, two mice have been sacrificed for inoculum verification. After collection, the samples were plated on potato dextrose agar + 0.1% Triton plates and incubated at 37 °C. For lung samples, after homogenization in 2 ml of PBS, 200 µl were plated directly from the concentrated samples and also from serial dilutions to facilitate counting.

Generation of murine BMDMs. BMDMs were generated by culturing BM cells obtained from 8- to 12-week-old female mice in Dulbecco's modified Eagle's medium (DMEM), supplemented with L929 cell-conditioned medium (30%). The resulting cultures consisted of macrophages (>95% purity), as determined by staining for F4/80 and flow cytometry.

Isolation and stimulation of BMDMs. The BMDMs were collected and resuspended in DMEM culture medium supplemented with streptomycin 1% and fetal bovine serum (FBS) 10% (DMEM complete). The cells were counted in a Bürker counting chamber, and their number was adjusted to 10^6/ml. For immunofluorescence experiments, a total of 1×10^5 BMDMs per condition in a final volume of 100 µl were allowed to adhere to polylysine-treated glass coverslips (Ø 12 mm) for 1 h followed by stimulation with conidia of *Rhizopus* or *A. fumigatus* at a multiplicity of infection (MOI) of 2:1 and 5:1, respectively, at 37 °C in a 5% CO_2 incubator for the indicated time point. After infection, cells were washed twice with PBS to remove medium and non-phagocytosed spores and cells were fixed on the coverslips for 15 min in 4% paraformaldehyde, followed by 10 min fixation with 100% ice-cold methanol and then stored in PBS at 4°C until immunofluorescence staining.

Immunofluorescence staining. For immunofluorescence imaging, cells were seeded on coverslips pretreated with polylysine, fixed with 4% paraformaldehyde for 15 min at room temperature, and followed by 10 min of fixation with ice-cold methanol at −20 °C. Next, the coverslips were washed twice with PBS, permeabilized by using 0.1% saponin (Sigma-Aldrich) prior to blocking for 30 min in PBS-BSA (PBS + 2% BSA). The coverslips were then incubated for 1 h with the indicated primary antibody (Ab), washed twice in PBS-BSA, then counterstained with the appropriate secondary Alexa Fluor secondary Ab (Molecular Probes), and followed by DNA staining with 10 µM TOPRO-3 iodide (642/661; Invitrogen). After extensive washing, slides were mounted in Prolong Gold antifade media (Molecular Probes). Images were acquired using a laser-scanning spectral confocal microscope (TCS SP2; Leica), LCS Lite software (Leica), and a ×40 Apochromat 1.25 NA oil objective using identical gain settings. A low fluorescence immersion oil (11513859; Leica) was used, and imaging was performed at room temperature. Serial confocal sections at 0.5 µm steps within a z-stack spanning a total thickness of 10 to 12 µm of the cell were taken and 3D images were generated using the LCS Lite software to assess for internalized conidia contained within phagosomes. Unless otherwise stated, mean projections of image stacks were obtained using the LCS Lite software and processed with Adobe Photoshop CS2. Phagosomes surrounded by a rim of fluorescence of the indicated protein marker were scored as positive.

Lysosomal extract preparation. Crude BMDM lysosomal extracts were obtained using the lysosome isolation kit instructions (Thermo Scientific, Boston, MA, USA), with small modification of a previously described protocol[52]. Briefly, at least 3×10^8 freshly collected BMDMs were counted, centrifuged at $400 \times g$ for 5 min at 4 °C and then washed twice with cold PBS. The supernatant was removed, the pellet was resuspended with reagent A and 1% (v/v) protease inhibitor, and then incubated in ice for exactly 2 min. Next, the cells were mildly sonicated on ice for 10 s and checked under a microscope with Tryptan blue solution staining to verify lysis of BMDMs. Subsequently, reagent B with 1% (v/v) protease inhibitor was added and the tube was inverted several times to mix the solution, which was then centrifuged at $500 \times g$ for 10 min at 4 °C. The supernatant was collected and gradient dilution buffer was added. The solution was centrifuged at $18000 \times g$ for 30 min at 4 °C and the pellet was dissolved in 250 µl gradient dilution buffer. Two rounds of sonication for 10 s each were performed, resulting in the generation of crude lysosome extract.

In vitro studies with crude lysosomal extracts. Crude lysosomal extracts were added to a 96-well plate in increasing concentration of 10%, 25%, and 50% with culture medium (DMEM-Glutamax supplemented with 10% FBS and 1% streptomycin) at pH 5.5. *Rhizopus oryzae* and *A. fumigatus* conidia were counted and added at a number of 5×10^4/well, reaching a total volume of 100 µl in each well. Culture medium at pH 5.5 was added to control wells. Plates were incubated for 24 h at 37°C in a 5% CO_2 incubator. The fungal metabolic activity was assessed with XTT ((2,3)-bis (2-methoxy 4-nitro 5-sulfenyl)-2*H*-tetrazolium carboxanilide; Sigma-Aldrich) reduction assay. One hundred microliters of tetrazolium salt XTT and menadione was added to each well at a final concentration of 0.25 mg/ml and 25 µM, respectively, and the plate was incubated for an additional 1 h. The absorbance of formazan, the XTT reduction product, was read at 450 and 655 nm on a Bio-Rad 680 microplate spectrophotometer. The percentage of the metabolic activity was determined as follows: % metabolic activity = $100\% \times (OD_{450} - OD_{655})$ experiment/$(OD_{450} - OD_{655})$ control. Fungal killing was evaluated by plating on a Sabouraud agar plate a 100-fold dilution of each well in sterile PBS.

Electron microscopy studies. Electron microscopy was performed using the methods reported previously[53]. Briefly, BMDMs were collected, counted, and inoculated in DMEM-Glutamax, 10% FBS, 1% streptomycin in 6-well plates. BMDMs were infected with conidia of either *R. oryzae* or *A. fumigatus* and cells were removed at the indicated time point of infection. Accordingly, infected BMDMs were fixed for 30 min at 4 °C with 2% glutaraldehyde in cold sodium cacodylate buffer (SCB) (0.1 M sodium cacodylate, 0.25 M sucrose, pH 7.4), and washed again with SCB. This was followed by two 30-min incubations in acid phosphatase reaction buffer (0.1 M sodium acetate, 1 mM glycerophosphate, and 2 mM $CeCl_3$), pH 5.2, at 37 °C. The cells were then rinsed three times with acid phosphatase reaction buffer, and re-fixed in 3% glutaraldehyde in SCB for 1 h at 4 °C. After two more washes in SCB, the obtained monolayers were post-fixed in cacodylate-buffered 1% OsO_4 for 2 h, dehydrated, and embedded in Epon 812 (Merck, Darmstadt, Germany). An ultratome (Leica, Reichert Ultracuts, Wien, Austria) was used to cut ultrathin sections, which were contrasted with 4% uranyl acetate for 45 min and lead citrate for 4 min at room temperature. Finally, the sections were examined using a Jeol 1200 EX2 electron microscope (JEOL, Tokyo, Japan).

Phagocytosis and killing assays in BMDMs and PMNs. For the killing assays, 10^6 BMDMs were left to adhere in 6-well plates for 1 h in 2 ml of DMEM complete media at 37 °C in a 5% CO_2 incubator, and subsequently infected with either *R. oryzae* or *A. fumigatus* conidia, at an MOI of 1:1. BMDMs were washed three times with warm PBS 30 min after the infection to remove non-phagocytosed conidia. At the indicated time point of infection (2 or 6 h), BMDMs were harvested by scraping, placed in Eppendorf tubes, lysed by sonication (three times for 10 s and once for 5 s for *A. fumigatus*-infected and *R. oryzae*-infected BMDMs, respectively), centrifuged at 1000 rpm for 10 min at 4 °C, and the pellet containing intracellular conidia was resuspended in 200 µl sterile PBS. *Aspergillus fumigatus* killing was assessed as previously described using propidium iodide staining[22]. For the evaluation of killing of *Rhizopus* conidia by BMDMs, intracellular conidia recovered after BMDM lysis were incubated at 37 °C in a 5% CO_2 incubator with DMEM complete medium for ~4 h, until germination was microscopically observed. Killing of *R. oryzae* was assessed using a Bürker counting chamber based on the percentage of germinating conidia. Germination of intracellular *Rhizopus* conidia by BMDMs was always normalized to the germination of control *R. oryzae* conidia following sonication (5 s) and cultured in DMEM complete medium for ~4 h in the absence of BMDMs, which was typically always >95%. In representative experiments, killing of *A. fumigatus* was also assessed based on the germination assay.

For phagocytosis assay, BMDMs and polymorphonuclear neutrophils (PMNs) from GFP-LC3 mice were stimulated with *R. oryzae* and *A. fumigatus* conidia at an MOI of 2:1 at 37 °C in a 5% CO_2 incubator for different time points. Cells were then fixed and stained for confocal microscopy as previously mentioned. Phagocytic index was expressed with the following formula: (total number of engulfed cells/total number of counted macrophages) × (number of macrophages containing engulfed cells/total number of counted macrophages) × 100.

Murine PMN isolation. Murine PMNs were isolated using a Percoll (Sigma) double gradient density centrifugation technique. Bone marrow from two immunocompetent GFP-LC3 mice was collected and flushed in room temperature in a sterile solution of PBS/EDTA. The cells were centrifuged at room temperature for 10 min at $350 \times g$ and resuspended in 2 ml PBS/EDTA. The cells were carefully placed on top of 2 ml of three different Percoll concentrations (75%, 67%, and 52%) in a 15 ml Falcon tube. The solution was centrifuged at room temperature for 30 min at $1100 \times g$, resulting in three zones, peripheral blood mononuclear cells, PMNs, and red blood cells (RBCs), from the top to the bottom, respectively. PMNs were collected and centrifuged in 4 °C for 10 min at $350 \times g$. The pellet was collected and resuspended in 0.5 ml water for 25 s to lyse the remaining RBCs. Subsequently, 0.5 ml of 1.8% NaCl was added and the cells were centrifuged in 4 °C for 10 min at $350 \times g$, washed with 2 ml HEPES buffer, and centrifuged again in 4 °C for 10 min at $350 \times g$. Finally, the pellet was re-diluted in 1 ml DMEM complete. The viability of PMNs, checked with trypan blue dye, was over 98% and purity of PMNs (identified as CD11b+/Ly6G+ cells) was >90% by flow cytometry.

FACS sorting and flow cytometry studies. To obtain single lung cell suspensions, lungs were perfused with 20 ml PBS through the right ventricle, cut into small pieces, and digested for 1 h at 37 °C in 1 mg/ml collagenase A (Roche) and 0.05 mg/ml DNase I (Roche) in Hank's balanced salt solution. For flow cytometric analysis, single lung cells were stained with the following antibodies: anti-CD45-APC (Clone

30-F11, BioLegend, #103111, 1:200 dilution), anti-MHCII-FITC (Clone M5/114.15.2, BioLegend, #107605, 1:100 dilution), anti-F4/80-PE (Clone BM8, BioLegend, #123109, 1:100 dilution), anti-CD11c-PerCP-Cy5.5 (Clone N418, BioLegend, #117328, 1:100 dilution), anti-CD11b-PE-Cy7 (Clone M1/70, BioLegend, #101215, 1:200 dilution), anti-Ly6G-PE (Clone 1A8, BioLegend, #127607, 1:200 dilution), and anti-Ly6C-FITC (Clone HK1.4, BioLegend, #128005, 1:200 dilution). Flow cytometric data were collected on a MoFloT High-Performance Cell Sorter and were analyzed with FlowJo, version 8.7.1 (Treestar). AMs and IMs were sorted by flow cytometry based on their differential F4/80/CD11c/MHCII expression, as previously described[54]. PMNs were sorted as MHCII−/CD11b+/Ly6G+ cells. Isolated cells were cultured in RPMI-1640 medium supplemented with 10% fetal calf serum, 2 mM L-glutamine, 1 mM sodium pyruvate, 0.1 mM nonessential amino acids, 50 μM β-mercaptoethanol, 50 μg/ml streptomycin, and 50 IU/ml penicillin (all from Invitrogen), fixed and stained for confocal imaging. Flow cytometric data were collected on a MoFloT High-Performance Cell Sorter and were analyzed with FlowJo, version 8.7.1 (Treestar).

For FACS analysis in CD11c-DTR mice, the following antibodies were used: anti-CD45-APC-Cy7 (Clone 30-F11, BioLegend, #103116, 1:200), anti-CD11c-PerCP-Cy5.5 (Clone N418, BioLegend, #117328, 1:200), anti-I-A/I-E-PE-Cy7 (M5/114.15.2, BioLegend, #107630, 1:200), and anti-Singlec-F Alexa Fluor® 647 (E50-2440, BD Pharmingen, #562680, 1:200). Cells were acquired in a FACS Aria IIu (BD Biosciences) and data were analyzed with the FACSDIVA software (BD Biosciences).

Histopathological and immunohistochemistry studies. Lungs were fixed in 10% formalin, paraffin embedded, cut in 4-μm sections, and stained with hematoxylin and eosin. For immunohistochemistry studies, the anti-CD11c Abs (HL3; BD Biosciences, 1:200 dilution) and anti-CD68 (FA-11, 137001, BioLegend, 1:200 dilution) primary antibodies were used for detection of CD11c and CD68 in tissue. The slide-mounted sections were baked for 10 min at 60 °C, deparaffinized with two xylene washes, rehydrated through a series of graded alcohol washes, rinsed in water, and washed with 0.1 M PBS (pH 7.4) containing 0.01% Tween-20. Heat-induced antigen retrieval was performed in a steamer using target retrieval solution (Dako S1700). Endogenous peroxidase was blocked with 3% H_2O_2 for 10 min. The slides were then incubated in blocking solution (serum-free protein block, Dako X0909) for 20 min to block nonspecific binding. The primary antibodies were added to the slides and incubated overnight in a humidified chamber at 40 °C. Detection was accomplished using an Envision_Horseradish Peroxidase Kit (Dako K0679). Immunostaining was revealed using 3,3′-diaminobenzidine. The slides were lightly counterstained with hematoxylin, progressively dehydrated through graded alcohols and xylene, and finally covered with a coverslip after mounting in DPX mounting medium. Slides were examined under an Olympus light microscope that was equipped with a ×40 objective. In certain experiments fungal conidia were counterstained with periodic acid-Schiff (PAS).

RNA isolation from *Rhizopus*-infected BMDMs. BMDMs (2×10^6 cells per condition) obtained following 6 days of differentiation of BM cells of 12-week-old female C57BL/6 mice were seeded in 12-well plates and left overnight at 37 °C in DMEM media. Next, BMDMs were washed 2× with culture media, infected at an MOI of 1:2 (macrophage:fungal conidia) with *R. delemar* (strain 99-880), and 1 h later washed five times to remove extracellular conidia. At the indicated time point of infection (1, 4, and 18 h), BMDMs were removed by scraping, centrifuged at 400 × *g*, and lysed with 450 μl of RLT buffer + β-mercaptoethanol using the RNeasy Plant Mini Kit (Qiagen). As a negative control, 1×10^7 *R. delemar* conidia were added to the tissue culture plates containing medium alone without host cells and processed in parallel. Another control included RNA extracted from uninfected BMDMs. Then, each sample was sonicated using a sonication probe on ice 20 × 1 s (set 40). Afterwards, isolation of RNAs was performed according to the manufacturer's instructions.

RNA-seq analysis. All RNA-seq libraries (strand-specific, paired-end) were prepared with the TruSeq RNA Sample Prep Kit (Illumina). The total RNA samples were subjected to poly (A) enrichment as part of the TruSeq protocol. One hundred and fifty nucleotide sequences were determined from both ends of each complementary DNA fragment using the HiSeq platform (Illumina) as per the manufacturer's protocol. Sequencing reads were annotated and aligned to the UCSC mouse reference genome (mm10, GRCm38.75) as well as the *R. delemar* (strain 99-880) genome using TopHat2[55]. The alignment files from TopHat2 were used to generate read counts for each gene and a statistical analysis of differential gene expression was performed using the DE-seq package from Bioconductor[56]. A gene was considered differentially expressed if the *P* value for differential expression was <0.05 and the absolute log (base 2) fold change, relative to single organism control, was ≥1.

Human studies. Approval for the collection of clinical information and tissue samples from the patient with mucormycosis was obtained and the Ethics Committee of the University Hospital of Heraklion, Crete, Greece (5159/2014). The patient provided written informed consent in accordance with the Declaration of Helsinki

Statistical analysis. The data were expressed as mean ± SEM. Statistical significance of differences was determined by two-sided nonparametric Mann–Whitney test and one-way analysis of variance with the indicated post hoc test for multiple comparisons ($P < 0.05$ was considered statistically significant). Survival analysis was performed by log-rank (Mantel–Cox) test. Analysis was performed using the GraphPad Prism software (version V). All in vitro experiments were performed at least in triplicate and replicated at least twice.

Data availability

All the data that support the findings of this study are available from the corresponding author (G.C.) upon reasonable request. All of the raw sequencing data from this study will have been submitted to the NCBI SRA database (http://www.ncbi.nlm.nih.gov) under accession code PRJNA407788.

Received: 4 January 2018 Accepted: 27 July 2018
Published online: 20 August 2018

References

1. Brown, G. D. et al. Hidden killers: human fungal infections. *Sci. Transl. Med.* **4**, 165rv113 (2012).
2. Kontoyiannis, D. P. et al. Prospective surveillance for invasive fungal infections in hematopoietic stem cell transplant recipients, 2001–2006: overview of the Transplant-Associated Infection Surveillance Network (TRANSNET) Database. *Clin. Infect. Dis.* **50**, 1091–1100 (2010).
3. Pappas, P. G. et al. Invasive fungal infections among organ transplant recipients: results of the Transplant-Associated Infection Surveillance Network (TRANSNET). *Clin. Infect. Dis.* **50**, 1101–1111 (2010).
4. Kontoyiannis, D. P. et al. Zygomycosis in a tertiary-care cancer center in the era of *Aspergillus*-active antifungal therapy: a case–control observational study of 27 recent cases. *J. Infect. Dis.* **191**, 1350–1360 (2005).
5. Trifilio, S. M. et al. Breakthrough zygomycosis after voriconazole administration among patients with hematologic malignancies who receive hematopoietic stem-cell transplants or intensive chemotherapy. *Bone Marrow Transplant.* **39**, 425–429 (2007).
6. Roden, M. M. et al. Epidemiology and outcome of zygomycosis: a review of 929 reported cases. *Clin. Infect. Dis.* **41**, 634–653 (2005).
7. Spellberg, B., Edwards, J. Jr. & Ibrahim, A. Novel perspectives on mucormycosis: pathophysiology, presentation, and management. *Clin. Microbiol. Rev.* **18**, 556–569 (2005).
8. Ibrahim, A. S., Spellberg, B., Walsh, T. J. & Kontoyiannis, D. P. Pathogenesis of mucormycosis. *Clin. Infect. Dis.* **54**, S16–S22 (2012).
9. Ibrahim, A. S. et al. The high affinity iron permease is a key virulence factor required for *Rhizopus oryzae* pathogenesis. *Mol. Microbiol.* **77**, 587–604 (2010).
10. Liu, M. et al. Fob1 and Fob2 proteins are virulence determinants of *Rhizopus oryzae* via facilitating iron uptake from ferrioxamine. *PLoS Pathog.* **11**, e1004842 (2015).
11. Boelaert, J. R. et al. Mucormycosis during deferoxamine therapy is a siderophore-mediated infection. In vitro and in vivo animal studies. *J. Clin. Investig.* **91**, 1979–1986 (1993).
12. Boelaert, J. R., Van Cutsem, J., de Locht, M., Schneider, Y. J. & Crichton, R. R. Deferoxamine augments growth and pathogenicity of *Rhizopus*, while hydroxypyridinone chelators have no effect. *Kidney Int.* **45**, 667–671 (1994).
13. Gebremariam, T. et al. Bicarbonate correction of ketoacidosis alters host–pathogen interactions and alleviates mucormycosis. *J. Clin. Invest.* **126**, 2280–2294 (2016).
14. Gebremariam, T. et al. CotH3 mediates fungal invasion of host cells during mucormycosis. *J. Clin. Invest.* **124**, 237–250 (2014).
15. Liu, M. et al. The endothelial cell receptor GRP78 is required for mucormycosis pathogenesis in diabetic mice. *J. Clin. Invest.* **120**, 1914–1924 (2010).
16. Lionakis, M. S., Iliev, I. D. & Hohl, T. M. Immunity against fungi. *JCI Insight* **2**, e93156 (2017).
17. Uwamahoro, N. et al. The pathogen *Candida albicans* hijacks pyroptosis for escape from macrophages. *mBio* **5**, e00003–e00014 (2014).
18. O'Meara, T. R. et al. Global analysis of fungal morphology exposes mechanisms of host cell escape. *Nat. Commun.* **6**, 6741 (2015).
19. Shah, A. et al. Calcineurin orchestrates lateral transfer of *Aspergillus fumigatus* during macrophage cell death. *Am. J. Respir. Crit. Care Med.* **194**, 1127–1139 (2016).
20. Li, C. H. et al. Sporangiospore size dimorphism is linked to virulence of *Mucor circinelloides*. *PLoS Pathog.* **7**, e1002086 (2011).
21. Kyrmizi, I. et al. Corticosteroids block autophagy protein recruitment in *Aspergillus fumigatus* phagosomes via targeting dectin-1/Syk kinase signaling. *J. Immunol.* **191**, 1287–1299 (2013).

22. Akoumianaki, T. et al. *Aspergillus* cell wall melanin blocks LC3-associated phagocytosis to promote pathogenicity. *Cell. Host Microbe* **19**, 79–90 (2016).
23. Levin, R., Grinstein, S. & Canton, J. The life cycle of phagosomes: formation, maturation, and resolution. *Immunol. Rev.* **273**, 156–179 (2016).
24. Latge, J. P. The cell wall: a carbohydrate armour for the fungal cell. *Mol. Microbiol.* **66**, 279–290 (2007).
25. Nosanchuk, J. D., Stark, R. E. & Casadevall, A. Fungal melanin: what do we know about structure? *Front. Microbiol.* **6**, 1463 (2015).
26. Mircescu, M. M., Lipuma, L., van Rooijen, N., Pamer, E. G. & Hohl, T. M. Essential role for neutrophils but not alveolar macrophages at early time points following *Aspergillus fumigatus* infection. *J. Infect. Dis.* **200**, 647–656 (2009).
27. Van Rooijen, N. & Sanders, A. Liposome mediated depletion of macrophages: mechanism of action, preparation of liposomes and applications. *J. Immunol. Methods* **174**, 83–93 (1994).
28. Drakesmith, H. et al. The hemochromatosis protein HFE inhibits iron export from macrophages. *Proc. Natl Acad. Sci. USA* **99**, 15602–15607 (2002).
29. Recalcati, S. et al. Differential regulation of iron homeostasis during human macrophage polarized activation. *Eur. J. Immunol.* **40**, 824–835 (2010).
30. Corna, G. et al. Polarization dictates iron handling by inflammatory and alternatively activated macrophages. *Haematologica* **95**, 1814–1822 (2010).
31. Partida-Martinez, L. P. & Hertweck, C. Pathogenic fungus harbours endosymbiotic bacteria for toxin production. *Nature* **437**, 884–888 (2005).
32. Chamilos, G. et al. Drosophila melanogaster as a model host to dissect the immunopathogenesis of zygomycosis. *Proc. Natl Acad. Sci. USA* **105**, 9367–9372 (2008).
33. Voelz, K., Gratacap, R. L. & Wheeler, R. T. A zebrafish larval model reveals early tissue-specific innate immune responses to *Mucor circinelloides*. *Dis. Model Mech.* **8**, 1375–1388 (2015).
34. Kumar, N. et al. Gain-of-function signal transducer and activator of transcription 1 (STAT1) mutation-related primary immunodeficiency is associated with disseminated mucormycosis. *J. Allergy Clin. Immunol.* **134**, 236–239 (2014).
35. Fahimzad, A., Chavoshzadeh, Z., Abdollahpour, H., Klein, C. & Rezaei, N. Necrosis of nasal cartilage due to mucormycosis in a patient with severe congenital neutropenia due to HAX1 deficiency. *J. Investig. Allergol. Clin. Immunol.* **18**, 469–472 (2008).
36. Vinh, D. C. et al. Mucormycosis in chronic granulomatous disease: association with iatrogenic immunosuppression. *J. Allergy Clin. Immunol.* **123**, 1411–1413 (2009).
37. Levitz, S. M., Selsted, M. E., Ganz, T., Lehrer, R. I. & Diamond, R. D. In vitro killing of spores and hyphae of *Aspergillus fumigatus* and *Rhizopus oryzae* by rabbit neutrophil cationic peptides and bronchoalveolar macrophages. *J. Infect. Dis.* **154**, 483–489 (1986).
38. Jorens, P. G. et al. Human and rat macrophages mediate fungistatic activity against *Rhizopus* species differently: in vitro and ex vivo studies. *Infect. Immun.* **63**, 4489–4494 (1995).
39. Waldorf, A. R., Levitz, S. M. & Diamond, R. D. In vivo bronchoalveolar macrophage defense against *Rhizopus oryzae* and *Aspergillus fumigatus*. *J. Infect. Dis.* **150**, 752–760 (1984).
40. Waldorf, A. R., Ruderman, N. & Diamond, R. D. Specific susceptibility to mucormycosis in murine diabetes and bronchoalveolar macrophage defense against *Rhizopus*. *J. Clin. Invest.* **74**, 150–160 (1984).
41. Guarner, J. & Brandt, M. E. Histopathologic diagnosis of fungal infections in the 21st century. *Clin. Microbiol. Rev.* **24**, 247–280 (2011).
42. Lehar, S. M. et al. Novel antibody–antibiotic conjugate eliminates intracellular *S. aureus*. *Nature* **527**, 323–328 (2015).
43. Davoudi, S., Anderlini, P., Fuller, G. N. & Kontoyiannis, D. P. A long-term survivor of disseminated *Aspergillus* and *Mucorales* infection: an instructive case. *Mycopathologia* **178**, 465–470 (2014).
44. Volling, K., Thywissen, A., Brakhage, A. A. & Saluz, H. P. Phagocytosis of melanized *Aspergillus conidia* by macrophages exerts cytoprotective effects by sustained PI3K/Akt signalling. *Cell Microbiol.* **13**, 1130–1148 (2011).
45. Artis, W. M., Fountain, J. A., Delcher, H. K. & Jones, H. E. A mechanism of susceptibility to mucormycosis in diabetic ketoacidosis: transferrin and iron availability. *Diabetes* **31**, 1109–1114 (1982).
46. Ibrahim, A. S. et al. The iron chelator deferasirox protects mice from mucormycosis through iron starvation. *J. Clin. Invest.* **117**, 2649–2657 (2007).
47. Soares, M. P. & Weiss, G. The iron age of host–microbe interactions. *EMBO Rep.* **16**, 1482–1500 (2015).
48. Weiss, G. & Schaible, U. E. Macrophage defense mechanisms against intracellular bacteria. *Immunol. Rev.* **264**, 182–203 (2015).
49. Skory, C. D. & Ibrahim, A. S. Native and modified lactate dehydrogenase expression in a fumaric acid producing isolate *Rhizopus oryzae* 99-880. *Curr. Genet.* **52**, 23–33 (2007).
50. Fava, F., Gioia, D. D. & Marchetti, L. Characterization of a pigment produced by *Pseudomonas fluorescens* during 3-chlorobenzoate co-metabolism. *Chemosphere* **27**, 825–835 (1993).
51. Ito, S. & Wakamatsu, K. Chemical degradation of melanins: application to identification of dopamine-melanin. *Pigment Cell Res.* **11**, 120–126 (1998).
52. Wozniak, K. L. & Levitz, S. M. Cryptococcus neoformans enters the endolysosomal pathway of dendritic cells and is killed by lysosomal components. *Infect. Immun.* **76**, 4764–4771 (2008).
53. Strasser, J. E. et al. Regulation of the macrophage vacuolar ATPase and phagosome–lysosome fusion by Histoplasma capsulatum. *J. Immunol.* **162**, 6148–6154 (1999).
54. Bedoret, D. et al. Lung interstitial macrophages alter dendritic cell functions to prevent airway allergy in mice. *J. Clin. Invest.* **119**, 3723–3738 (2009).
55. Kim, D. et al. TopHat2: accurate alignment of transcriptomes in the presence of insertions, deletions and gene fusions. *Genome Biol.* **14**, R36 (2013).
56. Anders, S., & Huber, W. Differential expression analysis for sequence count data. *Genome Biol.* **11**, R106 (2010).

Acknowledgements

We are grateful to Zacharenia Vlata from the IMBB FACS sorting facility for assistance with FACS analyses and to Teclegiorgis Gebremariam for helping with the animal studies. We are grateful to the EPR facilities available at the French research infrastructure IR-RPE CNRS 3443. I.K. is supported by the Onassis Foundation under the Special Grant and Support Program for Scholars Association Members (Grant No. R ZM 003-1/2016-2017; G.C. and A.M.A. are supported by a grant from the Greek State Scholarship Foundation (I.K.), G.C. is also supported by grants from the Hellenic General Secretariat for Research and Technology-Excellence program (ARISTEIA), and a Research Grant from Institute Merieux; A.S.I. is supported by Public Health Service grant from the National Institutes of Allergy and Immunology R01 AI063503 and U19AI110820. V.M.B. is supported by Public Health Service grant from the National Institutes of Allergy and Immunology U19AI110820.

Author contributions

A.M.A. and I.K. performed and analyzed most of the experiments in this study and participated in their design. K.T. and E.A. performed experiments with CD11c-DTR mice and analyzed data. E.D. and M.T. performed histopathology studies. C.B. performed experiments with albino *Rhizopus* conidia. S.S.M.S. performed studies on physicochemical characterization of *Rhizopus* melanin. V.M.B., A.C.S., and C.M.C. performed dual RNA-seq. T.A. and P.I. analyzed data and provided assistance in establishing protocols for immunostaining. K.S. participated in EM studies. C.P. and H.A.P. provided information on the patient with mucormycosis. V.B. and E.E. performed EPR studies on melanins. A.B. analyzed data and performed melanin purification studies. D.P.K. and G.S. analyzed data and provided helpful suggestions. A.S.I. participated in the design and supervision of experiments, performed experiments, analyzed data, and provided key materials, as well as suggestions throughout the study. G.C. conceived and supervised the study, performed experiments, was involved in the design and evaluation of all experiments, and wrote the manuscript together with A.S.I. along with comments from co-authors.

Additional information

Supplementary Information accompanies this paper at https://doi.org/10.1038/s41467-018-05820-2.

Competing interests: The authors declare no competing interests.

Reprints and permission information is available online at http://npg.nature.com/reprintsandpermissions/

Publisher's note: Springer Nature remains neutral with regard to jurisdictional claims in published maps and institutional affiliations.